NATIONAL ADVISORY COMMITTEE FOR AERONAUTICS

TECHNICAL MEMORANDUM

No. 1218

LECTURE SERIES "BOUNDARY LAYER THEORY"

PART II - TURBULENT FLOWS

By H. Schlichting

Translation of "Vortragsreihe" W.S. 1941/42, Luftfahrtforschungsanstalt Hermann Göring, Braunschweig

Washington
April 1949

TABLE OF CONTENTS

NATIONAL ADVISORY COMMITTEE FOR AERONAUTICS

TECHNICAL MEMORANDUM NO. 1218

LECTURE SERIES "BOUNDARY LAYER THEORY"

Part II – Turbulent Flows*

By H. Schlichting

CHAPTER XIII. GENERAL REMARKS ON TURBULENT FLOWS

a. Turbulent Pipe Flow

The flow laws of the actual flows at high Reynolds numbers differ considerably from those of the laminar flows treated in the preceding part. These actual flows show a special characteristic, denoted as "turbulence."

The character of a turbulent flow is most easily understood in the case of the pipe flow. Consider the flow through a straight pipe of circular cross section and with a smooth wall. For laminar flow each fluid particle moves with uniform velocity along a rectilinear path. Because of viscosity, the velocity of the particles near the wall is smaller than that of the particles at the center. In order to maintain the motion, a pressure decrease is required which, for laminar flow, is proportional to the first power of the mean flow velocity (compare chapter I, Part I). Actually, however, one observes that, for larger Reynolds numbers, the pressure drop increases almost with the square of the velocity and is very much larger than that given by the Hagen–Poiseuille law. One may conclude that the actual flow is very different from that of the Poiseuille flow.

The following test, introduced by Reynolds, is very instructive: If one inserts into the flowing fluid a colored filament one can observe, for small Reynolds numbers, that the colored filament is maintained downstream as a sharply defined thread. One may conclude that the fluid actually flows as required by the theory of laminar flow: a gliding along, side by side, of the adjoining layers without mutual mixing (laminar = layer flow). For large Reynolds numbers, on the other hand, one can observe the colored filament, even at a small distance downstream from the inlet, distributed over the entire cross section, that is, mixed

---

*"Vortragsreihe 'Grenzschichttheorie.' Teil B: Turbulente Strömungen." Zentrale für wissenschaftliches Berichtswesen der Luftfahrtforschung des Generalluftzeugmeisters (ZWB) Berlin-Adlershof, pp. 154–279. The original language version of this report is divided into two main parts, Teil A and Teil B, which have been translated as separate NACA Technical Memorandums, Nos. 1217 and 1218, designated Part I and Part II, respectively. This report is a continuation of the lecture series presented in part I, the equations, figures, and tables being numbered in sequence from the first part of the report. For general information on the series, reference should be made to the preface and the introduction of Part I.

to a great extent with the rest of the fluid. Thus the flow character has changed completely for large Reynolds numbers: A pronounced transverse mixing of adjacent layers takes place. Irregular additional velocities in the longitudinal and transverse directions are superposed on the main velocity. This state of flow is called turbulent. As a consequence of the mixing the velocity is distributed over the cross section more uniformly for turbulent than for laminar flow (compare fig. 17, part I). For turbulent flow there exists a very steep velocity increase in the immediate neighborhood of the wall and almost constant velocity in the central regions. Consequently the wall shearing stress is considerably larger for turbulent than for laminar flow; the same applies to the drag. This follows also from the fact that in turbulent flow a considerable part of the energy is used up in maintaining the turbulent mixing motion.

The exact analysis of a turbulent flow shows that at a point fixed in space the velocity is subjected to strong irregular fluctuations with time (fig. 72). If one measures the variation with time of a velocity component at a fixed point in space, one obtains, qualitatively, a variation as shown in figure 72. The flow is steady only on the average and may be interpreted as composed of a temporal mean value on which the irregular fluctuation velocities are superimposed.

The first extensive experimental investigations were carried out by Darcy (reference 60) in connection with the preliminary work for a large water-distributing system for the city of Paris. The first quantitative experiments concerning laminar pipe flow were made by Hagen (reference 95). The first systematic tests regarding the transition from laminar to turbulent flow were made by Osborn Reynolds (reference 61). He determined by experiment the connection between flow volume and pressure drop for turbulent flow and investigated very thoroughly the transition of the laminar to the turbulent form of flow. He found, in tests of various velocities and in pipes of various diameters, that transition always occurred at the same value of the Reynolds number: $\frac{\bar{u}d}{\nu}$. This Reynolds number is called the critical Reynolds number. The measurements gave for the pipe flow:

$$Re_{crit} = \left(\frac{\bar{u}d}{\nu}\right)_{crit} = 2300 \qquad (13.1)$$

For $Re < Re_{crit}$ the flow is laminar, for $Re > Re_{crit}$, turbulent. Later on it was ascertained that the numerical value of Re_{crit} is, moreover, very dependent on the particular test conditions. If the entering flow was very free of disturbances, laminar flow could be maintained up to Re = 24000. However, of main interest for the technical applications is the lowest critical Reynolds number existing for an arbitrary disturbance of the entering flow, due either to irregularities in the approaching flow or to vortices forming at the pipe inlet. Concerning the drag law of the pipe Reynolds found that the pressure drop is proportional to the 1.73 power of the mean flow velocity:

$$\Delta p \sim \bar{u}^{1.73}$$

b. Turbulent Boundary Layers

Recently it was determined that the flow along the surface of a body (boundary layer flow) also can be turbulent. We had found, for instance, for the flat plate in longitudinal flow that the drag for laminar flow is proportional to $\sqrt{U_o^3}$ (compare equation (9.18), Part I.) However, towing tests on plates for large Reynolds numbers carried out by Froude (reference 96) resulted in a drag law according to which $W \sim U_o^{1.85}$. Moreover, the drag coefficients in these measurements remained considerably higher than the drag coefficient of the laminar plate flow according to equation (9.19), Part I. Presumably this deviation is caused by the turbulence of the boundary layer.

A clear decision about the turbulent flow in the boundary layer was obtained by the classical experiments of Eiffel and Prandtl concerning the drag of spheres in 1914 (reference 62). These tests gave the following results regarding the drag of spheres (compare fig. 73). The curve of drag against velocity shows a sudden drop at a definite velocity V_{crit}, although it rises again with further increasing velocity. If one plots the drag coefficient $c_w = W/F \frac{\rho}{2} U_o^2$ (F = frontal area) against the Reynolds number $U_o d/\nu$, c_w shows a decrease to 2/5 of its original value at a definite Reynolds number (Re_{crit}). Prandtl explained this phenomenon in 1914. He was able to show that this drag decrease stems from the laminar boundary layer changing to turbulent ahead of the separation point. The resulting considerable rearward shift of the separation point causes a reduction of the vortex region (dead water) behind the sphere (fig. 74). This hypothesis could be confirmed by experiment: by putting a wire ring on the sphere (sphere diameter 28 centimeters, wire diameter 1 millimeter) one could attain the smaller drag at smaller V_{crit} and Re_{crit}. The wire ring is put on slightly ahead of the laminar separation point; it causes a vortex formation in the boundary layer, which is thus made turbulent ahead of the separation point and separates only farther toward the rear. By means of the wire ring the boundary layer is, so-to-say, "infected" with turbulence. Due to the mixing motions which continually lead high velocity air masses from the outside to the wall, the turbulent boundary layer is able to overcome, without separation, a larger pressure increase than the laminar boundary layer.

The turbulence of the friction layer is of great importance for all flows along solid walls with pressure increase (diffuser, wing suction side). It is, however, also present in the flow along a flat plate where the pressure gradient is zero. There the flow in the boundary layer is laminar toward the front, experiencing transition to the turbulent state further downstream. Whereas the laminar boundary layer thickness increases downstream with $x^{1/2}$, the turbulent boundary layer thickness increases

approximately as $x^{4/5}$; that is, for the turbulent boundary layer the increase of the boundary layer thickness is considerably larger, (fig. 75). The position of the transition point x_{crit} is given by (fig. 75):

$$\left(\frac{U_o x}{\nu}\right)_{crit} = 3 \text{ to } 5 \times 10^5 \tag{13.2}$$

In comparing the critical Reynolds numbers for the pipe and the plate one must select r and δ, respectively, as reference lengths. The equation for the flat plate is, according to Blasius (reference 8) (compare equation (9.21a))

$$\left.\begin{aligned} \delta &= 5\sqrt{\frac{\nu x}{U_o}} \\ \text{or} \quad \frac{U_o \delta}{\nu} &= 5\sqrt{\frac{U_o x}{\nu}} \end{aligned}\right\} \tag{13.3}$$

Thus, with $\left(\frac{U_o x}{\nu}\right)_{crit} = 25000$:

$$\left(\frac{U_o \delta}{\nu}\right)_{crit} = 5.500 = 2500 \text{ (flat plate)} \tag{13.4}$$

This critical Reynolds number must be compared with $\frac{U_{max}\, r}{\nu}$ at the transition point for the pipe. Due to the parabolic laminar velocity distribution in the pipe $u_{max} = 2\,\bar{u}$, and because $r = \frac{1}{2}\,d$, then, for the pipe, $u_{max} r/\nu = \bar{u}d/\nu$. According to equation (13.1), $\left(\frac{ud}{\nu}\right)_{crit} = 2300$ for the pipe. Thus the comparable critical Reynolds numbers for pipe and plate show rather good agreement.

CHAPTER XIV. OLDER THEORIES

The first efforts toward theoretical calculation of the turbulent flows go back to Reynolds. One distinguishes in the theory of turbulence two main problems:

1. The flow laws of the developed turbulent flow:

The space and time velocity variations affect the time average of the velocity; they act like an additional internal friction. The problem is to calculate the local distribution of the time average of the velocity components, and thus to gain further information concerning, for instance, the friction drag.

2. Origin of turbulence:

One investigates under what conditions a small disturbance, superposed on a laminar flow, increases with time. According to whether or not the disturbance increases with time, the laminar flow is called unstable or stable. The investigation in question is therefore a stability investigation, made to clarify theoretically the laminar-turbulent transition. These investigations aim particularly at the theoretical calculation of the critical Reynolds number. They are, in general, mathematically rather complicated.

The first problem, since it is the more important one for general flow problems will be our main concern. The second will be discussed briefly at the end of the lecture series.

As to the first problem, that of calculation of the developed turbulent flow, one may remark quite generally that a comprehensive theoretical treatment, as exists for laminar flow, is not yet possible. The present theory of the developed turbulent flow must be denoted as semi-empirical. It obtains its foundations to a great extent from experiment, works largely with the laws of mechanical similarity, and always contains several or at least one empirical constant. Nevertheless the theory has contributed much toward correlating the voluminous experimental data and also has yielded more than one new concept.

For the numerical treatment one divides the turbulent flow, unsteady in space and time, into mean values and fluctuation quantities. The mean value may a priori be formed with respect to either space or time. We prefer, however, the time average at a fixed point in space, and form such mean values of the velocity, pressure, shearing stress, etc. In forming the mean values one must not neglect to take them over a sufficiently long time interval T so that the mean value will be independent of T. Let the velocity vector with its three mutually perpendicular components be

$$*\underline{w} = i\underline{y} + j\underline{v} + k\underline{w} \tag{14.1}$$

For a turbulent flow the velocity components are therefore functions of the three space coordinates and the time:

$$\begin{aligned} u &= u\,(x,\ y,\ z,\ t) \\ v &= v\,(x,\ y,\ z,\ t) \\ w &= w\,(x,\ y,\ z,\ t) \end{aligned} \tag{14.2}$$

The time average for the component u, for instance, is formed as follows:

$$\overline{u}(x,\ y,\ z) = \frac{1}{T}\int_{t_o}^{t_o+T} u\ dt \tag{14.3}$$

*Throughout the text, underscored letters are used in place of corresponding German script letters used in the original text.

If $\overline{u}$, $\overline{v}$, $\overline{w}$ are independent of t_o and T, the motion is called steady on the average, or quasisteady. A steady turbulent flow, in the sense that the velocity at a point fixed in space is perfectly constant, does not exist. The velocity fluctuations are then defined by the equations

$$\left.\begin{aligned} u &= \overline{u} + u' \\ v &= \overline{v} + v' \\ w &= \overline{w} + w' \end{aligned}\right\} \qquad (14.4)$$

and in the same way for the pressure:

$$p = \overline{p} + p' \qquad (14.5)$$

The time average of the fluctuation quantities equals zero, according to definition, as the following consideration will show immediately:

$$\frac{1}{T}\int_{t_o}^{t_o+T} u'\,dt = \frac{1}{T}\int_{t_o}^{t_o+T} u\,dt - \frac{\overline{u}}{T}\int_{t_o}^{t_o+T} dt = \overline{u} - \overline{u} = 0 \qquad (14.6)$$

Thus:

$$\overline{u'} = \overline{v'} = \overline{w'} = 0 \qquad (14.7)$$

The Additional "Apparent" Turbulent Stresses

As a result of the velocity fluctuations additional stresses (= apparent friction) originate in the turbulent flow. This is readily illustrated for instance by the case of the simple shearing flow $\overline{u} = \overline{u}(y)$ (fig. 76). Here $\overline{v} = 0$; however, a fluctuation velocity v' in the transverse direction is present. The latter causes a momentum transfer between the adjoining layers across the main flow. This momentum transfer acts like an additional shearing stress τ. Whereas in laminar flow the friction is brought about by the molecular momentum exchange, the turbulent exchange of momentum is a macroscopic motion of, mostly, much stronger effect.

The equations of motion of the turbulent flow, with this turbulent apparent friction taken into consideration, can be obtained from the Navier–Stokes differential equations by substituting equation (14.4) into the latter and then forming the time averages in the Navier–Stokes differential equations. To that purpose the Navier–Stokes differential equations (3.16) are written in the form:

$$\left.\begin{aligned}
\rho\left\{\frac{\partial u}{\partial t}+\frac{\partial\left(u^2\right)}{\partial x}+\frac{\partial(uv)}{\partial y}+\frac{\partial(uw)}{\partial z}\right\} &= -\frac{\partial p}{\partial x}+\mu\left(\frac{\partial^2 u}{\partial x^2}+\frac{\partial^2 u}{\partial y^2}+\frac{\partial^2 u}{\partial z^2}\right)\\
\rho\left\{\frac{\partial v}{\partial t}+\frac{\partial(uv)}{\partial x}+\frac{\partial v^2}{\partial y}+\frac{\partial(vw)}{\partial z}\right\} &= -\frac{\partial p}{\partial y}+\mu\left(\frac{\partial^2 v}{\partial x^2}+\frac{\partial^2 v}{\partial y^2}+\frac{\partial^2 v}{\partial z^2}\right)\\
\rho\left\{\frac{\partial w}{\partial t}+\frac{\partial(wu)}{\partial x}+\frac{\partial(wv)}{\partial y}+\frac{\partial w^2}{\partial z}\right\} &= -\frac{\partial p}{\partial z}+\mu\left(\frac{\partial^2 w}{\partial x^2}+\frac{\partial^2 w}{\partial y^2}+\frac{\partial^2 w}{\partial z^2}\right)\\
\frac{\partial u}{\partial x}+\frac{\partial v}{\partial y}+\frac{\partial w}{\partial z} &= 0
\end{aligned}\right\} \qquad (14.8)$$

By introducing equations (14.4) and (14.5) and forming the time averages one first obtains from the continuity equation:

$$\frac{\partial \overline{u}}{\partial x}+\frac{\partial \overline{v}}{\partial y}+\frac{\partial \overline{w}}{\partial z}=0 \qquad (14.9)$$

and thus also:

$$\frac{\partial u'}{\partial x}+\frac{\partial v'}{\partial y}+\frac{\partial w'}{\partial z}=0 \qquad (14.10)$$

By introduction of equations (14.4) into the left side of equation (14.8) one obtains expressions as, for instance,

$$u^2=(\overline{u}+u')^2=\overline{u}^2+2\,\overline{u}\,u'+u'^2 \text{ etc.}$$

In the subsequent formation of the time average the squared terms in the barred quantities remain unchanged since they are already constant with respect to time. The mixed terms, as for instance $\overline{u}\,u'$, . . . and also the terms that are linear in the fluctuation quantities are eliminated in forming the average because of equation (14.7). However, the terms that are quadratic in the fluctuation quantities as $\overline{u'^2}$, $\overline{u'v'}$, . . . remain. Thus one obtains from the equation system (equation (14.8)), after forming the time average the following system of equations:

$$\left.\begin{aligned}
\rho\left(\bar{u}\frac{\partial\bar{u}}{\partial x}+\bar{v}\frac{\partial\bar{u}}{\partial y}+\bar{w}\frac{\partial\bar{u}}{\partial z}\right)&=-\frac{\partial\bar{p}}{\partial x}+\mu\Delta\bar{u}-\rho\left\{\frac{\partial\overline{u'^2}}{\partial x}+\frac{\partial\overline{u'v'}}{\partial y}+\frac{\partial\overline{u'w'}}{\partial z}\right\}\\
\rho\left(\bar{u}\frac{\partial\bar{v}}{\partial x}+\bar{v}\frac{\partial\bar{v}}{\partial y}+\bar{w}\frac{\partial\bar{v}}{\partial z}\right)&=-\frac{\partial\bar{p}}{\partial y}+\mu\Delta\bar{v}-\rho\left\{\frac{\partial\overline{u'v'}}{\partial x}+\frac{\partial\overline{v'^2}}{\partial y}+\frac{\partial\overline{u'w'}}{\partial z}\right\}\\
\rho\left(\bar{u}\frac{\partial\bar{w}}{\partial x}+\bar{v}\frac{\partial\bar{w}}{\partial y}+\bar{w}\frac{\partial\bar{w}}{\partial z}\right)&=-\frac{\partial\bar{p}}{\partial z}+\mu\Delta\bar{w}-\rho\left\{\frac{\partial\overline{u'w'}}{\partial x}+\frac{\partial\overline{u'w'}}{\partial y}+\frac{\partial\overline{w'^2}}{\partial z}\right\}
\end{aligned}\right\} \qquad (14.11)$$

The left side now formally agrees with the Navier–Stokes differential equations for steady flow if one writes instead of u, v, w the time averages of these quantities. On the right side additional terms which arise from the fluctuations have been added to the pressure and friction terms.

Remembering that in deriving the Navier–Stokes differential equations one could write the resultant surface force per unit volume by means of the components of a stress tensor according to equation (3.7) in the form

$$\left.\begin{aligned}
R = {}& i\left(\frac{\partial\sigma_x}{\partial x}+\frac{\partial\tau_{xy}}{\partial y}+\frac{\partial\tau_{xz}}{\partial z}\right)\\
&+ j\left(\frac{\partial\tau_{xy}}{\partial x}+\frac{\partial\sigma_y}{\partial y}+\frac{\partial\tau_{yz}}{\partial z}\right)\\
&+ \underline{k}\left(\frac{\partial\tau_{xz}}{\partial x}+\frac{\partial\tau_{yz}}{\partial y}+\frac{\partial\sigma_z}{\partial z}\right)
\end{aligned}\right\} \qquad (14.12)$$

one recognizes by comparison with (equation (14.11)) that one may introduce for the quantities added by the fluctuation motion a symmetrical stress tensor in the following manner:

$$\left.\begin{aligned}
\sigma_x &= -\rho\overline{u'^2} & \tau_{xy} &= -\rho\overline{u'v'} & \tau_{xz} &= -\rho\overline{u'w'}\\
\tau_{xy} &= -\rho\overline{u'v'} & \sigma_y &= -\rho\overline{v'^2} & \tau_{yz} &= -\rho\overline{v'w'}\\
\tau_{xz} &= -\rho\overline{u'w'} & \tau_{yz} &= -\rho\overline{v'w'} & \sigma_z &= -\rho\overline{w'^2}
\end{aligned}\right\} \qquad (14.13)$$

One has therefore, for the mean values of the quasisteady flow, the following equations of motion:

$$\left.\begin{aligned}
\rho\left(\bar{u}\frac{\partial\bar{u}}{\partial x}+\bar{v}\frac{\partial\bar{u}}{\partial y}+\bar{w}\frac{\partial\bar{u}}{\partial z}\right)&=-\frac{\partial\bar{p}}{\partial x}+\mu\Delta\bar{u}+\frac{\partial\sigma_x}{\partial x}+\frac{\partial\tau_{xy}}{\partial y}+\frac{\partial\tau_{xz}}{\partial z}\\
\rho\left(\bar{u}\frac{\partial\bar{v}}{\partial x}+\bar{v}\frac{\partial\bar{v}}{\partial y}+\bar{w}\frac{\partial\bar{v}}{\partial z}\right)&=-\frac{\partial\bar{p}}{\partial y}+\mu\Delta\bar{v}+\frac{\partial\tau_{xy}}{\partial x}+\frac{\partial\sigma_y}{\partial y}+\frac{\partial\tau_{yz}}{\partial z}\\
\rho\left(\bar{u}\frac{\partial\bar{w}}{\partial x}+\bar{v}\frac{\partial\bar{w}}{\partial y}+\bar{w}\frac{\partial\bar{w}}{\partial z}\right)&=-\frac{\partial\bar{p}}{\partial z}+\mu\Delta\bar{w}+\frac{\partial\tau_{xz}}{\partial x}+\frac{\partial\tau_{yz}}{\partial y}+\frac{\partial\sigma_z}{\partial z}
\end{aligned}\right\} \quad (14.14)$$

The continuity equation (equation (14.9)) also enters. The boundary conditions are the same as for laminar flow: adhering of the fluid to the wall, that is, on the solid walls all velocity components equal zero. According to equation (14.14) the mean values of the turbulent flow obey the same equations of motion as the velocity components of a laminar flow, with the friction forces, however, increased by the apparent stresses of the turbulent fluctuation motion. But since the fluctuation velocities u', v', . . . and particularly their space distribution are unknown, equations (14.14) and (14.13) are, at first, rather useless for the calculation of a turbulent flow.

Only when one will have succeeded in expressing the fluctuation quantities $\overline{u'^2}$, $\overline{u'v'}$, . . . in a suitable manner by the time averages $\bar{u}$, $\bar{v}$, . . ., will it be possible to use equations (14.14) to calculate, in particular, the mean values $\bar{u}$, $\bar{v}$, $\bar{w}$.

A first expression of this kind which brought however little success was originated by Boussinesq (reference 64). He introduced, aside from the ordinary viscosity coefficient, a new viscosity coefficient of the apparent turbulent friction. In analogy to the stress tensor for laminar flow which is, according to equation (3.13):

$$\begin{vmatrix}\sigma_x & \tau_{xy} & \tau_{xz}\\ \tau_{xy} & \sigma_y & \tau_{yz}\\ \tau_{xz} & \tau_{yz} & \sigma_z\end{vmatrix} = -\begin{vmatrix}p & 0 & 0\\ 0 & p & 0\\ 0 & 0 & p\end{vmatrix} + \mu\begin{vmatrix}\frac{\partial u}{\partial x} & \frac{\partial u}{\partial y} & \frac{\partial u}{\partial z}\\ \frac{\partial v}{\partial x} & \frac{\partial v}{\partial y} & \frac{\partial v}{\partial z}\\ \frac{\partial w}{\partial x} & \frac{\partial w}{\partial y} & \frac{\partial w}{\partial z}\end{vmatrix} + \mu\begin{vmatrix}\frac{\partial u}{\partial x} & \frac{\partial v}{\partial x} & \frac{\partial w}{\partial x}\\ \frac{\partial u}{\partial y} & \frac{\partial v}{\partial y} & \frac{\partial w}{\partial y}\\ \frac{\partial u}{\partial z} & \frac{\partial v}{\partial z} & \frac{\partial w}{\partial z}\end{vmatrix} \quad (14.15)$$

Boussinesq puts for the apparent turbulent friction:

$$\sigma_x = 2\rho\,\epsilon\,\frac{\partial\bar{u}}{\partial x} \qquad \tau_{xy} = \rho\,\epsilon\left(\frac{\partial\bar{u}}{\partial y}+\frac{\partial\bar{v}}{\partial z}\right) \quad . \quad . \quad . \quad (14.16)$$

Then there corresponds to the laminar viscosity coefficient μ the mixing factor $\rho\epsilon$:

$$\mu \sim \rho \epsilon \quad \text{or} \quad \nu \sim \epsilon$$

The kinematic viscosity of the turbulent flow (apparent friction) is usually very much larger than that for the ordinary laminar friction. (Hundred- or thousandfold or more). In general, one may therefore altogether neglect the ordinary viscosity terms $\mu\Delta\overline{u}$, . . . in equation (14.14). Only at the solid walls where due to the no-slip condition

$$\overline{u} = \overline{v} = \overline{w} = 0 \quad \text{as well as} \quad u' = v' = w' = 0$$

the apparent turbulent friction disappears, does the laminar friction again become dominant. Thus there exists in every turbulent friction layer in the immediate neighborhood of the wall a very narrow zone where the flow is laminar. The thickness of this laminar sublayer is only a small fraction of the turbulent boundary layer thickness.

One can easily understand from the example of the simple shear flow according to figure 76 that in a turbulent flow the mean value $\overline{u'v'}$ is different from zero. For this case, a correlation exists between the fluctuation velocities u' and v' in the following manner: The particles with negative v' have "mostly" a positive u', since they come from a region of larger mean velocity $\overline{u}$.* The parts with positive v', on the other hand, have "mostly" a negative u', because they come from a region with smaller $\overline{u}$, and retain in the transverse motion approximately the x-momentum of the layer from which they come. Thus, "mostly" $u'v' < 0$ and, therefore, the time average $\overline{u'v'} < 0$. Therefore, the shearing stress is this flow is:

$$\tau_{xy} = -\rho\,\overline{u'v'} > 0$$

In measuring turbulent flows one usually measures only the mean values $\overline{u}$, $\overline{v}$, . . . since only they are of practical interest. However, in order to obtain deeper insight into the mechanism of the turbulent flow, the fluctuation quantities have recently been measured and also their mean squares and products:

$$\sqrt{\overline{u'^2}} \qquad \sqrt{\overline{v'^2}} \qquad \sqrt{\overline{u'v'}}$$

According to measurements by Reichardt (reference 65) in a rectangular tunnel (width 1 millimeter, height 24 centimeters) the maximum value

---

*"Mostly" is to indicate that particles with different signs, though not excluded, are in the minority.

of $\sqrt{\overline{u'^2}}$, for instance, equals $0.13\,\overline{u}_{max}$, the maximum value of $\sqrt{\overline{v'^2}}$ equals $0.05\,\overline{u}_{max}$. Both maxima lie in the neighborhood of the wall. One may say, therefore, that in this case the turbulence is strongest near the wall.

In a flow that is homogeneous (wind tunnel), turbulent fluctuations are also always present to a varying degree. They determine the so-called degree of turbulence of a wind tunnel. Since the measurement of the fluctuation quantities is rather difficult (hot-wire method), a more convenient measuring method has been chosen, for the present, for determination of the degree of turbulence of a wind tunnel: namely, the determination of the critical Reynolds number for the sphere from force measurements or pressure distribution measurements. One defines as critical Reynolds number the one where the drag coefficient $c_w = 0.3$. It becomes clear that a unique connection exists between the critical Reynolds number and the turbulent fluctuation velocity in the sense that the critical Reynolds number of the sphere is the lower, the higher the turbulent fluctuation velocity. According to American measurements (reference 97) the connection between the longitudinal fluctuation and the measured critical Reynolds number for the sphere is as shown in the following table:

$\sqrt{\overline{u'^2}}/u$	0.004	0.0075	0.012	0.017	0.026
$Re_{crit}\ 10^{-5}$	2.8	2.4	2.0	1.6	1.2

In addition to the apparent increase of viscosity, the turbulent fluctuation motion has other effects: It tends to even out any temperature differences or variations in concentration existing in a flow. The diffusion of heat, for instance, is much larger than for laminar flow, because of the exchange motions which are much stronger in turbulent flow. A close connnection therefore exists, for instance, between the laws of flow and of heat transfer from a heated body to the fluid flowing by.

Ninth Lecture (February 2, 1942)

CHAPTER XV. MORE RECENT THEORIES; MIXING LENGTH

In order to make possible a quantitative calculation of turbulent flows, it is necessary to transform the expressions for the apparent turbulent stresses (equation (14.13)) in such a manner that they no longer contain the unknown fluctuation velocities but contain the components of the mean velocities. Consider, for that purpose, a particularly simple

flow, namely a plane flow which has the same direction everywhere and a velocity varying only on the different stream lines. The main-flow direction coincides with the x-direction; then:

$$\bar{u} = \bar{u}(y) \qquad \bar{v} = 0 \qquad \bar{w} = 0 \tag{15.1}$$

Of the shearing stresses, only the component $\tau_{x,y} = \tau$ is present, for which from equation (14.13) as well as from Boussinesq's equation, equation (14.15), there results:

$$\tau = -\rho \overline{u'v'} = \rho \epsilon \frac{d\bar{u}}{dy} \tag{15.2}$$

This formula shows that $|\tau|/\rho$ equals the square of a velocity. One puts, therefore, for use in later calculations,

$$v_* = \sqrt{\frac{|\tau|}{\rho}} = \sqrt{\left|\overline{u'v'}\right|} \tag{15.3}$$

and denotes v_* as shearing stress velocity. Thus this shearing stress velocity is a measure of the momentum transfer by the turbulent fluctuation motion.

According to Prandtl (reference 66), one may picture the turbulent flow mechanism, particularly turbulent mixing, in the following simplified manner: Fluid particles, each possessing a particular motion, originate in the turbulent flow; they move for a certain distance as coherent masses maintaining their velocity (momentum). One now assumes that such a fluid particle which originates in the layer $(y_1 - l)$ and has the velocity $\bar{u}(y_1 - l)$ moves a distance l = mixing length normal to the flow (fig. 77). If this fluid particle maintains its original velocity in the x-direction it will have, in its new location y_1, a smaller velocity than its new surroundings, the velocity difference being

$$-u_1' = \bar{u}(y_1) - \bar{u}(y_1 - l) \quad \text{with} \quad v' > 0$$

Likewise a fluid particle coming from the layer $(y_1 + l)$ to y_1 has at the new location a greater velocity than the surroundings there; the difference is

$$u_2' = \bar{u}(y_1 + l) - \bar{u}(y_1) \quad \text{with} \quad v' < 0$$

u_1' and u_2' give the turbulent velocity fluctuation in the layer y_1. One obtains for the mean value of this velocity fluctuation

$$\overline{|u'|} = \frac{1}{2}\left(|u_1'| + |u_2'|\right) = l\left|\left(\frac{d\bar{u}}{dy}\right)_1\right| \tag{15.4}$$

From this equation one obtains the following physical interpretation for the mixing length l:

The mixing length signifies the distance in the transverse direction which a fluid particle must travel at the mean velocity of its original layer so that the difference between its velocity and the velocity of the new location equals the mean velocity fluctuation of the turbulent flow. It is left open whether the fluid particles in their transverse motion fully maintain the velocity of their original layer, or whether they have partly assumed the velocity of the traverse layer and then travelled larger distances in the transverse direction. The Prandtl mixing length which is thereby introduced has a certain analogy to the mean free path of the kinetic theory of gases, with, however, the difference that there one deals with microscopic motions of the molecules, here with macroscopic motions of larger fluid particles.

One may picture the origin of the transverse fluctuation velocity v' in the following way:

Two fluid particles flowing from the layers $(y_1 + l)$ and $(y_1 - l)$ meet in the layer y_1 in such a manner that one lies behind the other: the faster $(y_1 + l)$ behind the slower $(y_1 - l)$. They then collide with the velocity $2u'$ and giveway laterally. Thereby originates the transverse velocity v', directed away from the layer y_1 to both sides. If, conversely, the slower of the two particles is behind the faster, they withdraw from each other with the velocity $2u'$. In this case the space formed between them is filled up out of the surroundings. Thus originates a transverse velocity v' directed toward the layer y_1. One concludes from this consideration that v' and u' are of the same order of magnitude and puts

$$\overline{|v'|} = \text{number} \quad \overline{|u'|} = \text{number} \quad l\frac{d\bar{u}}{dy} \tag{15.5}$$

In order to express the shearing stress according to equation (15.2) one has to consider the mean value $\overline{u'v'}$ more closely. The following conclusions can be drawn from the previous considerations.

The particles arriving in the layer y_1 with positive v' (from below, fig. 77) have "mostly" a negative u' so that $u'v'$ is negative. For the particles arriving with negative v', u' is "mostly" positive, so that $u'v'$ is again negative. "Mostly" signifies that particles with different sign are not wholly excluded, but are strongly outnumbered. The mean value $\overline{u'v'}$ is therefore different from zero and negative. Thus one puts

$$\overline{u'v'} = - k \, \overline{|u'|} \, \overline{|v'|} \tag{15.6}$$

with $k \neq 0$; $0 < k < 1$. The numerical factor k, also called the correlation coefficient is not known more closely. According to equation (15.5) and (15.4) one now obtains

$$\overline{u'v'} = - \text{number} \quad l^2 \left(\frac{d\bar{u}}{dy}\right)^2 \tag{15.7}$$

the "number" in this equation being different from the one in equation (15.5). If one includes the "number" in the unknown mixing length, one can also write

$$\overline{u'v'} = - l^2 \left(\frac{d\bar{u}}{dy}\right)^2 \tag{15.8}$$

and thus finally obtains for the turbulent shearing stress according to equation (15.2)

$$\tau = \rho \, l^2 \left(\frac{d\bar{u}}{dy}\right)^2$$

Considering that the sign of τ also must change with the sign of $\frac{d\bar{u}}{dy}$ it is more correct to write

$$\boxed{\tau = \rho \, l^2 \left| \frac{d\bar{u}}{dy} \right| \frac{d\bar{u}}{dy} \qquad \text{Prandtl's formula}} \tag{15.9}$$

This is the famous Prandtl mixing length formula which has been very successful for the calculation of turbulent flows.

If one compares this formula (equation (15.9)) with the equations of Boussinesq where one had put $\tau = \epsilon \frac{d\bar{u}}{dy}$ (ϵ = mixing factor = turbulent analogue of the laminar viscosity μ), one has for the mixing factor

$$\epsilon = \rho l^2 \left| \frac{d\bar{u}}{dy} \right| \tag{15.10}$$

The turbulent mixing factor ϵ is in most cases larger than the laminar viscosity μ by several powers of ten. Moreover the mixing factor ϵ is dependent on the velocity and on the location and tends toward zero near a wall, because there the mixing length goes toward zero.

If one compares Prandtl's formula equation (15.9) with Boussinesq's equation (15.2) one could perhaps think at first that not much has been gained, since the unknown quantity ϵ (= apparent viscosity) has been replaced by the new unknown l = mixing length. Nevertheless Prandtl's formula is considerably better than the old formula for the following reason: It is known from tests that the drag for turbulent flow is proportional to the square of the velocity. According to equation (15.9) one obtains this square law for drag by assuming the mixing length to be independent of the velocity, that is, by assuming the mixing length to be purely a function of position. It is considerably easier to make a plausible assumption for the length l = mixing length than for the apparent turbulent viscosity ϵ, and therein lies the considerable superiority of Prandtl's formula equation (15.9) over Boussinesq's equation (15.2).

In many cases the length l can be brought into a simple relation to the characteristic lengths of the respective flows. For the flow along a smooth wall l must, at the wall itself, equal zero, since all transverse motions are prevented at the wall. For the flow along a rough wall, however, the limiting value of l at the wall equals a length of the order of magnitude of the height of the roughness.

It would be very useful to have a formula permitting the determination of the dependence of the mixing length on the position for any arbitrary flow. Such an attempt has been made by v. Karman (reference 68). v. Karman makes the assumption that the inner mechanism of the turbulent flow is such that the motion at various points differs only with respect to time- and length-scale, but is otherwise similar (similarity hypothesis). Instead of the units of time and length one may select those of velocity and length. The velocity unit that is important for the turbulent motion is the shearing stress velocity v_* according to equation (15.3). The corresponding unit of length is the mixing length l.

In order to find the quantity l from the data of the basic flow $\bar{u}(y)$, v. Karman applies the Taylor development* for $u(y)$ in the neighborhood of the point y_1.

$$u(y) = u(y_1) + (y - y_1)\left(\frac{du}{dy}\right)_1 + \frac{1}{2!}(y - y_1)^2\left(\frac{d^2u}{dy^2}\right)_1 + \ldots\ldots \tag{15.11}$$

---

* In the following, the bar over the mean velocity will be omitted, for simplification.

The length l cannot depend on the velocity $u(y_1)$, since according to Newton's principle of relativity the addition of a constant velocity has no influence on the course of motion. Thus

$$\left(\frac{du}{dy}\right)_1 \qquad \left(\frac{d^2u}{dy^2}\right)_1$$

and the higher derivatives remain as characteristic data of the basic flow. The simplest length to be formed from it is

$$\frac{du}{dy} \Bigg/ \frac{d^2u}{dy^2}$$

v. Karman puts therefore

$$l = \kappa_1 \left| \frac{du}{dy} \Bigg/ \frac{d^2u}{dy^2} \right| \tag{15.12}$$

According to this formula l is not dependent on the amount of velocity but only on the velocity distribution. Thus l is a pure position function as required above. In equation (15.12) κ_1 is an empirical constant which must be determined from the experiment. To arrive further at the turbulent shearing stress, v. Karman also maintains Prandtl's equation (15.9).

In generalizing equation (15.9) one obtains, according to Prandtl, the complete expression for the turbulent stress tensor of a plane flow in the form

$$\begin{pmatrix} \sigma_x & \tau_{xy} \\ \tau_{xy} & \sigma_y \end{pmatrix} = \rho l^2 \left|\frac{du}{dy}\right| \begin{pmatrix} 2\frac{\partial u}{\partial x} & \frac{\partial u}{\partial y} + \frac{\partial v}{\partial x} \\ \frac{\partial u}{\partial y} + \frac{\partial v}{\partial x} & 2\frac{\partial v}{\partial y} \end{pmatrix} \tag{15.13}$$

The common factor on the right side signifies the turbulent mixing factor according to equation (15.10).

Tenth Lecture (February 9, 1942)

Flow Along a Smooth Wall

We will immediately make a first application of Prandtl's formula (equation (15.9)) for the flow along a smooth wall. The normal distance from the wall is denoted as y. Let the wall coincide with the x-axis. For the velocity distribution then, $u = u(y)$. For this case one sets the mixing length in the neighborhood of the wall proportional to the distance from the wall

$$l = \kappa y \tag{15.14}$$

the constant κ must be determined from the experiment. Moreover one makes the assumption that the shearing stress τ is constant in the entire flow region; then the shearing stress velocity v_* according to equation (15.3) also is constant. If one further neglects the laminar friction, one obtains from equations (15.2), (15.9), (15.14)

$$v_*^2 = \kappa^2 y^2 \left(\frac{du}{dy}\right)^2$$

or

$$\frac{du}{dy} = \frac{v_*}{\kappa y}$$

and by integration

$$u = \frac{v_*}{\kappa} \ln y + \text{constant} \tag{15.15}$$

In determining the constant of integration one must pay attention to the fact that the turbulent law equation (15.9) does not apply right up to the wall but that very near to the wall an extremely thin laminar layer is present. From the laminar viscosity μ and the turbulent shearing stress velocity v_* one can form the length ν/v_*. The constant of integration in equation (15.15) is determined from the condition that $u = 0$ for $y = y_0$. Thus there results, according to equation (15.15)

$$u = \frac{v_*}{\kappa} (\ln y - \ln y_0) \tag{15.16}$$

The as yet unknown distance from the wall y_0 is set proportional to the length ν/v_*, thus

$$y_o = \beta \frac{\nu}{v_*} \tag{15.17}$$

where β signifies a dimensionless constant. Thus one finally obtains for the velocity distribution at the smooth wall

$$u = \frac{v_*}{\kappa} \left(\ln \frac{y v_*}{\nu} - \ln \beta \right) \tag{15.18}$$

that is, a logarithmic velocity distribution law. It contains two empirical constants κ and β. According to measurements $\kappa = 0.4$. From equation (15.18) one can see that the dimensionless velocity $u/v_* = \varphi$ can be represented as a function of the dimensionless distance from the wall $\eta = v_* y/\nu$. The latter is a sort of Reynolds number, formed with the distance from the wall y and the shearing stress velocity v_*. Thus one obtains for larger Reynolds numbers from equation (15.18) the following universal velocity distribution law

$$\varphi(\eta) = A \ln \eta + B \tag{15.19}$$

with $A = 1/\kappa = 2.5$. For smaller Reynolds numbers, where the laminar friction also has a certain influence, tests gave the velocity distribution law

$$\varphi(\eta) = C \eta^n \tag{15.20}$$

or

$$\frac{u}{v_*} = C \left(\frac{y v_*}{\nu} \right)^n \tag{15.20a}$$

with the exponent n equalling about $1/7$. These universal velocity distribution laws according to measurements for pipe flow are given in figure 78. They will be discussed in more detail in the following chapter.

CHAPTER XVI. PIPE FLOW

a. The Smooth Pipe

Among the various turbulent flows of practical importance, pipe flow was investigated with particular thoroughness because of its great practical importance. We shall therefore consider the pipe flow first. It will be noted at this point that the flow laws of the pipe flow may be applied to other cases, as for instance the plane plate in longitudinal flow. Consider a straight pipe of circular cross section and with a smooth wall. Let y be the radial coordinate measured from the pipe axis. The

balance of forces between the shearing stress τ and the pressure drop $p_1 - p_2$ on a piece of pipe of length L yields as before for the laminar flow according to equation (2.1a), the relation:

$$\tau = \frac{p_1 - p_2}{L} \frac{y}{2} \tag{16.1}$$

This formula applies equally to laminar and turbulent flow. In it τ now signifies the sum of the laminar shearing stresses and of the apparent turbulent shearing stresses. Over a cross section, τ is proportional to y. The shearing stress at the wall τ_o may be determined experimentally by measurement of the pressure drop:

$$\tau_o = \frac{p_1 - p_2}{L} \frac{r}{2} \tag{16.2}$$

For the turbulent flow the connection between pressure drop and flow volume $Q = \pi r^2 \bar{u}$ must be obtained from tests.* In the literature there exists a very great number of pipe resistance formulas. Only those serve our purpose which satisfy Reynolds' law of similarity. One of them is the formula of H. Blasius (reference 69), set up particularly carefully, which is valid for a smooth wall and for Reynolds numbers $Re = \bar{u}d/\nu \leq 100\,000$.

If one introduces, as before in equation (2.6), the dimensionless pipe resistance coefficient λ by the equation

$$\frac{p_1 - p_2}{L} = \frac{\lambda}{d} \frac{\rho}{2} \bar{u}^2 \tag{16.3}$$

λ is, according to Blasius:

$$\lambda = 0.3164 \left(\frac{\bar{u}\, d}{\nu}\right)^{-1/4} \tag{16.4}$$

Comparing equations (16.2) and (16.3) one finds:

$$\tau_o = \frac{\lambda}{8} \rho \bar{u}^2 \tag{16.5}$$

and therefore according to equation (16.4):

$$\tau_o = 0.03955\ \rho\, \bar{u}^{7/4}\, \nu^{1/4}\, d^{-1/4} \tag{16.6}$$

---

*In the following, $\bar{u}$ is, for the pipe flow, the mean flow velocity at the cross section, as distinguished from the time average in the previous sections.

If one introduces, moreover, instead of the diameter d the radius r, the numerical factor in this linear equation must be divided by $2^{1/4} = 1.19$. Thus τ_o becomes:

$$\tau_o = 0.03325\ \rho\ \bar{u}^{7/4}\ \nu^{1/4}\ r^{-1/4} = \rho\ v_*^2 \qquad (16.7)$$

where the shearing stress velocity is defined by the wall shearing stress:

$$v_* = \sqrt{\frac{\tau_o}{\rho}} \qquad (16.8)$$

If one finally factors the quantity v_*^2 in equation (16.7) into $v_*^{7/4} \times v_*^{1/4}$, one obtains:

$$\left(\frac{\bar{u}}{v_*}\right)^{7/4} = \frac{1}{0.03325}\left(\frac{v_* r}{\nu}\right)^{1/4} \text{ or } \frac{\bar{u}}{v_*} = 6.99\left(\frac{v_* r}{\nu}\right)^{1/7} \qquad (16.9)$$

This equation is very similar to equation (15.20a); however, the mean velocity now takes the place of the local velocity and the pipe radius takes the place of the distance from the wall. One passes first from the mean velocity to the maximum velocity u_1; based on measurements of Nikuradse (reference 70) $\bar{u} = 0.8\ u_1$, and therewith follows from equation (16.9):

$$\frac{u_1}{v_*} = 8.74\left(\frac{v_* r}{\nu}\right)^{1/7}$$

If this formula is assumed to be valid for any distance from the wall, one obtains:

$$\frac{u}{v_*} = 8.74\left(\frac{v_* y}{\nu}\right)^{1/7} \qquad (16.10)$$

or

$$\varphi = 8.74\ \eta^{1/7} \qquad (16.11)$$

This is the so-called 1/7-power law for the velocity distribution; its form was already given in equation (15.20a). The coefficients n and η_b

still unknown there, have now been determined on the basis of the resistance law of the pipe flow. Figure 78 shows, according to measurements of Nikuradse (reference 70) that this law is well satisfied in the range of Reynolds numbers up to 100,000. Naturally this law of velocity distribution can apply only to the region of Reynolds numbers where the pipe resistance law given by equation (16.4) is valid, since it was derived from this law.

For purposes of later calculations we shall derive from equation (16.10) the shearing stress velocity v_*. One obtains:

$$v_* = 0.150\, u^{7/8}\left(\frac{\nu}{y}\right)^{1/8} \tag{16.12}$$

with $8.74^{7/8} = 6.65$ and $\frac{1}{6.65} = 0.150$. From equation (16.12) follows:

$$\tau_o = \rho\, v_*^2 = 0.0225\rho u^{7/4}\left(\frac{\nu}{y}\right)^{1/4} \tag{16.13}$$

This relation will be needed later.

Comparing measured velocity distributions with equation (16.10) one can state that outside of the range of validity of equation (16.10), namely for $Re > 100{,}000$, a better approximation is obtained by the power 1/8, 1/9, or 1/10 instead of 1/7. The measurements concerning the pipe resistance (fig. 81) show an upward deviation from the formula of Blasius for larger Reynolds numbers.

The logarithmic velocity distribution law, equation (15.19), derived in the previous chapter has been verified by Nikuradse (reference 70) on the basis of his measurements for the smooth pipe. For this purpose from the measured pressure drop for each velocity profile one first determines the wall shearing stress according to equation (16.2) and from that, according to equation (16.8), the shearing stress velocity $v_* = \sqrt{\tau_o/\rho}$. Then the dimensionless velocity $\varphi = u/v_*$ can be plotted against the dimensionless distance from the wall $\eta = yv_*/\nu$. The measurements of Nikuradse in a very large range of Reynolds numbers, $Re = 4 \times 10^3$ up to 3240×10^3, lie very accurately on a straight line if one plots φ against $\log \eta$ (fig. 78). The straight line has the equation:

$$\boxed{\varphi = 2.5 \ln \eta + 5.5} \tag{16.14}$$

This gives, by comparison with equation (15.18), the following numerical values for the coefficients κ and β

$$\kappa = 0.400 \qquad \beta = 0.111 \tag{16.15}$$

Mixing Length

From the measured velocity distribution and the measured pressure drop the distribution of the mixing length over the pipe cross section can be determined according to equations (16.2), (16.1), and (15.9). $\tau = \tau_o \frac{y}{r}$ (y = distance from the pipe axis). This determination of the mixing length from the measurements in the pipe was made by Nikuradse (reference 70). For large Reynolds numbers, where the influence of viscosity is negligible, one obtains a distribution of the mixing length l/r over y/r which is independent of the Re-number (fig. 79). The following interpolation formula can be given for this distribution:

$$\frac{l}{r} = 0.14 - 0.08\left(1 - \frac{y}{r}\right)^2 - 0.06\left(1 - \frac{y}{r}\right)^4 \tag{16.16}$$

In this equation y signifies the distance from the wall. The development of equation (16.16) for small y/r (neighborhood of the wall) gives

$$l = 0.4y - 0.44\frac{y^2}{r} + \cdots \tag{16.16a}$$

In the neighborhood of the wall the mixing length is, therefore, proportional to the distance from the wall. Equation (16.16) for the distribution of the mixing length applies not only to the smooth pipe, but, according to the measurements of Nikuradse (reference 71) also to the rough pipe, as can be seen from figure 79. From this fact one can derive in a very simple manner a universal form for the law of velocity distribution, valid for the smooth as well as for the rough pipe. One puts for the mixing length distribution: $l = \kappa y\, f\left(\frac{y}{r}\right)$ with $f\left(\frac{y}{r}\right) \to 1$ for $\frac{y}{r} \to 0$. Furthermore follows from the linear distribution of the shearing stress over the cross section:

$$\tau = \tau_o\left(1 - \frac{y}{r}\right) \quad (y = \text{distance from the wall})$$

together with equation (15.9)

$$\frac{du}{dy} = \frac{1}{l}\sqrt{\frac{\tau}{\rho}} = \frac{v_*}{\kappa}\frac{\sqrt{1 - \frac{y}{r}}}{y f(y/r)} \tag{16.17}$$

and hence by integration:

$$u = \frac{v_*}{\kappa} \int_{y_o/r}^{y/r} \frac{\sqrt{1 - \frac{y}{r}}\, d\,\frac{y}{r}}{\frac{y}{r} f\left(\frac{y}{r}\right)} \tag{16.18}$$

the lower limit of intergration y_o where the velocity equals zero is, according to the considerations of the previous section, proportional to ν/v_*; thus: $y_o/r = F_1\left(\frac{v_* r}{\nu}\right)$. From equation (16.18) follows:

$$u_{max} = \frac{v_*}{\kappa} \int_{y_o/r}^{1} \frac{\sqrt{1 - y/r}\, d\, y/r}{\frac{y}{r} f\left(\frac{y}{r}\right)} \tag{16.18a}$$

and therefore, from equations (16.18) and (16.18a):

$$\boxed{u_{max} - u = v_* F\,(y/r)} \tag{16.19}$$

This law, with the same function $F(y/r)$, applies equally to smooth and rough pipes. It states that the curves of the velocity distribution over the pipe cross section for all Reynolds numbers and all roughnesses can be made congruent by shifting along the velocity axis, if one plots $u_{max} - u/v_*$ against y/r (fig. 80). The explicit expression for the function $F(y/r)$ is obtained immediately from equation (16.14), according to which

$$u_{max} - u = 2.5 v_* \ln \frac{r}{y} = 5.75\, v_* \log \frac{r}{y} \tag{16.20}$$

Universal Resistance Law

According to their derivation the velocity-distribution-law (equations (16.19) and (16.20)) are to be regarded as valid for arbitrary Reynolds number since the laminar viscosity was neglected as compared with the turbulent viscosity. We shall now derive from the velocity-distribution-law equation (16.20) a resistance law which, in contrast to Blasius', applies up to Reynolds numbers of arbitrary magnitude.

From equation (16.20) one may determine by integration over the cross section the mean flow velocity $\overline{u}$. One finds:

$$\overline{u} = u_{max} - 3.75\ v_* \tag{16.21}$$

The test results of Nikuradse (reference 70) gave a number slightly different from 3.75, namely:

$$\overline{u} = u_{max} - 4.07\ v_* \tag{16.22}$$

According to equation (16.5):

$$\lambda = 8\left(\frac{v_*}{u}\right)^2 \tag{16.23}$$

From the universal velocity distribution law of the smooth pipe equation (16.14) follows:

$$u_{max} = v_*\left\{2.5\ \ln\frac{rv_*}{\nu} + 5.5\right\}$$

and hence the connection with equation (16.21):

$$\overline{u} = v_*\left\{2.5\ \ln\frac{rv_*}{\nu} + 1.75\right\} \tag{16.24}$$

The Reynolds number enters into the calculation by means of the identity:

$$\frac{rv_*}{\nu} = \frac{1}{2}\frac{\overline{u}d}{\nu}\frac{v^*}{\overline{u}} = \frac{\overline{u}d}{\nu}\frac{\sqrt{\lambda}}{4\sqrt{2}}$$

Thus results from equations (16.23) and (16.24):

$$\lambda = \frac{8}{\left\{2.5\ \ln\left(\frac{\overline{u}d}{\nu}\sqrt{\lambda}\right) - 2.5\ \ln 4\sqrt{2} + 1.75\right\}^2}$$

$$= \frac{1}{\left\{2.035\ \log\left(\frac{ud}{\nu}\sqrt{\lambda}\right) - 0.91\right\}^2}$$

or:

$$\frac{1}{\sqrt{\lambda}} = 2.035 \log\left(\frac{\bar{u}d}{\nu}\sqrt{\lambda}\right) - 0.91 \qquad (16.25)$$

Accordingly a straight line must result for the resistance law of the smooth pipe, if one plots $1/\sqrt{\lambda}$ against $\log\left(\frac{\bar{u}d}{\nu}\sqrt{\lambda}\right)$. This is very well confirmed by Nikuradse's measurement (fig. 81). The numerical values according to the measurements differ only slightly from those of this theoretical derivation. From Nikuradse's measurements was found:

$$\boxed{\frac{1}{\sqrt{\lambda}} = 2.0 \log\left(\frac{\bar{u}d}{\nu}\sqrt{\lambda}\right) - 0.8} \qquad (16.26)$$

Universal Resistance Law For Smooth Pipes

This is the final resistance law for smooth pipes. On the basis of its derivation it may be extrapolated up to Reynolds numbers of arbitrary magnitude. Thus measurements for larger Reynolds numbers than those of Nikuradse's tests are not required. Up to Re = 100,000 this universal resistance law is in good agreement with the Blasius law according to equation (16.4). For higher Reynolds numbers the Blasius law deviates considerably from the measurements (fig. 81).

Concerning the determination of λ from equation (16.26), where it appears on both sides, it should be added that it can be easily obtained by successive approximation.

Eleventh Lecture (February 16, 1942)

b. The Rough Pipe

The characteristic parameter for the flow along a rough wall is the ratio of grain size k of the roughness to the boundary layer thickness, particularly to the thickness of the laminar sublayer δ_l which is always present within the turbulent friction layer in the immediate neighborhood of the wall. The thickness of the laminar sublayer is δ_l = number $\frac{\nu}{v*}$. The effectiveness of roughness of a certain grain size depends, therefore, on the dimensionless roughness coefficient $k/\delta_l \sim \frac{kv*}{\nu}$

In the experimental investigations of the resistance of turbulent flows over rough walls, the rough pipe has been studied very thoroughly since it is of great practical importance. Besides depending on the Reynolds number, the resistance of a rough pipe is a function of the relative roughness r/k. One distinguishes for the resistance law of a rough pipe three regions.

The subsequently given boundaries of these regions are valid for sand roughness k_s like those investigated by Nikuradse (reference 71).

1. Hydraulically smooth: The grain size of the roughness is so small that all roughnesses lie within the laminar sublayer. In this case the roughness has no drag increasing effect. This case exists for small Reynolds numbers and for values of the characteristic roughness number: $0 \leq \frac{v_* k_s}{\nu} \leq 5$.

2. Fully developed roughness flow: The grain size of the roughness is so large that all roughnesses project from the laminer sub-layer. The friction drag then consists predominantly of the form drag of the single roughness elements. A purely square drag law applies. For the pipe the resistance coefficient λ is then independent of Re and only dependent on the relative roughness k/r. This law exists for very large Reynolds numbers. For sand roughness this law applies for: $\frac{v_* k_s}{\nu} \geq 70$.

3. Intermediate region: Only a fraction of the roughness elements project from the laminar sublayer. The drag coefficient depends on r/k as well as on Re. This law exists for medium Reynolds numbers and, for the sand roughness, for: $5 \leq \frac{v_* k_s}{\nu} \leq 70$.

The dependence of the pipe resistance coefficient on the Reynolds number and on the relative roughness according to the measurements of Nikuradse (reference 71) can be seen from figure 82 as well as, in particular, the three laws just given.

The velocity distribution on a rough wall is given, basically, in the same way as for the smooth wall by equation (15.16). One has only to substitute for the constant of integration y_o another value: y_o proportional to the roughness grain size. One puts for sand roughness $y_o = \gamma k_s$ and hence obtains from equation (15.16)

$$\frac{u}{v_*} = \frac{1}{\kappa} \left\{ \ln \frac{y}{k_s} - \ln \gamma \right\} \tag{16.27}$$

The constant γ is, moreover, a function of the roughness form and the roughness distribution. Comparison with experiments of Nikuradse (reference 71) on pipes roughened artificially by sand yields for the velocity distribution the general formula:

$$u = v_* \left(2.5 \ln \frac{y}{k_s} + B \right) \tag{16.28}$$

the constant B being different in each domain described above; it depends on $v_* k_s/\nu$.

For the fully developed roughness flow B = 8.5, thus:

$$u = v_*\left(2.5 \ln \frac{y}{k_s} + 8.5\right) \text{(fully rough)} \tag{16.29}$$

whence follows:

$$u_{max} = v_*\left(2.5 \ln \frac{r}{k_s} + 8.5\right) \tag{16.30}$$

and:

$$u_{max} - u = v_* \, 2.5 \ln \frac{r}{y} \tag{16.30a}$$

in agreement with equation (16.20). Thus there applies also to rough pipes, as equation (16.21) did before to the smooth pipe, the relation:

$$\overline{u} = u_{max} - 3.75 \, v_* \tag{16.31}$$

From here one can, by a calculation which is perfectly analogous to the previous one for the smooth pipe, easily arrive at the resistance law of the rough pipe for fully developed roughness flow. By insertion of u_{max} according to equation (16.30) into equation (16.31) one obtains:

$$\overline{u} = v_*\left(2.5 \ln \frac{r}{k_s} + 4.75\right) \tag{16.32}$$

or:

$$\lambda = 8\left(\frac{v_*}{\overline{u}}\right)^2 = \frac{8}{\left(2.5 \ln \frac{r}{k_s} + 4.75\right)^2} \tag{16.33}$$

or:

$$\lambda = \frac{1}{\left(2.0 \log \frac{r}{k_s} + 1.68\right)^2} \tag{16.34}$$

This is the square resistance law of the fully developed roughness flow. Comparison with the test results of Nikuradse (fig. 83) shows that one obtains better agreement if one changes the number 1.68 to 1.74. Thus the resistance law of the pipe flow for fully developed roughness is:

$$\lambda = \frac{1}{\left(2.0 \log \frac{r}{k_s} + 1.74\right)^2} \tag{16.35}$$

In the plots of $\frac{1}{\sqrt{\lambda}}$ against $\log r/k_s$ (fig. 83) the test results fall very accurately on a straight line.

For flow along a rough wall in the intermediate region the constant B in equation (16.28) is, moreover, a function of the roughness coefficient $v_* k_s/\nu$. For this case also one can derive the resistance law immediately from the velocity distribution. According to equation (16.28):

$$B = \frac{u}{v_*} - 2.5 \ln \frac{y}{k_s} = \frac{u_{max}}{v_*} - 2.5 \ln \frac{r}{k_s} \tag{16.36}$$

On the other hand, according to equations (16.31) and (16.23):

$$\frac{u_{max}}{v_*} = \frac{u}{v_*} + 3.75 = \frac{2\sqrt{2}}{\sqrt{\lambda}} + 3.75 \tag{16.37}$$

so that one obtains from equation (16.36):

$$B\left(\frac{v_* k_s}{\nu}\right) = \frac{u}{v_*} - 2.5 \ln \frac{y}{k_s} = \frac{2\sqrt{2}}{\sqrt{\lambda}} - 2.5 \ln \frac{r}{k_s} + 3.75 \tag{16.38}$$

One can, therefore, determine the constant B as a function of $v_* k_s/\nu$ either from the velocity distribution or from the resistance law. The plot in figure 84 shows good agreement between the values determined by these two methods. At the same time the determination of the resistance law from the velocity distribution is confirmed.

The formula for B includes the case of the smooth pipe. B is, according to equation (16.14),

$$B = \frac{u}{v_*} - 2.5 \ln \frac{y}{k_s} = 2.5 \ln \frac{v_* k_s}{\nu} + 5.5 \qquad (16.39)$$

Thus a straight line results for B in the plot against $\log v_* k_s/\nu$.

Other Roughnesses

Because of the great practical importance of the roughness-problem a few data concerning roughnesses other than the special sand roughness will be given. Nikuradse's sand roughness may also be characterized by the fact that the roughness density was at its maximum value, because the wall was covered with sand as densely as possible. For many practical roughnesses the roughness density is considerably smaller. In such cases the drag then depends, for one thing, on form and height of the roughness, and, moreover, on the roughness density. It is useful to classify any arbitrary roughness in the scale of a standard roughness. Nikuradse's sand roughness suggests itself as roughness reference (roughness scale) because it was investigated for a very large range of Reynolds numbers and relative roughnesses. Classification with respect to the roughness scale is simplest for the region of fully developed roughness. According to what was said previously, for this region the velocity distribution is given by:

$$\frac{u}{v_*} = 5.75 \log \frac{y}{k_s} + B_s \qquad B_s = 8.5 \qquad (16.40)$$

and the resistance coefficient by:

$$\lambda = \frac{1}{\left(2.0 \log \frac{r}{k_s} + 1.74\right)^2} \qquad (16.41)$$

One now relates to an arbitrary roughness k an equivalent sand roughness k_s by the ratio

$$k_s = \alpha k \qquad (16.42)$$

Where by equivalent sand roughness k_s is meant that grain size of sand roughness which has, according to equation (16.41) the same resistance as the given roughness k.

Basically, of course, the equivalent sand roughness k_s can be determined by a resistance measurement on the pipe. However, such measurements

for arbitrary roughnesses are difficult to perform. Measurements on arbitrary roughnesses in a tunnel with plane walls are more convenient. To this purpose an exchangeable wall of a tunnel with rectangular cross section is provided with the roughness to be investigated (fig. 85). From the measurement of the velocity distribution in such a tunnel with a rough and a smooth longitudinal wall one obtains, for the logarithmic plot against the distance from the wall, a triangular velocity distribution (compare fig. 85). From the logarithmic plot of the velocity distribution over the rough wall

$$u = n_r \log y + m_r \tag{16.43}$$

one obtains by comparison with the universal law according to equation (16.28) for the shearing stress velocity at the wall:

$$v_{*r} = \frac{n_r}{5.75} \tag{16.44}$$

Further, one determines for the roughness to be investigated the constant B of the velocity distribution law, namely:

$$B = \frac{u}{v_{*r}} - 5.75 \log \frac{y}{k} \tag{16.45}$$

By comparison of equation (16.45) with (16.40) one obtains for the equivalent sand roughness:

$$5.75 \log \frac{k_s}{k} = 8.5 - B \tag{16.46}$$

In this way one may determine the drag for arbitrary roughnesses from a simple measurement in the roughness tunnel. This method may be also carried over to the case of the intermediate region.

CHAPTER XVII. THE FRICTION DRAG OF THE FLAT PLATE IN LONGITUDINAL FLOW

The turbulent friction drag of the plate in longitudinal flow is of very great practical importance, for instance as friction drag of wings, airplane fuselages, or ships. The exact measurement of the friction drag for the large Reynolds numbers of practice is extremely difficult. Thus

it is particularly important that one can, according to Prandtl (references 73 and 74), calculate the friction drag of surfaces from the results of pipe flow studies. This conversion from the pipe to the plate can be made for the smooth as well as for the rough plate.

a. The Smooth Plate

One assumes, for simplification, that the boundary layer on the plate is turbulent from the leading edge. Let the coordinate system be selected according to figure 86. The boundary layer thickness $\delta(x)$ increases with the length of run x. Let b be the width of the plate. For the transition from pipe to plate the free stream velocity U_o of the plate corresponds to the maximum velocity u_{max} in the pipe, and the boundary layer thickness δ to the pipe radius r.

One now makes the fundamental assumption that the same velocity distribution exists in the boundary layer on the plate as in the pipe. This is certainly not exactly correct since the velocity distribution in the pipe is influenced by a pressure drop, whereas on the plate the pressure gradient equals zero. However, slight differences in velocity distribution are insignificant since it is the momentum integral which is of fundamental importance for the drag. For the drag $W(x)$ of one side of the plate of length x, according to equations (10.1) and (10.2):

$$W(x) = b\int_0^x \tau_o(x)\,dx = b\rho\int_0^{\delta(x)} u\,(U_o - u)\,dy \qquad (17.1)$$

whence

$$\frac{1}{b}\frac{dW}{dx} = \tau_o(x) \qquad (17.1a)$$

The equation (17.1) can also be written in the form

$$W(x) = b\rho U_o^2\delta(x)\int_0^1 \frac{u}{U_o}\left(1 - \frac{u}{U_o}\right) d\frac{y}{\delta} \qquad (17.2)$$

For the velocity distribution in the boundary layer one now assumes the 1/7-power law found for the pipe. Replacing u_{max} by U_o and r by δ_1 one may write this law, according to equation (16.11):

$$\frac{u}{U_o} = \left(\frac{y}{\delta}\right)^{1/7} = \eta'^{1/7} \tag{17.3}$$

Hence the momentum integral becomes

$$J = \int_o^1 \frac{u}{U_o}\left(1 - \frac{u}{U_o}\right) d\,\frac{y}{\delta} = \int_o^1 \eta'^{1/7}\left(1 - \eta'^{1/7}\right) d\eta' = \frac{7}{72} \tag{17.4}$$

and thus

$$W(x) = \frac{7}{72}\, b\rho U_o^{\,2}\delta(x) \tag{17.5}$$

Hence follows, according to equation (17.1a)

$$\tau_o = \frac{7}{72}\,\rho U_o^{\,2}\,\frac{d\delta}{dx} \tag{17.6}$$

On the other hand, one had found before for the smooth pipe, equation (16.13) again replacing r by δ and u_{max} by U_o:

$$\tau_o = 0.0225\,\rho U_o^{\,7/4}\left(\frac{\nu}{\delta}\right)^{1/4} \tag{17.7}$$

By equating equations (17.6) and (17.7) results:

$$\frac{7}{72}\,\rho U_o^{\,2}\,\frac{d\delta}{dx} = 0.0225\,\rho U_o^{\,7/4}\left(\frac{\nu}{\delta}\right)^{1/4}$$

This is a differential equation for $\delta(x)$. The integration yields:

$$\left.\begin{aligned} \frac{4}{5}\,\delta^{5/4} &= \frac{72}{7}\,0.0225\left(\frac{\nu}{U_o}\right)^{1/4} x \\ \delta(x) &= 0.37\left(\frac{\nu}{U_o}\right)^{1/5} x^{4/5} \end{aligned}\right\} \tag{17.8}$$

$$\boxed{\delta(x) = \frac{0.37x}{\sqrt[5]{Re_x}}} \qquad Re_x = \frac{U_o x}{\nu} \tag{17.9}$$

For the turbulent boundary layer the boundary layer thickness, therefore, increases with $x^{4/5}$. The corresponding equation for the laminar flow was, according to equation (9.21a), $\delta = 5\sqrt{\nu x/U_o}$.

By substitution of equation (17.8) into equation (17.5) one obtains

$$W(x) = 0.036\, b\rho U_o^2 x\, (Re_x)^{-1/5}$$

or for the drag coefficient $c_f = W/\frac{\rho}{2} U_o^2 xb$:

$$c_f = 0.072\, (Re_x)^{-1/5}$$

Comparing this result with test results on plates one finds the numerical value 0.072 to be somewhat too low.

$$\boxed{c_f = 0.074\, (Re_x)^{-1/5}} \qquad \text{valid for } 5 \times 10^5 < Re < 10^7 \tag{17.10}$$

corresponds better to the measurements. This law holds true only for $Re_x < 10^7$, corresponding to the fact that the Blasius pipe resistance law and the 1/7-power law of the velocity distribution, which form the basis of this plate drag law, are not valid for large Reynolds numbers. This law is represented in figure 87 together with the laminar-flow law according to equation (9.19). The initial laminar flow on the front part of the plate can be taken into consideration by a subtraction, according to Prandtl (reference 73):

$$\boxed{c_f = 0.074\, Re_x^{-1/5} - \frac{1700}{Re_x}} \qquad 5 \times 10^5 < Re_x < 10^7 \tag{17.11}$$

The plate drag law for very large Reynolds numbers can be obtained in essentially the same way by starting from the universal logarithmic law for the velocity distribution equation (16.41) which, according to

its derivation, is valid up to Reynolds numbers of arbitrary magnitude. Here the calculation becomes considerably more complicated. The development of the calculation is clarified if one first introduces the velocity distribution in a general form. We had introduced for the pipe flow the dimensionless variables $\varphi = \frac{u}{v_*}$ and $\eta = \frac{yv_*}{\nu}$. The values at the edge of the boundary layer are to be denoted by the index 0, thus

$$\varphi_o = \frac{U_o}{v_*} \qquad \eta_o = \frac{\delta v_*}{\nu} \tag{17.12}$$

Then:

$$u = v_* \varphi = U_o \frac{\varphi}{\varphi_o} \tag{17.13}$$

$$y = \frac{\nu \varphi_o}{U_o} \eta \qquad dy = \frac{\nu \varphi_o}{U_o} d\eta \tag{17.14}$$

From the equation $\tau_o = \frac{1}{b} \frac{dW}{dx}$ follows, with W according to equation (17.1)

$$\rho v_*^2 = \rho \frac{d}{dx} \left\{ \int_0^\delta u(U_o - u)\, dy \right\}$$

$$v_*^2 = \frac{d\eta_o}{dx} \frac{d}{d\eta_o} \left\{ \int_0^\delta u(U_o - u)\, dy \right\}$$

and according to equation (17.13):

$$\frac{U_o^2}{\varphi_o^2} = \frac{\nu \varphi_o}{U_o} \frac{d}{d\eta_o} \int_0^{\eta_o} u(U_o - u) d\eta \frac{d\eta_o}{dx}$$

$$\frac{U_o}{\varphi_o^2} = \nu\varphi_o \frac{d\eta_o}{dx} \frac{d}{d\eta_o}\int_o^{\eta_o} \frac{u}{U_o}\left(1 - \frac{u}{U_o}\right) d\eta$$

$$= \nu\varphi_o \frac{d\eta_o}{dx} \frac{d}{d\eta_o}\int_o^{\eta_o} \frac{\varphi}{\varphi_o}\left(1 - \frac{\varphi}{\varphi_o}\right) d\eta$$

$$\frac{U_o}{\varphi_o^2} = \nu \frac{d\eta_o}{dx} \frac{d}{d\eta_o}\int_o^{\eta_o} \left(\varphi - \frac{\varphi^2}{\varphi_o}\right) d\eta \qquad (17.15)$$

In forming the integral $\frac{d}{d\eta_o}\int_o^{\eta_o}\left(\varphi - \frac{\varphi^2}{\varphi_o}\right)d\eta$ one must note the following facts: The differentiation with respect to the upper limit gives zero, since for $\eta = \eta_o$, $\varphi = \varphi_o$. In the differentiation of the integrand φ is to be regarded as constant, and φ_o as a function of η_o. Therefore

$$\frac{d}{d\eta_o}\int_o^{\eta_o} \left(\varphi - \frac{\varphi^2}{\varphi_o}\right) d\eta = \frac{d\varphi_o}{d\eta_o}\int_o^{\eta_o} \frac{\varphi^2}{\varphi_o^2}\, d\eta$$

Thus follows from equation (17.15):

$$U_o = \nu \frac{d\eta_o}{dx} \frac{d\varphi_o}{d\eta_o}\int_o^{\eta_o} \varphi^2 d\eta \qquad (17.16)$$

One puts, for simplification,

$$F(\eta_o) = \frac{d\varphi_o}{d\eta_o}\int_o^{\eta_o} \varphi^2 d\eta \qquad (17.17)$$

and obtains from equation (17.16):

$$dx = \frac{\nu}{U_o} F(\eta_o)\, d\eta_o$$

If one assumes this law to be valid from the leading edge of the plate ($x = 0$), that is, that the flow is turbulent starting from the front, the integration gives:

$$x = \frac{\nu}{U_o} \Phi(\eta_1) \tag{17.18}$$

with

$$\Phi(\eta_1) = \int_{\eta_o=o}^{\eta_1} F(\eta_o) d\eta_o \tag{17.19}$$

Equation (17.18) can also be written so that the Re-number formed with the length of run x appears:

$$Re_x = \frac{U_o x}{\nu} = \Phi(\eta_1) \tag{17.20}$$

with:

$$\Phi(\eta_1) = \int_{\eta_o=o}^{\eta_1} \frac{d\varphi_o}{d\eta_o} \left(\int_{u_o}^{\eta_o} \varphi^2 d\eta \right) d\eta_o \tag{17.19a}$$

Equation (17.20) gives the relation between the dimensionless boundary layer thickness $\eta_1 = v_* \delta / \nu$ and the Re-number $U_o x / \nu$.

The drag remains to be calculated. From

$$\tau_o = \rho v_*^2 = \rho \frac{U_o^2}{\varphi_o^2}$$

follows, because $W = b \int_o^x \tau_o \, dx$

$$W = b\ \rho\ U_o\ \nu \int_{\eta_o=o}^{\eta_1} \frac{F(\eta_o)}{\varphi_o^2}\, d\eta_o = b\ \rho\ U_o\ \nu\psi(\eta_1) \tag{17.21}$$

where

$$\psi(\eta_1) = \int_{\eta_o=o}^{\eta_1} \frac{F(\eta_o)}{\varphi_o^2}\, d\eta_o \tag{17.22}$$

The drag coefficient $c_f = W/\frac{\rho}{2} U_o^2 b\ x$ becomes finally

$$c_f = \frac{2\nu}{U_o x}\psi(\eta_1) = 2\,\frac{\psi(\eta_1)}{\Phi(\eta_1)} \tag{17.23}$$

Hence c_f also turns out to be a function of η_1. Equations (17.20) and (17.23) together give a parametric representation of c_f as a function of Re_x, where the parameter is the boundary layer thickness $\eta_1 = \frac{v_*\delta}{\nu}$.

Numerical Results

In order to arrive at numerical results, one must introduce a special function for $\varphi(\eta)$. For the 1/7-power law according to equation (16.11) that is, with $\varphi = C\eta^{1/7}$, one would obtain the drag law according to equation (17.10). One uses the universal logarithmic velocity distribution law, equation (16.14).

$$\varphi = 2.5\ \ln\ \eta + 5.5$$

In order to make the carrying out of the integrations more convenient, one writes

$$\varphi = 2.5\ \ln\ (1 + 9\eta)$$

Then φ becomes, for $\eta = 0$, $\varphi = 0$. The adding of the one changes $\varphi(\eta)$ a little, only for very small η and has only little influence on the integrals. If one writes the law at first in the general form

$$\varphi = a \ln (1 + b\eta) \tag{17.24}$$

the calculation of the integrals equations (17.17), (17.19), (17.22), with $z = 1 + b\eta$ yields

$$\left.\begin{aligned} F(\eta) &= a^3 \left(\ln^2 z - 2 \ln z + 2 - \frac{2}{z}\right) \\ \Phi(\eta) &= \frac{a^3}{b}\left(z \ln^2 z - 4z \ln z - 2 \ln z + 6z - 6\right) \\ \Psi(\eta) &= \frac{a}{b}\left\{z + 1 - \frac{2(z-1)}{\ln z}\right\} \end{aligned}\right\} \tag{17.25}$$

With the numerical values

$$a = 2.493 \qquad b = 8.93$$

one obtains for the drag law the following table:

$\frac{\eta}{10^3}$	Re 10^{-6}	$c_f\ 10^3$
0.500	0.337	5.65
1.00	0.820	4.75
2.00	1.96	4.05
3.00	3.25	3.71
5.00	6.10	3.34
12.0	17.7	2.81
20.0	32.5	2.57
50.0	96.5	2.20
100.0	217.5	1.96
500.0	1401.0	1.55

This table can be replaced by the following interpolation formula:

$$c_f = \frac{0.472}{(\log \mathrm{Re}_x)^{2.58}}$$

Comparison with test results shows that the agreement improves if the number 0.472 is slightly varied, by putting

$$\boxed{c_f = \frac{0.455}{(\log \mathrm{Re}_x)^{2.58}}} \qquad 10^6 < \mathrm{Re}_x < 10^9 \qquad (17.26)$$

Prandtl – Schlichting's Plate Drag Law

The laminar approach length may again be taken into consideration by the same subtraction as before; thus:

$$\boxed{c_f = \frac{0.455}{(\log \mathrm{Re}_x)^{2.58}} - \frac{1700}{\mathrm{Re}_x}} \qquad 5 \times 10^5 < \mathrm{Re}_x < 10^9 \qquad (17.27)$$

Whereas the system of formulas equation (17.25) is valid up to Re-numbers of arbitrary magnitude, the interpolation formulas, equations (17.26) and (17.27), have the upper limit $\mathrm{Re} = 10^9$. However, this limit takes care of all Re-numbers occurring in practice. The theoretical formula (equation (17.27)) is also plotted in figure 87. Figure 88 gives a comparison with test results on plates, wings, and airship bodies. The agreement is quite good.

Very recently this plate drag law has been somewhat improved by Schultz-Grunow (reference 89). Until then, the turbulent velocity profile measured in the pipe (1/7-power law, logarithmic law) had been carried over directly to the plate, mainly because accurate velocity distribution measurements of the plate boundary layer did not exist. The exact measurement of the plate boundary layer showed, however, that the plate profile does not completely coincide with the pipe profile. The test points show, for large distance from the wall, a slight upward deviation from the logarithmic law found for the pipe. Thus the loss of momentum on the plate is somewhat smaller than that calculated with the logarithmic law. Schultz-Grunow repeated the calculation of the drag law according to the formula system given above with the velocity distribution law for the plate measured by him. His result is represented by the interpolation formula

$$c_f = \frac{0.427}{(-0.407 + \log \mathrm{Re}_x)^{2.64}} \qquad 10^6 < \mathrm{Re}_x < 10^9 \qquad (17.28)$$

This law is also plotted in figure 87. The differences from the Prandtl-Schlichting law are only slight.*

The corresponding rotationally-symmetrical problem, that is, the turbulent boundary layer on a body of revolution at zero incidence, was treated by C. B. Millikan (reference 79). The 1/7-power law of the velocity distribution was taken as basis. Application to the general case has not yet been made.

Twelfth Lecture (February 23, 1942)

b. The Rough Plate

The conversion from pipe resistance to the plate drag may be carried out for the rough plate in the same manner as described previously for the smooth plate. One assumes a plate uniformly covered with the same roughness k. Since the boundary layer thickness δ increases from the front toward the rear, the ratio k/δ which is significant for the drag decreases from the front toward the rear. Behind the initial laminar run, therefore, follows at first the region of the fully developed roughness flow; the so-called intermediate region follows and farthest toward the rear there is, finally, if the plate is long enough, the region of the hydraulically smooth flow. These regions are determined by specification of the numerical values for the roughness coefficient $v_* k_s/\nu$. In order to obtain the drag of the rough plate, one must perform the conversion from pipe flow to plate flow for each of these three regions individually. This calculation was carried out by Prandtl and Schlichting (reference 76), based on the results of Nikuradse (reference 71) for the pipe tests with sand roughness. For this conversion one starts from the universal velocity distribution law of the rough pipe according to equation (16.28), the quantity B being dependent also on the characteristic roughness value $v_* k_s/\nu$, according to figure 84. The calculation takes basically the same course as described in detail for the smooth plate in chapter XVIIa. It is, however, rather complicated and will not be reproduced here. One obtains as final result for the total drag coefficient of the sand-rough plate a diagram (fig. 89) which represents the drag coefficient as a function of the Reynolds number $U_0 l/\nu$ with the relative roughness l/k_s as parameter. Just as for the pipe, a given relative roughness l/k_s has a drag increasing effect not for all Re-numbers, but only above a certain Re-number. This diagram is applicable also for roughnesses other than sand roughness, if one uses the equivalent sand roughness. In the diagram (fig. 89) the square drag law is attained, just as for the pipe, for every relative

* The tables pertaining to the plate drag formulas are given in table 7, chapter XXII.

roughness l/k_s provided the Re-number is sufficiently large. The interpolation formula

$$c_f = \left(1.89 + 1.62 \log \frac{l}{k_s}\right)^{-2.5} \tag{17.29}$$

applies to this law.

c. The Admissible Roughness

The problem of the admissible roughness of a wall in a flow is very important in practice since it concerns the effort that might reasonably be expended in smoothing a surface for the purpose of drag reduction. Admissible roughness signifies that roughness above which a drag increase would occur in the given turbulent friction layer (which, therefore, still is in effect hydraulically smooth). The admissible relative roughness k_s/l decreases with increasing Re-number $U_o l/\nu$ as one can see from figure 89. It is the point where the particular curve l/k_s diverges from the curve of the smooth wall. One finds the values for the admissible relative roughness according to the following table; they can also be combined into the one formula

$$\frac{U_o \, k_{s\ admiss.}}{\nu} = 10^2 \tag{17.30}$$

$\frac{U_o l}{\nu}$	10^5	10^6	10^7	10^8	10^9
$\left(\frac{k_s}{l}\right)_{admiss.}$	10^{-3}	10^{-4}	10^{-5}	10^{-6}	10^{-7}

From equation (17.30) one recognizes that the admissible roughness height is by no means a function of the plate length. This fact is significant for instance for the admissible roughness of a wing. Equation (17.30) states that for equal velocity the admissible roughness height is the same for a full scale wing as for a model wing. Let us assume a numerical example:

Wing: chord $l = 2$m

Velocity $U_o = 300$ km/h $= 83$ m/sec

From equation (17.30) results an admissible magnitude of roughness $k_s = 0.02$ mm. This degree of smoothness is not always attained by the wing surfaces manufactured in practice, so that the latter have a certain roughness drag. In the considerations just made one deals with an increase of the friction drag in an a priori turbulent friction layer.

However, the roughness may also change the drag by disturbing the laminar friction layer to such an extent that the point of laminar/turbulent transition is shifted toward the front. Thereby the drag can be increased or reduced according to the shape of the body. The drag is increased by this displacement of the transition point if the body in question has predominant friction drag (for instance wing profile). The drag might be reduced, circumstances permitting, for a body with predominant pressure drag (for instance, the circular cylinder). One calls the roughness height which causes the transition the "critical roughness height". According to Japanese measurements (reference 77) this critical roughness height for the laminar friction layer is given by

$$\frac{v_* k_{crit}}{\nu} = 15 \tag{17.31}$$

A numerical example follows:

Assume, as prescribed before, a

$$\text{wing} \quad l = 2\text{m}$$

$$U_o = 300 \text{ km/h} = 83 \text{ m/sec}$$

then $Re = U_o l/\nu = 10^7$. Consider the point of the wing $x = 0.1l$, thus $Re_x = U_o x/\nu = 10^6$. Up to this point the boundary layer might remain laminar under the effect of the pressure drop. The wall shearing stress for the laminar boundary layer is according to equation (9.17)

$$\frac{\tau_o}{\rho} = 0.332 \, U_o^2 \sqrt{\frac{\nu}{U_o x}} = 0.332 \, \frac{6900}{10^3} = 2.29 \, \frac{m^2}{sec^2}$$

hence:

$$v_* = \sqrt{\tau_o/\rho} = 1.52 \text{ m/sec}$$

and according to equation (17.31)

$$k_{crit} = 15 \, \frac{\nu}{v_*} = \frac{15}{1.52} \, \frac{1}{7} \, 10^{-4} = 0.14 \text{ mm}$$

The critical roughness height causing the transition is, therefore, about ten times as high as the roughness height admissible in the turbulent friction layer. The laminar friction layer therefore "tolerates" a greater roughness than the turbulent one.

The following can be said about the influence of the roughness on the form drag: Sharp-edged bodies are indifferent to surface roughnesses because for them the transition point is fixed by the edges, as for instance for the plate normal to the flow. Short curved bodies, on the other hand, as for instance the circular cylinder, are sensitive. For the circular cylinder the critical Reynolds number, for which the known large pressure drag reduction occurs, is largely dependent on the roughness. With increasing relative roughness k/R (R = radius of the circular cylinder) Re_{crit} decreases. According to British measurements (reference 90) the drag curves for a circular cylinder with different relative roughnesses have a course as indicated in figure 90. The boundary layer is so disturbed by the roughness that the laminar/turbulent transition occurs for a considerably smaller Re-number than for the smooth cylinder. The roughness has here the same effect as Prandtl's trip wire, that is, in a certain region of Re-numbers it decreases the drag. It is true, however, that the supercritical drag coefficient is then always larger for the rough circular cylinder than for the smooth one.

CHAPTER XVIII. THE TURBULENT FRICTION LAYER IN ACCELERATED AND RETARDED FLOW

The cases of turbulent friction layer treated so far are relatively simple insofar as the velocity outside of the friction layer along the wall is constant. Here as for the laminar flow the case of special interest is where the velocity of the potential flow is variable along the wall (pressure drop and pressure rise). As for laminar flow, the form of the boundary layer profile along the wall is variable. In practice this case exists for instance for the friction layer on the wing, on the turbine blade, and in the diffuser. Of special interest is the question of whether separation of the boundary layer occurs and, if so, where the separation point is located. The problem consists therefore for a prescribed potential flow in following the turbulent friction layer by calculation. The calculation of the turbulent friction drag is of importance. The corresponding problem for the laminar friction layer was solved by the Pohlhausen method (chapter X).

For the turbulent friction layer the method of Gruschwitz (reference 78) proved best. Gruschwitz makes the asumption that the velocity profiles of the turbulent boundary layer for pressure drop and

rise can be represented as a one-parameter family, if one plots u/U against y/ϑ. ϑ signifies the momentum thickness which is, according to equation (6.32), defined by:

$$U^2\vartheta = \int_0^\delta u(U - u)\, dy \tag{18.1}$$

As form parameter one selects

$$\eta = 1 - \left(\frac{u(\vartheta)}{U}\right)^2 \tag{18.2}$$

$u(\vartheta)$ denoting the velocity in the friction layer at the distance from the wall $y = \vartheta$. That η actually is a serviceable form parameter can be recognized from figure 91 where a family of turbulent boundary layer profiles is plotted according to Gruschwitz. Gruschwitz found from his measurements that the turbulent separation point is given by

$$\eta = 0.8 \qquad \text{(Separation)} \tag{18.3}$$

The form parameter η is analogous to the Pohlhausen-parameter λ of the laminar friction layer. However, a considerable difference exists between η and λ: for the laminar friction layer an analytical relation exists between λ and the pressure gradient and the boundary layer thickness, namely according to equation (10.41)

$$\lambda = \frac{\delta^2}{\nu}\frac{dU}{dx} \tag{18.4}$$

Such a relation is thus far lacking for the turbulent boundary layer, since one does not yet possess an analytical expression for the turbulent velocity profiles*. One needs therefore an empirical equivalent for equation (18.4).

For the special case of the turbulent friction layer without pressure gradient where the 1/7-power law $u/U = (y/\delta)^{1/7}$ applies for the velocity profile, one finds from equations (18.1) and (18.2)

---

* Compare, however, chapter XXIIb, where under certain assumptions such an analytical connection is indicated.

$$\frac{\vartheta}{\delta} = \frac{7}{72} \qquad \eta = 0.487 \tag{18.5}$$

Since in the case of the turbulent boundary layer, an analytical expression for the velocity distribution does not exist, the calculation is limited to the determination of the four characteristics of the friction layer: form parameter η, wall shearing stress τ_o, displacement thickness δ^*, momentum thickness ϑ. Four equations are required for their calculation.

As for the laminar boundary layer, the momentum theorem yields the first equation; the momentum theorem may, according to equation (10.36) be written in the form:

$$\boxed{\frac{\tau_o}{\rho U^2} = \frac{d\vartheta}{dx} + \left(1 + \frac{1}{2}\frac{\delta^*}{\vartheta}\right)\frac{\vartheta}{U^2}\frac{dU^2}{dx}} \qquad \text{(I)} \tag{18.6}$$

The second equation is yielded by the function

$$\boxed{\frac{\delta^*}{\vartheta} = H(\eta)} \qquad \text{(II)} \tag{18.7}$$

obtained by Gruschwitz by evaluation of the measured velocity profiles (fig. 92), and regarded as generally valid. It can be derived also by calculation from the form of the velocity profile (compare appendix chapter XXII) and yields:

$$\eta = 1 - \left(\frac{H - 1}{H(H + 1)}\right)^{H-1} \tag{18.8}$$

The third equation is empirically derived by Gruschwitz from his measurements. He considers that the energy variation of a particle moving parallel to the wall at the distance $y = \vartheta$ is a function of u_ϑ, U, ϑ, ν. Dimension considerations suggest the following relation:

$$\frac{\vartheta}{q}\frac{dg_1}{dx} = F(\eta, \mathrm{Re}) \tag{18.9}$$

$q = \frac{\rho}{2} U^2$ and $g_1 = p + \frac{\rho}{2} u_\vartheta^2$ signify the total pressure in the layer $y = \vartheta$. The evaluation of the test results showed that a dependence on

the Re-number is practically non-existent, and that one can represent equation (18.9) in the following manner:

$$\frac{\vartheta}{q}\frac{dg_1}{dx} = 0.00894\ \eta - 0.00461 \tag{18.10}$$

Furthermore, the identity

$$g_o - g_1 = p + \frac{\rho}{2}U^2 - p - \frac{\rho}{2}u_\vartheta^2$$

$$= \frac{\rho}{2}U^2\left(1 - \frac{u^2\vartheta}{U^2}\right) = q\ \eta$$

is valid. One puts

$$q\ \eta = \zeta \tag{18.11}$$

and has therefore

$$\frac{dg_1}{dx} = -\frac{d\zeta}{dx} \tag{18.12}$$

Now equation (18.10) can be written:

$$\boxed{\vartheta\frac{d\zeta}{dx} = -0.00894\ \zeta + 0.00461\ q} \qquad \text{(III)} \tag{18.13}$$

The fourth equation is still missing and is replaced by the following estimation of τ_o: According to the calculations for the plate in longitudinal flow, equation (17.7) was:

$$\frac{\tau_o}{\rho U^2} = 0.0225\left(\frac{U\delta}{\nu}\right)^{-1/4} = 0.0225\ (Re_\delta)^{-1/4} \tag{18.14}$$

If one takes into consideration that for the 1/7-power law of the velocity distribution:

$$\delta^* = \frac{1}{8}\delta; \qquad \vartheta = \frac{7}{72}\delta$$

one can write equation (18.14) also:

$$\boxed{\frac{\tau_o}{\rho U^2} = 0.01338\,(Re_{\delta^*})^{-1/4} = 0.01256\,(Re_{\vartheta})^{-1/4}} \quad (IV) \qquad (18.15)$$

For calculation of ϑ and η ($\zeta = q\,\eta$, respectively) one must now solve the following system of equations:

$$\boxed{\begin{aligned} &\frac{d\zeta}{dx} + 0.00894\,\frac{\zeta}{\vartheta} = 0.0461\,\frac{q}{\vartheta} \\ &\frac{d\vartheta}{dx} + \left(1 + \frac{H}{2}\right)\frac{\vartheta}{q}\,\frac{dq}{dx} = \frac{\tau_o}{\rho U^2} \end{aligned}} \qquad (18.16)$$

$q = \frac{\rho}{2}U^2$ is a given function of x; H and $\frac{\tau_o}{\rho U^2}$ are given functions of $\eta = \zeta/q$ or ϑ, respectively. This system of equations is to be solved downstream from the transition point.

Initial values: As initial value for ϑ one takes the value from the laminar friction layer at the transition point:

$$\vartheta_{o\,turb.} = \vartheta_{o\,lam.} \qquad (18.17)$$

This is based on the consideration that the loss of momentum does not vary at the transition point since it gives the drag. The initial value of η is somewhat arbitrary. Gruschwitz takes

$$\eta_o = 0.1$$

and states that a different choice has little influence on the result.

With these initial values the system of equations (18.16) may be solved graphically, according to a method of Czuber (compare appendix, Chapter XXII, where an example is given). A first approximation for ϑ is obtained by first solving the second equation with constant values for $\tau_o/\rho U^2$ and H;

$$\frac{\tau_o}{\rho U^2} = 0.002; \qquad H = 1.5 \qquad (18.18)$$

are appropriate. Thereby the second equation is a differential equation of the first order for ϑ. This first approximation $\vartheta_1(x)$ is then substituted into the first equation, which then becomes a differential equation of the first order for $\zeta(x)$; let its solution be denoted by $\zeta_1(x)$. Thus one has also a first approximation for η: $\eta_1(x)$. With $\eta_1(x)$ one determines the course of $H(\eta)$ according to figure 92 and is now able to improve τ_o according to equation (18.15). These values of both H and τ_o are now inserted in the second equation, and a second approximation $\vartheta_2(x)$ is obtained. By substitution of $\vartheta_2(x)$ into the first equation one obtains the second approximation $\zeta_2(x)$, etc. The method converges so well that the answer is essentially attained in the second approximation.

The separation point is given by

$$\eta = 0.8$$

Incidental to the boundary layer calculation one obtains the following characteristic values of the friction layer as functions of the arc length x:

$$\vartheta(x), \quad \delta^*(x), \quad \eta(x), \quad \tau_o(x).$$

The boundary layer calculation for the profile J 015, $c_a = 0$ is given as example in figure 93. The transition point was assumed at the velocity maximum. The calculation of the laminar boundary layer for the same case was indicated in chapter XII. The details of this example are compiled in the appendix, chapter XXII.

It should be mentioned that the calculation for the turbulent boundary layer must be performed anew for every Re-number $U_o l/\nu$, whereas only one calculation was necessary for the laminar boundary layer. The reasons are, first, that the transition point travels with the Re-number, and second, that the initial value of ϑ/t varies with Re, since for the laminar boundary layer $\frac{\vartheta}{t}\sqrt{\frac{U_o t}{\nu}}$ at the transition point is fixed.

It must be noted that the values obtained for τ_o become incorrect in the neighborhood of the separation point: At the separation point τ_o must equal zero, whereas equation (18.15) gives everywhere $\tau_o \neq 0$.

Boundary Layer Without Pressure Gradient

In this case $q(x)$ = Constant. Equation (18.13) can be written:

$$\frac{\vartheta}{q}\frac{d\zeta}{dx} = -0.00894\eta + 0.00461 \tag{18.19}$$

or, because $q(x)$ = constant;

$$\frac{d\zeta}{dx} = \frac{d(\eta q)}{dx} = q\frac{d\eta}{dx} \tag{18.20}$$

Thus equation (18.19) becomes:

$$\vartheta\frac{d\eta}{dx} = -0.00894\eta + 0.00461 \tag{18.21}$$

A solution of this equation is:

$$\eta = \frac{0.00461}{0.00894} = 0.516 \tag{18.22}$$

Since at the beginning of the turbulent friction layer η is smaller than this value (transition point $\eta = 0.1$) and since according to equation (18.21) $d\eta/dx > 0$, η must in this case approach the value $\eta = 0.516$ asymptotically from below. For the velocity profile of the 1/7-power law, $\eta = 0.487$ (compare equation (18.15)). The profile attained asymptotically for uniform pressure (p = constant) therefore almost agrees with the 1/7-power law that was previously applied to the plate in longitudinal flow.

A great many boundary layer calculations according to this method are performed in the dissertation by Pretsch (reference 80).

Thirteenth Lecture (March 2, 1942)

CHAPTER XIX. FREE TURBULENCE

a. General Remarks; Estimations

After considering so far almost exclusively the turbulent flow along solid walls, we shall now treat a few cases of the so-called free turbulence. By that one understands turbulent flows where no solid walls

are present. Examples are the spreading of a jet and its mixing with the surrounding fluid at rest; or the wake flow behind a body towed through the fluid at rest (fig. 94). Qualitatively these turbulent flows take a course similar to that for the laminar case (compare chapter IX); quantitatively, however, considerable differences exist, since the turbulent friction is very much larger than the laminar friction. In a certain way, the cases of free turbulence are, with respect to calculations, simpler than turbulent flows along a wall, since the laminar sublayer is not present and the laminar friction as compared with the turbulent one can therefore be neglected for the entire flow domain. The free turbulence may be treated satisfactorily with Prandtl's concept of the turbulent shearing stress according to equation (15.9):

$$\tau = \rho\, l^2 \left|\frac{\partial u}{\partial y}\right| \frac{\partial u}{\partial y} \tag{19.1}$$

the mixing length l being assumed a pure position function. The turbulent friction has the effect of making the jet width increase and the velocity at its center decrease with increasing distance along the jet.

We now perform rough calculations, according to Prandtl (reference 2, Part I), for a few cases of free turbulence which give information about the laws governing the increase of width and the decrease of "depth" with the distance x.

It has proved useful for such turbulent jet problems to set the mixing length l proportional to the jet width b:

$$\frac{l}{b} = \beta = \text{constant} \tag{19.2}$$

Furthermore, the following rule has held true: The increase of the width b of the mixing zone with time is proportional to the fluctuation of the transverse velocity v':

$$\frac{Db}{Dt} \sim v' \tag{19.3}$$

D/Dt signifies the substantial derivative; thus: $\frac{D}{Dt} = u\frac{\partial}{\partial x} + v\frac{\partial}{\partial y}$.

According to our previous estimation, equation (15.5): $v' = l\frac{\partial u}{\partial y}$;

Therefore:

$$\frac{Db}{Dt} \sim l \frac{\partial u}{\partial y} \tag{19.4}$$

Furthermore, the mean value of $\frac{\partial u}{\partial y}$ equals approximately:

$$\frac{\partial u}{\partial y} = \text{number } \frac{u_{max}}{b}$$

and thus:

$$\frac{Db}{Dt} = \text{number } \frac{l}{b} u_{max} = \text{number } \beta u_{max} \tag{19.5}$$

Jet (Plane and Circular)

We shall estimate, by means of these relations, how the width increases with the distance x and the velocity at the center decreases. At first, for the circular as well as for the plane jet:

$$\frac{Db}{Dt} = \text{number } u_{max} \frac{db}{dx} \tag{19.6}$$

It follows, by comparison with equation (19.5):

$$\frac{db}{dx} = \text{number } \frac{l}{b} = \text{number}$$

$$b = \text{number } x + \text{constant}$$

If the origin of coordinates is suitably selected (it need not coincide with the orifice) one has therefore:

$$\boxed{b = \text{number } x} \quad \text{(plane and circular jet)} \tag{19.7}$$

The relation between u_{max} and x is obtained from the momentum theorem. Since the pressure is constant, in the x-direction, the x-momentum must be independent of x, thus:

$$J = \rho \int u^2 \, d F = \text{constant}$$

whence follows for the circular jet:

$$J = \text{number } \rho\, u_{max}^2\, b^2$$

or:

$$u_{max} = \text{number } \frac{1}{b}\sqrt{\frac{J}{\rho}}$$

and because of equation (19.7):

$$\boxed{u_{max} = \text{number } \frac{1}{x}\sqrt{\frac{J}{\rho}}} \quad \text{(circular jet)} \qquad (19.8)$$

For the plane jet, if J' signifies the momentum per unit length of the jet:

$$J' = \text{number } \rho\, u_{max}^2\, b$$

$$u_{max} = \text{number } \frac{1}{\sqrt{b}}\sqrt{\frac{J'}{\rho}}$$

and because of equation (19.7):

$$\boxed{u_{max} = \text{number } \frac{1}{\sqrt{x}}\sqrt{\frac{J'}{\rho}}} \quad \text{(plane jet)} \qquad (19.9)$$

Wake (plane and circular)

The calculation for the wake is somewhat different, since the momentum which gives directly the drag of the body must be calculated in a slightly different way. The momentum integral is now (compare equation (9.40)):

$$W = J = \rho \int u\,(U_o - u)\, d\,F \qquad (19.10)$$

At large distance from the body $u' = U_o - u$ is small compared with U_o (fig. 95) so that $u' \ll U_o$ and

$$u(U_o - u) = (U_o - u') u' \approx U_o u'$$

Thus one obtains for the circular wake:

$$\frac{\rho}{2} c_w F U_o^2 \sim \rho U_o u' \pi b^2$$

$$\frac{u'}{U_o} \sim \frac{c_w F}{\pi b^2} \tag{19.11}$$

Instead of equation (19.6) now applies:

$$\frac{Db}{Dt} = U_o \frac{db}{dx} \tag{19.12}$$

and instead of equation (19.5):

$$\frac{Db}{Dt} = \text{number } \frac{l}{b} u' \tag{19.13}$$

Equating of equations (19.12) and (19.13) gives:

$$U_o \frac{db}{dx} \sim \frac{l}{b} u' = \beta u' \tag{19.14}$$

By comparison with equation (19.11) one obtains:

$$b^2 \frac{db}{dx} \sim \frac{\beta}{\pi} c_w F$$

$$\boxed{b \sim \sqrt[3]{\beta c_w F x}} \quad \text{(Wake Circular)} \tag{19.15}$$

By insertion in equation (19.11) results:

$$\boxed{\frac{u'}{U_o} \sim \frac{1}{\pi}\left(\frac{c_w F}{\beta^2 x^2}\right)^{1/3}} \quad \text{(Wake circular)} \tag{19.16}$$

For the plane wake behind a long rod, wing, or the like with the diameter d and the length L, $W = c_w \frac{\rho}{2} U_o^2 L d$ and

$$W = J \sim \rho U_o u' b L$$

and hence:

$$\frac{u'}{U_o} \sim \frac{c_w d}{2 b} \tag{19.17}$$

and from this in combination with equation (19.14):

$$2 b \frac{db}{dx} \sim \beta c_w d$$

$$\boxed{b \sim \sqrt{\beta c_w d x}} \quad \text{(wake plane)} \tag{19.18}$$

By substitution in equation (19.17) results:

$$\boxed{\frac{u'}{U_o} \sim \frac{1}{2}\left(\frac{c_w d}{\beta x}\right)^{1/2}} \quad \text{(Wake plane)} \tag{19.19}$$

Thus, for the circular wake, the width increases with $\sqrt[3]{x}$, and the velocity decreases with $x^{-2/3}$; for the plane wake, the width increases with $\sqrt{x}$, and the velocity decreases with $x^{-1/2}$.

The power laws for the width and the velocity at the center are compiled once more in the following table. The corresponding laminar cases which were partially treated in chapter IX, are included. Moreover, the case of the free jet boundary is given, that is the mixing of a homogeneous air flow with the adjoining air at rest. (Compare figure 97.)

Case	Laminar		Turbulent	
	Width b	Velocity at Center u_{max} or u' respectively	Width b	Velocity at Center u_{max} or u' respectively
Plane jet	$x^{2/3}$	$x^{-1/3}$	x	$x^{-1/2}$
Circular jet	x	x^{-1}	x	x^{-1}
Plane wake	$x^{1/2}$	$x^{-1/2}$	$x^{1/2}$	$x^{-1/2}$
Circular wake	$x^{1/2}$	x^{-1}	$x^{1/3}$	$x^{-2/3}$
Free jet boundary	$x^{1/2}$	x^{0}	x	x^{0}

POWER LAWS FOR THE INCREASE WITH WIDTH AND THE DECREASE OF VELOCITY WITH THE DISTANCE x

For a few of the cases treated here the velocity distribution will be calculated explicitly below. The calculation on the basis of the Prandtl mixing length theorem was performed for the free jet boundary, the plane jet, and the circular jet by W. Tollmien (reference 81), for the plane wake by H. Schlichting (reference 82) and for the circular wake by L. M. Swain (reference 83).

The equations of motion for the plane stationary case are, according to equation (14.14), if the laminar friction terms are completely neglected:

$$\left.\begin{aligned} u\frac{\partial u}{\partial x} + v\frac{\partial u}{\partial y} &= -\frac{1}{\rho}\frac{\partial p}{\partial x} + \frac{1}{\rho}\frac{\partial \sigma_x}{\partial x} + \frac{1}{\rho}\frac{\partial \tau_{xy}}{\partial y} \\ u\frac{\partial v}{\partial x} + v\frac{\partial v}{\partial y} &= -\frac{1}{\rho}\frac{\partial p}{\partial y} + \frac{1}{\rho}\frac{\partial \tau_{xy}}{\partial x} + \frac{1}{\rho}\frac{\partial \sigma_y}{\partial y} \\ \frac{\partial u}{\partial x} + \frac{\partial v}{\partial y} &= 0 \end{aligned}\right\} \quad (19.20)$$

b. The Plane Wake Flow

We shall now calculate the velocity distribution for the plane wake flow. A cylindrical body of diameter d and span h is considered. Further, let

$$u' = U_o - u \tag{19.21}$$

be the wake velocity. One applies the momentum theorem to a control area according to figure 95, the rear boundary B C of which lies at such a large distance from the body that the static pressure there has the undisturbed value. As shown in detail in chapter IX, equation (9.40), one obtains:

$$W = h\,\rho \int_{BC} u\,(U_o - u)\,dy$$

$$W = h\,\rho \int_{BC} (U_o - u')\,u'\,dy \tag{19.22}$$

For large distances behind the body $u' \ll U_o$ so that one may approximately neglect the term u'^2 in comparison with $U_o\,u'$ in equation (19.22). Hence:

$$x \to \infty: \quad W = h\,\rho\,U_o \int_{BC} u'\,dy \tag{19.22a}$$

Since, on the other hand $W = c_w\,d\,h\,\frac{\rho}{2}\,U_o^2$, there becomes:

$$\int_{-b}^{+b} u'\,dy = \frac{1}{2}\,c_w\,d\,U_o \tag{19.23}$$

This problem can be treated with the boundary layer differential equations; they read according to equation (19.20) with the Prandtl expression for the turbulent shearing stress according to equation (15.9), with p and σ_x neglected:

$$\left.\begin{aligned} u\frac{\partial u}{\partial x} + v\frac{\partial u}{\partial y} &= \frac{1}{\rho}\frac{\partial \tau}{\partial y} = 2l^2\frac{\partial u}{\partial y}\frac{\partial^2 u}{\partial y^2} \\ \frac{\partial u}{\partial x} + \frac{\partial v}{\partial y} &= 0 \end{aligned}\right\} \tag{19.24}$$

For the mixing length one puts, according to equation (19.2):

$$l = \beta\ b \tag{19.25}$$

Further:

$$u' = u_1 + u_2 + \ldots * \tag{19.26}$$

$$\eta = \frac{y}{b} \tag{19.27}$$

For the wake velocity u_1 and the width b the power laws for the decrease and increase, respectively, with x were already found in equations (19.18) and (19.19). One therefore writes:

$$\frac{u_1}{U_o} = \left(\frac{x}{c_w d}\right)^{-1/2} f(\eta) \tag{19.28}$$

$$b = B\ (c_{wd}\ x)^{1/2} \tag{19.29}$$

According to equations (19.27) and (19.29)

$$\frac{\partial \eta}{\partial y} = \frac{1}{B(c_w d\ x)^{1/2}}. \qquad \frac{\partial \eta}{\partial x} = -\frac{1}{2}\frac{\eta}{x}$$

The estimation of the terms in equation (19.24) with respect to their order of magnitude in x gives:

$$\frac{\partial u}{\partial x} \sim x^{-3/2};\quad \frac{\partial v}{\partial y} \sim x^{-3/2};\quad \frac{\partial u}{\partial y} \sim x^{-1};\quad \frac{\partial^2 u}{\partial y^2} \sim x^{-3/2};\quad v \sim x^{-1}$$

*The terms u_2 . . . signify additional terms of higher approximation, which disappear according to a higher power of x than does u_1.

Hence the term $v \frac{\partial u}{\partial y} \sim x^{-2}$ whereas the largest terms $\sim x^{-3/2}$. Thus equation (19.24) is simplified to:

$$- U_o \frac{\partial u_1}{\partial x} = 2 l^2 \frac{\partial u_1}{\partial y} \frac{\partial^2 u_1}{\partial y^2} \tag{19.30}$$

The neglected terms are taken into account only in the next approximation. The further calculation gives:

$$\frac{\partial u_1}{\partial x} = U_o \left(\frac{x}{c_w d}\right)^{-1/2} \left[- \frac{1}{2} \frac{\eta}{x} f' - \frac{1}{2x} f \right]$$

$$\frac{\partial u_1}{\partial y} = U_o \left(\frac{x}{c_w d}\right)^{-1/2} f' \frac{1}{B (c_w d\, x)^{1/2}}$$

$$\frac{\partial^2 u_1}{\partial y^2} = U_o \left(\frac{x}{c_w d}\right)^{-1/2} f'' \frac{1}{B^2 c_w d\, x}$$

$$2 l^2 \frac{\partial u_1}{\partial y} \frac{\partial^2 u_1}{\partial y^2} = 2 \beta^2 U_o^2 \left(\frac{x}{c_w d}\right)^{-1} f' f'' \frac{1}{B (c_w d x)^{1/2}}$$

After insertion in equation (19.30) and eliminating the factor $U_o^2 \frac{1}{x} \left(\frac{x}{c_w d}\right)^{-1/2}$ the following differential equation results for $f(\eta)$

$$\frac{1}{2} (f + \eta f') = \frac{2\beta^2}{B} f' f'' \tag{19.31}$$

The boundary conditions are:

$$y = b: \quad u_1 = 0; \quad \frac{\partial u_1}{\partial y} = 0$$

That is:

$$\eta = 1: \quad f = f' = 0 \tag{19.32}$$

The differential-equation (19.30) may immediately be integrated once and gives:

$$\frac{1}{2} f \eta = \frac{\beta^2}{B} f'^2 + \text{Constant}$$

Because of the boundary conditions, the integration constant must equal zero; thus:

$$\frac{1}{2} f \eta = \frac{\beta^2}{B} f'^2$$

This may be integrated in closed form:

$$f^{1/2} \eta^{1/2} = \sqrt{\frac{2\beta^2}{B}} \frac{df}{d\eta}$$

$$\frac{df}{\sqrt{f}} = \sqrt{\frac{B}{2\beta^2}} \sqrt{\eta}\, d\eta$$

$$2f^{1/2} = \sqrt{\frac{B}{2\beta^2}} \frac{2}{3} \eta^{3/2} + \text{Constant}$$

$$f = \left(\frac{1}{3} \sqrt{\frac{B}{2\beta^2}} \eta^{3/2} + C \right)^2$$

Because $f = 0$ for $\eta = 1$, $C = -\frac{1}{3} \sqrt{\frac{B}{2\beta^2}}$ and hence:

$$f = \frac{1}{9} \frac{B}{2\beta^2} \left(1 - \eta^{3/2} \right)^2 \tag{19.33}$$

The condition $f' = 0$ for $\eta = 1$ is simultaneously satisfied according to equation (19.33). In f'', that is $\frac{\partial^2 u}{\partial y^2}$, a singularity results at the center $(\eta = 0)$ and on the edge. For $\eta = 0$, $f'' = \infty$; the velocity profile there has zero radius of curvature. At the edge there exists a discontinuity in curvature. In contrast to the laminar boundary layer solutions, where the velocity asymptotically approaches the value of the potential flow, one obtains here velocity profiles which adjoin the potential flow at a finite distance from the center.

The constant B remains to be determined:

$$\int_{-b}^{+b} u' \, dy = *2\int_{0}^{b} u' \, dy = 2\int_{0}^{b} u_1 \, dy = 2U_o \, c_w d \, B \int_{0}^{1} f(\eta) \, d\eta$$

From equation (19.33) one finds: $2\int_{0}^{1} \left(1 - \eta^{3/2}\right)^2 d\eta = \frac{9}{10}$ and hence:

$$2\int_{0}^{1} f(\eta) \, d\eta = \frac{B}{20\beta^2}$$

and, by comparison with equation (19.23):

$$2\int_{0}^{b} u' \, dy = c_w d \, \frac{B^2}{20\beta^2} U_o = \frac{1}{2} c_w d \, U_o$$

or:

$$\frac{B^2}{20\beta^2} = \frac{1}{2}; \quad B = \sqrt{10}\,\beta \tag{19.34}$$

Thus the final result for the width of the wake and the velocity distribution from equations (19.28) and (19.29) is:

---

*Reviewer's note: Integrating from −1 to +1, as was done in the original German version, results in an imaginary term, which was avoided in the translation by integrating from 0 to +1 and doubling the result.

$$b = \sqrt{10}\,\beta\,(c_w d\,x)^{1/2}$$

$$\frac{u_1}{U_o} = \frac{\sqrt{10}}{18\beta}\left(\frac{x}{c_w d}\right)^{-1/2}\left[1 - \left(\frac{y}{b}\right)^{3/2}\right]^2 \qquad (19.35)$$

The constant $\beta = l/b$ is the only empirical constant of this theory; it must be determined from the measurements.

Comparison with the tests of Schlichting (reference 82) shows that the two power laws (equations (19.28) and (19.29)) are well satisfied, and also that the form of the velocity distribution shows good agreement with equation (19.35), figure 96. The constant β is determined as

$$\beta = \frac{l}{b} = 0.207$$

The solution found is a first approximation for large distances; according to the measurements it is valid for $x/c_w d \geq 50$. For smaller distances one may calculate additional terms which are proportional to x^{-1}, $x^{-3/2}$, . . . for the wake velocity in equation (19.26).

The rotationally-symmetrical wake problem was treated by Miss L. M. Swain (reference 83). For the first approximation results exactly the same function for the velocity distribution; only the power laws for the width b and the velocity at the center u_m' are different, namely $b \sim x^{1/3}$ and $u_m' \sim x^{-2/3}$, as already indicated in equations (19.15) and (19.16).

Fourteenth Lecture (March 9, 1942)

c. The Free Jet Boundary

The plane problem of the mixing of a homogeneous air stream with the adjoining air at rest shall also be treated somewhat more accurately (fig. 97). It is approximately present for instance at the edge of the free jet of a wind tunnel. The problem was solved by Tollmien (reference 81).

The velocity profiles at various distances x are affine. One sets

$$u = U_o f(\eta) = U_o F'(\eta) \qquad (19.36)$$

where

$$\eta = \frac{y}{x}; \quad (b \sim x) \tag{19.37}$$

and

$$F(\eta) = \int f(\eta)\, d\eta$$

Furthermore set

$$l = c\, x = C\, b \tag{19.38}$$

The equation of motion reads:

$$u \frac{\partial u}{\partial x} + v \frac{\partial u}{\partial y} = \frac{1}{\rho} \frac{\partial \tau}{\partial y} = 2\, l^2 \frac{\partial u}{\partial y} \frac{\partial^2 u}{\partial y^2} \tag{19.39}$$

One integrates the continuity equation by the stream function:

$$\Psi = \int u\, dy = U_o\, x \int f(\eta)\, d\eta = U_o\, x\, F(\eta) \tag{19.40}$$

Then:

$$\frac{\partial u}{\partial x} = -\frac{U_o}{x} \eta F''; \quad \frac{\partial u}{\partial y} = \frac{U_o}{x} F''; \quad \frac{\partial^2 u}{\partial y^2} = \frac{U_o}{x^2} F'''$$

$$v = -\frac{\partial \Psi}{\partial x} = -U_o\, (F - \eta F') \tag{19.40a}$$

Substitution into the equation of motion (19.39) gives, after division by U_o^2/x;

$$FF'' + 2c^2\, F''F''' = 0 \tag{19.41}$$

The boundary conditions are:

at the inner edge:

$$\left.\begin{array}{lll} \eta = \eta_1: & u = U_o: & F' = 1 \\ & \dfrac{\partial u}{\partial y} = 0: & F'' = 0 \\ & v = 0: & F = \eta_1 \end{array}\right\} \qquad (19.42)$$

at the outer edge:

$$\left.\begin{array}{lll} \eta = \eta_2: & u = 0: & F' = 0 \\ & \dfrac{\partial u}{\partial y} = 0: & F'' = 0 \end{array}\right\}$$

Since the boundary points η_1 and η_2 are still free, these five boundary conditions can be satisfied by the differential equation of the third order equation (19.41). By introduction of the new variable:

$$\eta^* = \frac{\eta}{\sqrt[3]{2c^2}} \qquad (19.43)$$

the differential equation (19.41) is transformed into ($'$ = differentiation with respect to η^*)

$$F\,F'' + F''\,F''' = 0 \qquad (19.44)$$

The solution $F'' = 0$, which gives u = Constant, is eliminated. The general solution of the linear differential equation

$$F + F''' = 0 \qquad (19.45)$$

is

$$F = e^{\lambda\eta^*}$$

with λ signifying the roots of the equation $\lambda^3 + 1 = 0$, thus:

$$\lambda_1 = -1; \qquad \lambda_{2,3} = \frac{1}{2} \pm \frac{i}{2}\sqrt{3}$$

Hence the general solution is:

$$F = C_1 e^{-\eta^*} + C_2 e^{\frac{\eta^*}{2}} \cos\left(\frac{\sqrt{3}}{2}\eta^*\right) + C_3 e^{\frac{\eta^*}{2}} \sin\left(\frac{\sqrt{3}}{2}\eta^*\right) \qquad (19.46)$$

If, moreover, one measures the η-coordinate from the inner boundary point, thus puts:

$$\overline{\eta^*} = \eta^* - \eta^*_1$$

the solution (equation (19.46)) can also be written:

$$F = d_1 e^{-\overline{\eta^*}} + d_2 e^{\frac{\overline{\eta^*}}{2}} \cos\left(\frac{\sqrt{3}}{2}\overline{\eta^*}\right) + d_3 e^{\frac{\overline{\eta^*}}{2}} \sin\left(\frac{\sqrt{3}}{2}\overline{\eta^*}\right)$$

From the boundary conditions (equation (19.42)) result for the constants the values:

$$\eta^*_1 = 0.981; \qquad \eta^*_2 = -2.04; \qquad \overline{\eta^*_2} = -3.02$$

$$d_1 = -0.0062; \qquad d_2 = 0.987; \qquad d_3 = 0.577$$

For the width of the mixing region one obtains:

$$b = x(\eta_1 - \eta_2) = x\sqrt[3]{2c^2}\,(\eta^*_1 - \eta^*_2)$$

$$b = 3.02\sqrt[3]{2c^2}\,x$$

The constant c must be determined from experiments. From measurements it is found that

$$b = 0.255\,x \qquad (19.47)$$

Hence

$$\sqrt[3]{2c^2} = 0.0845; \qquad c = 0.0174$$

and

$$\frac{l}{b} = 0.0682 \tag{19.48}$$

It is striking that here the ratio l/b is essentially smaller than for the wake.

The distribution of the velocity components u and v over the width of the mixing zone is represented in figure 98.

From the second equation of motion one may calculate the pressure difference between the air at rest p_o and the homogeneous air stream p_1. One finds:

$$p_i - p_o = 0.0048 \frac{\rho}{2} U_o^2 \tag{19.49}$$

Thus an excess pressure of one-half percent is present in the jet. For the inflow velocity of the entrained air one finds according to equation (19.40a):

$$v_{-\infty} = -F(\eta_2)\, U_o = +0.379 \sqrt{2c^2}\, U_o$$

and with the measured value of c;

$$v_{-\infty} = 0.032\, U_o \tag{19.49a}$$

d. The Plane Jet

In a similar manner one may also calculate the plane turbulent jet flowing from a long narrow slot (compare fig. 94). The laws for the increase of the width and the decrease of the center velocity have already been given in equations (19.7) and (19.9): $b \sim x$; $u_m \sim \frac{1}{\sqrt{x}}$. The calculation of the velocity distribution was carried out by Tollmien (reference 81); it leads to a non-linear differential equation of the second order the integration of which is rather troublesome. Measurements for this case were performed by Förthmann (reference 91). In figure 99

the measurements are compared with the theoretical curve. The agreement is rather good. Only in the neighborhood of the velocity maximum is there a slight systematic deviation. There the theoretical curve is more pointed than the measured curve; the theoretical curve, namely, again has at the maximum a vanishing radius of curvature.

According to the Prandtl formula, equation (15.9), the exchange becomes zero at the velocity maximum, whereas actually a small exchange is still taking place.

e. Connection Between Exchange of Momentum, Heat and Material

In concluding the chapter on turbulent flows I should like to make a few remarks about the connection between the turbulent exchange and the heat and material transfer in a turbulent flow.

In the Prandtl theorem equation (15.9) for the apparent turbulent stress:

$$\tau = \rho\, l^2 \left|\frac{\partial u}{\partial y}\right| \frac{\partial u}{\partial y} = A \frac{\partial u}{\partial y} \tag{19.50}$$

one can interpret:

$$A = \rho\, l^2 \left|\frac{\partial u}{\partial y}\right| \left[\frac{\text{kg sec}}{\text{m}^2}\right]$$

as a mixing factor. It has the same dimension as the laminar viscosity μ. Furthermore, the shearing stress τ may be interpreted as a momentum flow:

$$\tau = \frac{\text{momentum}}{\text{m}^2\ \text{sec}} = \text{momentum flow} \tag{19.51}$$

Momentum = mass $\times$ velocity = $\left[\text{kg sec}\right]$.

Another effect of the turbulent mixing phenomena, besides the increased apparent viscosity by transport of momentum, is the transport of all properties inherent in flowing matter, as heat, concentration of impurities, etc. If this concentration is not uniform, more heat or impurity is carried away by the turbulent exchange from the places of higher concentration than is brought back from the places of lower concentration. Thus there results, on the average, transfer from the places of higher to those of lower concentration.

This results, for temperature differences, in a turbulent heat transfer; for concentration differences (for instance, of salt), in a turbulent diffusion. They can, in analogy to equation (19.50) be expressed as follows:

$$\text{Momentum flow} = \frac{\text{momentum transport}}{\text{m}^2\ \text{sec}} = A_T \frac{d}{dy}\left(\frac{\text{momentum}}{\text{unit mass}}\right)$$

$$\text{Heat flow} = \frac{\text{heat transport}}{\text{m}^2\ \text{sec}} = A_Q \frac{d}{dy}\left(\frac{\text{heat}}{\text{unit mass}}\right)$$

$$\text{Flow of material} = \frac{\text{transport of material}}{\text{m}^2\ \text{sec}} = A_M \frac{d}{dy}\left(\frac{\text{material}}{\text{unit mass}}\right)$$

The heat content of the unit mass is $c_p\Theta$ (Θ = temperature, c_p = specific heat = $\left[\frac{\text{cal m}}{\text{kg sec}^2\ \text{degree}}\right]$). For chemical or mechanical concentrations the concentration of material per unit mass is called the concentration c; it is therefore the ratio of two masses and therefore dimensionless. Thus the above equations may also be written in the following forms:

$$\left.\begin{aligned} \tau &= A_T \frac{du}{dy} \\ Q &= -A_Q \frac{d(c_p\Theta)}{dy} \\ M &= -A_M \frac{dc}{dy} \end{aligned}\right\} \qquad (19.52)$$

The question arises as to whether A_T, A_Q, A_M are numerically the same or different. If the momentum is transported exactly like heat or material concentration — Prandtl's theorem is based on this assumption — it would follow that $A_T = A_Q = A_M$ and, for instance, the velocity and temperature distributions in a turbulent mixing region would have to be equal. However, measurements show partially different behavior.

One has to distinguish between wall turbulence and free turbulence. Concerning free turbulence, calculations of G. I. Taylor (reference 92) and measurements of Fage and Falkner (reference 93) showed for the velocity and temperature profile of the plane wake flow

$$\frac{A_Q}{A_T} = 2 \qquad \text{(free turbulence)} \qquad (19.53)$$

The heat exchange is, therefore, larger than the momentum exchange. Consequently the temperature profile is wider than the velocity profile. The theory given for that phenomenon by G. I. Taylor operates with the conception that the particles, in their turbulent exchange movements, do not maintain their momentum (Prandtl), but their vortex strength $\frac{\partial u}{\partial y}$. (Prandtl's momentum exchange theory ~ Taylor's vorticity transfer theory). However, there are cases not satisfied by the Taylor theory (for instance the case of the rotationally symmetrical wake). That the heat exchange for free turbulence is considerably larger than the momentum exchange is also shown by experiments of Gran Olsson (reference 88) concerning the smoothing out of the temperature and velocity distributions behind grids of heated rods. With increasing distance behind the grid the temperature differences even out much more rapidly than the differences in velocity.

For wall turbulence the difference between the mixing factors for momentum and temperature is smaller. H. Reichardt (reference 87) was able to show, from measurements of the temperature distribution in the boundary layer on plates in longitudinal flow by Elias (reference 86) and in pipes by H. Lorenz (reference 14), that here

$$\frac{A_Q}{A_T} = 1.4 \text{ to } 1.5 \qquad \text{(wall turbulence)} \qquad (19.54)$$

Herewith we shall conclude the considerations of free turbulence.

CHAPTER XX: DETERMINATION OF THE PROFILE DRAG FROM THE LOSS OF MOMENTUM

The method, previously discussed in chapter IX, of determining the profile drag from the velocity distribution in the wake is rather important for wind tunnel measurements as well as for flight tests; we shall therefore treat it in somewhat more detail. The determination of the drag by force measurements is too inaccurate for many cases, in the wind tunnel for instance due to the large additional drag of the wire suspension; in some cases (flight test) it is altogether impossible. In these cases the determination of the drag from the wake offers the only serviceable possibility.

The formula derived before in chapter IX, equation (9.41) for determination of the drag from the velocity distribution in the wake is valid only for relatively large distances behind the body. It had been assumed that in the rear control plane (test plane) the static pressure equals the pressure of the undisturbed flow. However, in practically carrying out such tests in the wind tunnel or in flight tests one is

forced to approach the body more closely. Then the static pressure gives rise to an additional term in the formula for the drag. For measurements close behind the body (for instance, for the wing, for $x < t$) this term is of considerable importance, so that it must be known rather accurately. A formula was indicated, first by Betz (reference 84), later by B. M. Jones (reference 85) which takes this correction into consideration. Although at present most measurements are evaluated according to the simpler Jones formula, we shall also discuss Betz' formula since its derivation in particular is very interesting.

a. The Method of Betz

One imagines a control surface surrounding the body as shown in figure 100. In the entrance plane I ahead of the body there is flow with free-stream total pressure g_o, behind the body in plane II, the total pressure $g_2 < g_o$. The lateral boundaries are to lie at so large a distance from the body that the flow there is undisturbed. In order to satisfy the continuity condition for the control surface the velocity u_2 in plane II must be partially greater than the undisturbed velocity U_o. Consider the plane problem; let the body have the height h.

Application of the momentum theorem to the control surface gives:

$$W = h\left[\int_{-\infty}^{+\infty}\left(p_1 + \rho u_1^2\right)dy - \int_{-\infty}^{+\infty}\left(p_2 + \rho u_2^2\right)dy\right] \qquad (20.1)$$

In order to make this formula useful for test evaluation the integrals must be transformed in such a manner that the integrals need to be extended only over the "wake". For the total pressures

$$\left.\begin{aligned} &\text{at infinity:} && g_o = p_o + \frac{\rho}{2}U_o^2 \\ &\text{in plane I:} && g_o = p_1 + \frac{\rho}{2}u_1^2 \\ &\text{in plane II:} && g_2 = p_2 + \frac{\rho}{2}u_2^2 \end{aligned}\right\} \qquad (20.2)$$

Outside of the wake the total pressure everywhere equals g_o. Hence equation (20.1) becomes

$$W = h\left[\int_{-\infty}^{+\infty}\left(g_o - g_2\right)dy + \frac{\rho}{2}\int_{-\infty}^{+\infty}\left(u_1^2 - u_2^2\right)dy\right] \qquad (20.3)$$

Thus the first integral already has the desired form, since the integrand differs from zero only within the wake. In order to give the same form to the second integral, one introduces a hypothetical substitute flow $u_2'(y)$ in plane II which agrees with u_2 everywhere outside of the wake, but differs from u_2 within the wake by the fact that the total pressure for u_2' equals g_o. Thus

$$g_o = p_2 + \frac{\rho}{2}u'^2_2 \qquad (20.4)$$

Since the actual flow u_1, u_2 satisfies the continuity equation the flow volume across section II for the hypothetical flow u_1, u_2' is too large. It shows a source essentially at the location of the body which has the strength

$$Q = h\int\left(u_2' - u_2\right)dy \qquad (20.5)$$

A source in a frictionless parallel flow experiences a forward thrust

$$R = -\rho U_o Q \qquad (20.6)$$

One now again applies the momentum theorem according to equation (20.3) for the hypothetical flow with the velocity u_1 at the cross section I and the velocity u'_2 at the cross section II. Since $g_2' = g_o$ and the resultant force, according to equation (20.6), equals R, one obtains

$$-\rho U_o Q = \frac{\rho}{2}h\int\left(u_1^2 - u'^2_2\right)dy \qquad (20.7)$$

By subtraction of equation (20.7) from equation (20.3) there results

$$W + \rho U_o Q = h\left[\int\left(g_o - g_2\right)dy + \frac{\rho}{2}\int\left(u'^2_2 - u_2^2\right)dy\right] \qquad (20.8)$$

or because of equations (20.5) and (20.6):

$$W = h\left[\int\left(g_o - g_2\right)dy + \frac{\rho}{2}\int\left(u'^2_2 - u_2^2\right)dy - \rho\, U_o\int\left(u'_2 - u_2\right)dy\right]$$

One may now perform each of these integrations only across the wake, since outside of the wake $u'_2 = u_2$. Due to $u'^2_2 - u_2^2 = \left(u'_2 - u_2\right)\left(u'_2 + u_2\right)$ a transformation gives the following formula:

$$\boxed{W = h\left[\int\left(g_o - g_2\right)dy + \frac{\rho}{2}\int\left(u'_2 - u_2\right)\left(u'_2 + u_2 - 2U_o\right)dy\right]} \quad (20.9)$$

Betz' Formula

In order to determine W according to this equation, one has to measure in the test cross section behind the body the following values:

1. Total pressure g_2 (therewith g_o is the value of g_2 outside of the wake).
2. Static pressure p_2.

Furthermore, p = static pressure at infinity.

Hence one obtains all quantities required for the evaluation of equation (20.9).

It is useful for the evaluation of wind tunnel tests to introduce dimensionless quantities. With $F = ht$ as area of reference for the drag:

$$W = c_w\, h\, t\, \frac{\rho}{2}\, U_o^2$$

and hence from equation (20.9):

$$\boxed{c_w = \int\frac{g_o - g_2}{q_o}\, d\left(\frac{y}{t}\right) + \int\left(\sqrt{\frac{g_o - p_2}{q_o}} - \sqrt{\frac{g_2 - p_2}{q_o}}\right)\left(\sqrt{\frac{g_o - p_2}{q_o}} + \sqrt{\frac{g_2 - p_2}{q_o}} - 2\right)d\left(\frac{y}{t}\right)} \quad (20.10)$$

For the case in which $p_2 = p_o = 0$, at the test cross section one can write this equation, because $g_o = q_o$:

$$c_w = \int\left(1 - \frac{g_2}{q_o}\right) d\,\frac{y}{t} - \int\left(1 - \sqrt{\frac{g_2}{q_o}}\right)\left(1 - \sqrt{\frac{g_2}{q_o}}\right) d\,\frac{y}{t}$$

$$= \int\left(1 - \frac{g_2}{q_o}\right) d\,\frac{y}{t} - \int\left(1 - 2\sqrt{\frac{g_2}{q_o}} + \frac{g_2}{q_o}\right) d\,\frac{y}{t}$$

$$c_w = 2\int \sqrt{\frac{g_2}{q_o}}\left(1 - \sqrt{\frac{g_2}{q_o}}\right) d\,\frac{y}{t}$$

$$c_w = 2\int \frac{u_2}{U_o}\left(1 - \frac{u_2}{U_o}\right) d\,\frac{y}{t} \qquad (20.11)$$

This agrees with equation (9.41).* Thus in this case Betz' formula changes, as was to be expected, into the previous simple formula.

b. The Method of Jones

Later B. M. Jones (reference 85) indicated a similar method which in its derivation and final formula is somewhat simpler than Betz' method.

Let cross section II (fig. 101) (the test cross section) lie close behind the body; there the static pressure p_2 is still noticeably different from the static pressure p_o. Let cross section I be located so far behind the body that the static pressure there equals the undisturbed static pressure. Then there applies for cross section I according to equation (9.41)*

$$W = h\,\rho \int_I u_1\left(U_o - u_1\right) dy_1 \qquad (20.12)$$

In order to relate the value of u_1 back to measurements at cross section II, continuity for a stream filament is first applied:

$$\rho\, u_1\, dy_1 = \rho\, u_2\, dy_2 \qquad (20.13)$$

---

* In chapter IX the total drag of the body (both sides of the plates) was designated by 2 W; here the entire drag equals W!

Jones makes the further assumption that the flow from cross section II to cross section I is without loss, that is, that the total pressure is constant along each stream line from II to I:

$$g_2 = g_1 \tag{20.14}$$

First, according to equations (20.12) and (20.13):

$$W = h\rho \int u_2\left(U_o - u_1\right) dy_2 \tag{20.15}$$

Furthermore:

$$\left.\begin{aligned} p_o + \frac{\rho}{2} U_o^2 &= g_o = q_o \qquad \text{with} \quad p_o = 0 \\ p_o + \frac{\rho}{2} u_1^2 &= g_1 = g_2 \\ p_2 + \frac{\rho}{2} u_2^2 &= g_2 \end{aligned}\right\} \tag{20.16}$$

and hence

$$\frac{u_2}{U_o} = \sqrt{\frac{g_2 - p_2}{q_o}}; \qquad \frac{u_1}{U_o} = \sqrt{\frac{g_2}{q_o}} \tag{20.17}$$

From equation (20.12) follows, with $W = c_w \, t \, h \, \frac{\rho}{2} U_o^2$:

$$c_w = 2 \int \frac{u_2}{U_o} \left(1 - \frac{u_1}{U_o}\right) d \, \frac{y_2}{t}$$

and because of equation (20.17):

$$\boxed{c_w = 2 \int_{II} \sqrt{\frac{g_2 - p_2}{q_o}} \left(1 - \sqrt{\frac{g_2}{q_o}}\right) d \, \frac{y_2}{t}} \tag{20.18}$$

Formula of Jones

Thus all quantities may be measured in cross section II close to the body. This formula is simpler for the evaluation than Betz' formula, equation (20.10).

In the limit, when the static pressure in the test cross section becomes $p_2 = p_o$, this formula, of course, must also transform into the simple formula equation (20.11). One obtains for $p_2 = p_o = 0$ from equation (20.18):

$$c_w = 2\int \sqrt{\frac{g_2}{q_o}}\left(1 - \sqrt{\frac{g_2}{q_o}}\right) d\,\frac{y}{t} = 2\int \frac{u_2}{U_o}\left(1 - \frac{u_2}{U_o}\right) d\,\frac{y}{t}$$

This is in agreement with equation (9.41).

Fifteenth Lecture (March 16, 1942)

CHAPTER XXI: ORIGIN OF TURBULENCE

a. General Remarks

In this section a short summary of the theory of the origin of turbulence will be given. The experimental facts concerning laminar/turbulent transition for the pipe flow and for the boundary layer on the flat plate have been discussed in chapter XIII. The position of the transition point is extremely important for the drag problem, for instance for the friction drag of a wing, since the friction drag depends to a great extent on the position of the transition point.

The so-called critical Reynolds number determines transition. For the pipe $(\bar{u}d/\nu)_{crit} = 2300$, and for the boundary layer on the plate $(U_o x/\nu)_{crit} = 3$ to 5×10^5. However, experimental investigations show the value of the critical Reynolds number is very dependent on the initial disturbance. The value of Re_{crit} is the higher the smaller the initial disturbance. For the pipe flow the magnitude of the initial disturbance is given by the shape of the inlet, for the plate flow by the degree of turbulence of the oncoming flow. For the pipe, for instance, a critical Reynolds number $(\bar{u}d/\nu)_{crit} = 40{,}000$ can be attained with very special precautionary measures.

According to today's conception regarding the origin of turbulence, transition is a stability phenomenon. The laminar flow in itself is a solution of the Navier-Stokes differential equations up to arbitrarily high Reynolds numbers. However, for large Re-numbers the laminar flow

becomes unstable, in the sense that small chance disturbances (fluctuations in velocity) present in the flow increase with time and then alter the entire character of the flow. This conception stems from Reynolds (reference 101). Accordingly, it ought to be possible to obtain the critical Reynolds number from a stability investigation of the laminar flow.

Theoretical efforts to substantiate these assumptions of Reynolds mathematically reach rather far back. Besides Reynolds, Rayleigh (reference 102) in particular worked on the problem. These theoretical attempts did not meet with success for a long time, that is, no instability could be established in the investigated laminar flows. Only very recently has success been attained, for certain cases, in the theoretical calculation of a critical Reynolds number.

One assumes for the theoretical investigations that upon the basic flow which satisfies the Navier-Stokes differential equations a disturbance motion is superimposed. One then investigates whether the disturbance movement vanishes again under the influence of friction or whether it increases with time and thus leads to ever growing deviations from the basic flow. The following relations will be introduced for the plane case:

$$\left.\begin{array}{ll} \text{basic flows:} & U(x, y);\ V(x, y);\ P(x, y) \\ \text{disturbance movement:} & u'(x, y);\ v'(x, y);\ p'(x, y) \\ \text{resultant movement:} & U + u';\ V + v';\ P + p' \end{array}\right\} \qquad (21.1)$$

P, p' signify pressure. The investigation of the stability of such a disturbed movement was carried out essentially according to two different methods:

1. Calculation of the energy of the disturbance movement.

2. Calculation of the development of the disturbance movement with time according to the method of small oscillations.

I am going to say only very little about the first method since it was rather unsuccessful. The second method was considerably more successful and will therefore be treated in more detail later.

The first method was elaborated mainly by H. A. Lorenz (reference 103). The following integral expression may be derived for the energy balance of the disturbance movement:

$$\frac{D}{Dt}\int E\,dV = \rho\int M\,dV - \mu\int N\,dV \qquad (21.2)$$

In it $E = \frac{\rho}{2}\left(u'^2 + v'^2\right)$ signifies the kinetic energy of the disturbance movement. The integration is performed over a space which participates in the movement of the basic flow and at the boundaries of which the velocity equals zero. $\frac{D}{Dt}$ signifies the substantial derivative. Thus one finds on the left side of equation (21.2) the increase with time of the energy of the disturbance movement. On the right side,

$$\left.\begin{aligned} M &= -\left[u'^2\frac{\partial U}{\partial x} + v'^2\frac{\partial V}{\partial y} + u'v'\left(\frac{\partial U}{\partial y} + \frac{\partial V}{\partial x}\right)\right] \\ N &= \left(\frac{\partial v'}{\partial x} - \frac{\partial u'}{\partial y}\right)^2 \end{aligned}\right\} \quad (21.3)$$

The first integral signifies the energy transfer from the main to the secondary movement, the second the dissipation of the energy of the secondary movement. If the right side is greater than zero, the intensity of the secondary movement increases with time, and the basic flow is thus unstable. An assumed disturbance movement u', v' satisfies merely the continuity equation, but no heed is paid to its compatibility with the equations of motion. If one could prove that the right side is negative for any arbitrary disturbance movement u', v' this would serve as proof of the stability of the basic flow. On the other hand, the instability would be proved as soon as the right side is positive for a possible disturbance. Unfortunately general investigations in this direction are very difficult and have not led to much success. H. A. Lorenz (reference 103) treated as an example the Couette-flow (fig. 102), assuming an elliptical vortex as a superimposed disturbance movement. He found for this case $\left(\frac{U_o d}{\nu}\right)_{krit} = 288$, whereas Couette's measurements for this case gave the value 1900.

b. The Method of Small Oscillations

For the second method (method of small oscillations) the disturbance movement is actually calculated, that is, its dependance on the spatial coordinates x, y and the time t is developed on the basis of the hydrodynamic equations of motion. We shall explain this method of small oscillations in the case of a plane flow. In view of the applications of this method we shall immediately assume a special basic flow: the component U, namely, is to be dependent only on y and t and $V \equiv 0$. Such basic flows had been previously called "layer flows". They exist for instance in tunnel flow and pipe flow, approximately, however, also in the boundary layer since here the dependence of the velocity component U on the longitudinal coordinate x is very much smaller than the dependence on the transverse coordinate y. One now assumes a basic flow

$$U(y, t); \quad V \equiv 0; \quad P(x, y) \tag{21.4}$$

This basic flow, by itself, then satisfies the Navier–Stokes equations, thus

$$\left.\begin{aligned} \frac{\partial U}{\partial t} + \frac{1}{\rho}\frac{\partial P}{\partial x} &= \nu \frac{\partial^2 U}{\partial y^2} \\ \frac{\partial P}{\partial y} &= 0 \end{aligned}\right\} \tag{21.5}$$

A disturbance movement which is also two–dimensional is superimposed upon this basic flow:

$$\text{disturbance motion:} \quad u'(x,y,t); \quad v'(x,y,t); \quad p'(x,y,t) \tag{21.6}$$

One then has as the

$$\text{resultant motion:} \quad u = U + u'; \quad v = 0 + v'; \quad p = P + p' \tag{21.7}$$

This resultant motion is required to satisfy the Navier–Stokes differential equations and one investigates whether the disturbance motion dies away or increases with time. The selection of the initial values of the disturbance motion is rather arbitrary, but it must of course satisfy the continuity equation. The superimposed disturbances are assumed as "small", in the sense that all quadratic terms of the disturbance components are neglected relative to the linear terms. According to whether the disturbance motion fades away or increases with time, the basic flow is called stable or unstable.

By insertion in the Navier–Stokes differential equations (3.18) one obtains, neglecting the quadratic terms in the disturbance velocities

$$\left.\begin{aligned} \frac{\partial U}{\partial t} + \frac{\partial u'}{\partial t} + U\frac{\partial u'}{\partial x} + v'\frac{\partial U}{\partial y} + \frac{1}{\rho}\frac{\partial P}{\partial x} + \frac{1}{\rho}\frac{\partial p'}{\partial x} &= \nu\left(\frac{\partial^2 U}{\partial y^2} + \Delta u'\right) \\ \frac{\partial v'}{\partial t} + U\frac{\partial v'}{\partial x} + \frac{1}{\rho}\frac{\partial P}{\partial y} + \frac{1}{\rho}\frac{\partial p'}{\partial y} &= \nu \Delta v' \\ \frac{\partial u'}{\partial x} + \frac{\partial v'}{\partial y} &= 0 \end{aligned}\right\} \tag{21.8}$$

If one now notes the fact that the basic flow by itself satisfies the Navier–Stokes differential equations, equation (21.5), equation (21.8) is simplified to:

$$\left.\begin{aligned} \frac{\partial u'}{\partial t} + U\frac{\partial u'}{\partial x} + v'\frac{\partial U}{\partial y} + \frac{1}{\rho}\frac{\partial p'}{\partial x} &= \nu \Delta u' \\ \frac{\partial v'}{\partial t} + U\frac{\partial v'}{\partial x} + \frac{1}{\rho}\frac{\partial p'}{\partial y} &= \nu \Delta v' \\ \frac{\partial u'}{\partial x} + \frac{\partial v'}{\partial y} &= 0 \end{aligned}\right\} \qquad (21.9)$$

The pertinent boundary conditions are: Vanishing of the disturbance components u' and v' on the bounding walls. From the system equation (21.9) of three equations with three unknown quantities u', v', p' one may at first eliminate p' by differentiating the first equation with respect to y and the second with respect to x and then subtracting the second from the first. This gives, with continuity taken into consideration:

$$\left.\begin{aligned} &\frac{\partial^2 u'}{\partial t \partial y} + U\frac{\partial^2 u'}{\partial x \partial y} + v'\frac{\partial^2 U}{\partial y^2} - \frac{\partial^2 v'}{\partial t \partial x} - U\frac{\partial^2 v'}{\partial x^2} \\ &\quad = +\nu\left(\frac{\partial^3 u'}{\partial x^2 \partial y} + \frac{\partial^3 u'}{\partial y^3} - \frac{\partial^3 v'}{\partial x \partial y^2} - \frac{\partial^3 v'}{\partial x^3}\right) \end{aligned}\right\} \qquad (21.10)$$

In addition to this there is the continuity equation (21.9). There are now two equations with two unknown quantities u', v'.

Form of the Disturbance Movement

For cases where the basic flow predominantly flows in one direction as for instance boundary–layer or pipe flow, the disturbance motion is assumed to be a wave progressing in the x–direction (= main flow direction), the amplitude of which depends solely on y. The continuity equation of the disturbance motion may in general be integrated by a disturbance function for which the following expression may be used:

$$\psi(x,y,t) = \varphi(y)e^{i\alpha(x-ct)} \qquad (21.11)^*$$

Where:

$\lambda = 2\pi/\alpha$ the wave length of the disturbance (α = real)

$c = c_r + i\,c_i$

c_r = velocity of wave propagation

c_i = amplification factor; $c_i < 0$: stable; $c_i > 0$: unstable

$\varphi(y) = \varphi_r(y) + i\,\varphi_i(y)$ = amplitude of the disturbance movement

From equation (21.11) one obtains for the components of the disturbance movement

$$\left.\begin{aligned} u' &= \frac{\partial\psi}{\partial y} = \varphi'(y)e^{i\alpha(x-ct)} \\ v' &= -\frac{\partial\psi}{\partial x} = -i\alpha\varphi(y)e^{i\alpha(x-ct)} \end{aligned}\right\} \qquad (21.13)$$

By substitution into equation (21.10) one obtains the following differential equation for the disturbance amplitude φ:

$$i\alpha\left(U\varphi'' - c\varphi'' - \varphi U'' + \alpha^2 c\varphi - U\alpha^2\varphi\right) = \nu\left(\varphi'''' - 2\alpha^2\varphi'' + \alpha^4\varphi\right)$$

or

$$(U-c)(\varphi'' - \alpha^2\varphi) - U''\varphi = \frac{-i\nu}{\alpha}(\varphi'''' - 2\alpha^2\varphi'' + \alpha^4\varphi) \qquad (21.14)$$

One introduces dimensionless quantities into this equation by referring all velocities to the maximum velocity U_m of the basic flow (that is for the friction layer the potential flow outside of the boundary layer and all lengths to a suitable reference length δ) (for instance, for

---

*The convenient complex formulation is used here. The real part of the flow function, which alone has physical significance, is therefore

$$\mathrm{Re}(\psi) = e^{c_i t}\left\{\varphi_r \cos\left[\alpha\left(x - c_r t\right)\right] - \varphi_i \sin\left[\alpha\left(x - c_r t\right)\right]\right\} \qquad (21.12)$$

the boundary layer flow, the boundary layer thickness). Furthermore, differentiation with respect to the dimensionless quantity y/δ will be designated by a prime mark ($'$).

One then obtains from equation (21.14)

$$\boxed{(U - c)(\varphi'' - \alpha^2\varphi) - U''\varphi = -\frac{i}{\alpha R}(\varphi'''' - 2\alpha^2\varphi'' + \alpha^4\varphi)} \qquad (21.15)$$

DISTURBANCE DIFFERENTIAL EQUATION

where $R = \frac{U_m\delta}{\nu}$. This is the disturbance differential equation for the amplitude φ of the disturbance movement. The boundary conditions are, for instance, for a boundary layer flow

$$\left.\begin{aligned} &y = 0 \text{ (wall)}: \quad u' = v' = 0: \quad \varphi = \varphi' = 0 \\ &y = \infty \qquad\quad : \quad u' = v' = 0: \quad \varphi = \varphi' = 0 \end{aligned}\right\} \qquad (21.16)$$

The stability investigation is an eigenvalue problem of this differential equation for the disturbance amplitude $\varphi(y)$ in the following sense: A basic flow $U(y)$ is prescribed which satisfies the Navier–Stokes differential equations. Also prescribed is the Reynolds number R of the basic flow and the reciprocal wave length $\alpha = 2\pi/\lambda$ of the disturbance movement. From the differential equation (21.15) with the boundary conditions equation (21.16) the eigenvalue $c = c_r + i\,c_i$ is to be determined. The sign of the imaginary part of this characteristic value determines the stability of the basic flow. For $c_i < 0$ the particular flow (U, R) is, for the particular disturbance α, stable; for $c_i > 0$, unstable. The case $c_i = 0$ gives the neutrally stable disturbances. One can represent the result of the stability calculation for an assumed basic flow $U(y)$ in an α, R–plane in such a manner that a pair of values c_r, c_i belongs to each point of the α, R–plane. In particular the curve $c_i = 0$ in the α, R–plane separates the stable from the unstable disturbances. It is called the neutral stability curve (fig. 103). In view of the test results one expects only stable disturbances to be present at small Reynolds numbers for all wave lengths α, unstable disturbances, however, for at least a few α at large Reynolds numbers. The tangent to the neutral stability curve parallel to the α–axis gives the critical Reynolds number of the respective basic flow (fig. 103).

Methods of Solution and General Properties of the Disturbance

Differential Equation

Since the stability limit ($c_1 = 0$) is expected to occur at large Reynolds numbers, it suggests itself to suppress the friction terms in the general disturbance differential equation and to obtain approximate solutions from the so-called frictionless disturbance differential equation which reads

$$\boxed{(U - c)\,(\varphi'' - \alpha^2\varphi) - U''\varphi = 0} \tag{21.17}$$

Only two of the four boundary conditions, equation (21.16), of the complete disturbance differential equation can now be satisfied since the frictionless disturbance differential equation is of the second order. The remaining boundary conditions are:

$$y = 0: \quad v' = 0, \ \varphi = 0; \quad y = \infty: \quad v' = 0: \quad \varphi = 0 \tag{21.18}$$

The cancellation of the friction terms in the disturbance differential equation is very serious, because the order of the differential equation is thereby lowered from 4 to 2 and thus important properties of the general solution of the disturbance differential equation of the fourth order possibly are lost. (Compare the previous considerations in chapter IV concerning the transition from the Navier-Stokes differential equations to potential flow.)

An important special solution of equation (21.17) is the one for a constant basic flow, U = constant, which is needed for instance for the stability investigation of a boundary layer flow as a joining solution for an outer potential flow. One obtains from equation (21.17) for

$$U = \text{constant}: \quad \varphi = e^{\pm \alpha y}$$

However, due to the boundary conditions for φ at $y = \infty$, the only permissible solution is

$$\varphi = e^{-\alpha y} \tag{21.19}$$

We shall prove at first two general theorems of Rayleigh on the neutral and unstable oscillations of the frictionless disturbance differential equation.

Theorem I: The wave velocity c_r for a velocity profile with $U''(y) \leq 0$ must, for a neutral oscillation ($c_i = 0$, $c = c_r$), equal the basic velocity at a point so that there exists within the flow a point $U - c = 0$.

Proof: (indirect) One makes the assumption $c > U_m$ (= maximum velocity of the basic flow). One then forms from equation (21.17) the following differential expressions:

$$L(\varphi) = \varphi'' - \alpha^2\varphi - \frac{U''}{U - c}\varphi = 0 \tag{21.20a}$$

and

$$\overline{L(\varphi)} = \overline{\varphi}'' - \alpha^2\overline{\varphi} - \frac{U''}{U - \overline{c}}\overline{\varphi} = 0 \tag{21.20b}$$

$\overline{L(\varphi)}$ signifies the expression obtained from $L(\varphi)$, if one inserts everywhere the conjugate complex quantities. Because of the boundary conditions

$$y = 0: \quad \varphi = \overline{\varphi} = 0$$

$$y = \infty: \quad \varphi = \overline{\varphi} = 0$$

One forms further the expression $\overline{\varphi}L(\varphi) + \varphi\,\overline{L(\varphi)}$ and integrates it between the limits $y = 0$ and $y = \infty$. The integrals may be taken up to $y = \infty$, since for large y, $\varphi \sim e^{-\alpha y}$. Because of equation (21.20a, b) J_1 must then be

$$J_1 = \int_{y=0}^{\infty} \left[\overline{\varphi}\, L(\varphi) + \varphi\, \overline{L(\varphi)} \right] dy = 0 \tag{21.21}$$

After insertion of equation (21.20a and b) results, because $\overline{c} = c$,

$$J_1 = \int_{y=0}^{\infty} \left(\overline{\varphi}\,\varphi'' + \overline{\varphi}''\varphi - 2\alpha^2\varphi\overline{\varphi} - 2\,\frac{U''}{U - c}\,\varphi\overline{\varphi} \right) dy = 0$$

or

$$J_1 = \left[\bar{\varphi}\varphi' + \bar{\varphi}'\varphi\right]_0^\infty - 2\int_0^\infty \varphi'\bar{\varphi}'dy - 2\int_0^\infty \left(\alpha^2 + \frac{U''}{U-c}\right)\varphi\bar{\varphi}\,dy = 0$$

The first term vanishes due to the boundary conditions, hence there remains

$$J_1 = -2\int_{y=0}^\infty \left[\varphi'\bar{\varphi}' + \left(\alpha^2 + \frac{U''}{U-c}\right)\varphi\bar{\varphi}\right]dy = 0 \qquad (21.22)$$

$\varphi'\bar{\varphi}'$ as well as $\varphi\bar{\varphi}$ are positive throughout; if $U'' \leq 0$ and $c > U_m$, $U''/U - c \geq 0$ and hence the integrand in equation (21.22) is positive throughout. Thus the integral cannot become zero. The assumption made at the beginning $c > U_m$ therefore leads to a contradiction.

For basic flows with $U'' \leq 0$, as for instance boundary-layer flows in a pressure drop, the wave propagation velocity therefore must be smaller than U_m for neutral disturbances. Hence a point $U - c = 0$ exists within the flow. This point is a singular point of the frictionless disturbance differential equation (21.17) and plays as such a special role for the investigation of this differential equation. The wall distance y at which $U - c = 0$ is called $y = y_K$ = critical layer.

This first Rayleigh theorem proved above applies – as shall be noted here without proof – in the same manner tc flows with $U'' > 0$.

Sixteenth Lecture (March 23, 1942)

Theorem II: A necessary condition for the presence of amplified oscillations $(c_i > 0)$ is the presence of an inflection point within the basic flow $(U'' = 0)$.

Proof: (indirect) According to assumption, $c_i \neq 0$; thus $U - c \neq 0$ for all y. With $L(\varphi)$ and $\overline{L(\varphi)}$ one forms, according to equation (21.20a) and (21.20b), a similar expression as before. This latter, integrated from $y = 0$ to $y = \infty$, must again give 0, thus

$$J_2 = \int_{y=0}^\infty \left[\bar{\varphi}\,L(\varphi) - \varphi\,\overline{L(\varphi)}\right]dy = 0 \qquad (21.23)$$

By substitution according to equation (21.20a and b) results with $\bar{c} = c_r - i\,c_i$

$$J_2 = \int_{y=0}^{\infty} \left[\bar{\varphi}\varphi'' - \varphi\bar{\varphi}'' - \varphi\bar{\varphi}\left(\frac{U''}{U-c} - \frac{U''}{U-\bar{c}} \right) \right] dy = 0$$

or

$$J_2 = \left[\bar{\varphi}\varphi' - \varphi\bar{\varphi}' \right]_0^{\infty} - 2i\,c_i \int_0^{\infty} \frac{U''}{|U-c|^2}\,\varphi\bar{\varphi}\,dy = 0 \qquad (21.24)$$

The first term again vanishes because of the boundary conditions. Since $\varphi\bar{\varphi}$ is positive throughout and $|U-c| \neq 0$, the integral can only vanish if U'' changes its sign, that is, an inflection point of the velocity profile $U'' = 0$ must be present within the flow. It has, therefore, been proved: In order to make the presence of amplified oscillations possible, an inflection point must exist in the velocity profile of the basic flow, or, expressed briefly, such oscillations are possible only for inflection point profiles.

Later on Tollmien (reference 110) proved that the presence of an inflection point is not only a necessary but also a sufficient condition for the existence of amplified oscillations. Hence the following simple statement is valid: Inflection point profiles are unstable. It must be mentioned that all these considerations apply in the limiting case $R \to \infty$ since the proofs were obtained from the frictionless disturbance differential equation.

We know from our previous considerations about the laminar boundary layer that inflection point profiles always exist in the region of pressure rise, whereas in the pressure drop region the boundary layer profiles are always without an inflection point, (fig. 104). Hence we recognize that the pressure rise or pressure drop is of decisive significance for the stability of a boundary layer flow.

The converse of the theorem just set up is also valid, namely, that for $R \to \infty$ velocity profiles without inflection point are always stable. From this, however, one must not conclude that profiles without inflection point are stable for all Reynolds numbers. A closer investigation for Reynolds numbers of finite magnitude shows that there profiles without an inflection point also become unstable. One is faced with the peculiar fact that the transition from Re = ∞ to Re-number of finite magnitude, that is, the addition of a small viscosity to a frictionless flow, has a

destabilizing effect, whereas one intuitively expects the opposite. As later considerations will show in more detail, the typical difference between the neutral stability curves of a basic flow with and without inflection point appears as represented in figure 105. For the velocity profile without an inflection point the lower and the upper branch of the neutral curve have, for $R \longrightarrow \infty$, the same asymptote $\alpha = 0$. For the velocity profile with inflection point the lower and upper branch of the neutral curve have, for $R \longrightarrow \infty$, different asymptotes so that for $R = \infty$ a certain wave length region of unstable disturbances exists. Furthermore the critical Reynolds number is smaller for velocity profiles with an inflection point than for those without an inflection point.

Hence it is to be expected for very large Re-number, to a first, very rough approximation, that the transition point in the boundary layer of a body lies at the pressure minimum. Figure 106 shows schematically the pressure distribution for a rather strongly cambered wing profile at a small lift coefficient. The transition point would be expected in this case just behind the nose on the pressure side, slightly more toward the rear on the suction side.

Solution of the Disturbance Differential Equation

In order to perform the actual calculation for the boundary-value problem just formulated, one needs at first a fundamental system $\varphi_1, \ldots \varphi_4$ of the general disturbance differential equation (21.15). One imagines the basic flow $U(y)$ given in the form of a power series development:

$$U(y) = U_o' \, y + \frac{U_o''}{2!} y^2 + \ldots . \qquad (21.24)$$

If one introduces this expression into equation (21.15) and then wants to construct a solution from the complete differential equation which satisfies the boundary conditions (equation (21.16)), one encounters extreme difficulties of calculation, due to the two conditions to be satisfied for $y = \infty$. In order to obtain any solution at all, one has to make various simplifications. The simplifications concern:

1. The basic flow: Instead of the general Taylor-series equation (21.24) one takes only a few terms, thus for instance a linear or a quadratic velocity distribution.

2. The disturbance differential equation: For calculation of the particular solutions the disturbance differential equation is considerably simplified.

Regarding 1, it should be noted that linear velocity distributions frequently have been investigated with respect to stability, as for

instance the Couette flow according to figure 102 or a polygonal approximation for curved velocity profiles according to figure 107. This facilitates the calculation due to the fact that then the singular point $U - c = 0$ is avoided in the frictionless disturbance differential equation (21.17) for neutral disturbances. However, all investigations with linear velocity distributions (references 104, 105, 106) were unsuccessful with the frictionless as well as with the complete differential equation. No critical Reynolds number resulted. When one later took for a basis parabolic profiles, these negative results became intelligible. One must, therefore, take at least a parabolic distribution as a basis for the basic flow.

Regarding 2, it should be noted that one can provide approximate solutions for the solutions of the complete differential equation (21.15) from the frictionless differential equation (21.17) since the solutions are required only for large Re-number R. The frictionless differential equation however can yield no more than two particular solutions; two more have to be calculated, taking the largest friction terms in equation (21.15) into consideration.

The course of the calculation for the particular solutions will be briefly indicated. One limits oneself to neutral disturbances, assumes a parabolic velocity distribution, and imagines the latter developed in the neighborhood of the critical layer.

$$y = y_K: \quad U - c = U - c_r = 0$$

$$U - c = U'_K\left(y - y_K\right) + \frac{U''_K}{2}\left(y - y_K\right)^2 \tag{21.25}$$

The first pair of solutions φ_1, φ_2 is then obtained from the frictionless disturbance differential equation (21.17) by substitution of equation (21.25). According to known theorems about linear differential equations with a singular point a linearly independent pair of solutions has the form

$$\begin{aligned} \varphi_1 &= \left(y - y_K\right) P_1\left(y - y_K\right) \\ \varphi_2 &= P_2\left(y - y_K\right) + \frac{U''_K}{U'_K}\left(y - y_K\right) \log\left(y - y_K\right) P_1\left(y - y_K\right) \end{aligned} \tag{21.26}$$

P_1 and P_2 are power series with a constant term different from zero. The particular solution φ_2 is especially interesting.

$$\varphi'_2 \longrightarrow \infty \text{ for } y = y_K$$

That is, the u'-component of the disturbance velocity becomes infinitely large in the critical layer. This can also be understood directly from the frictionless disturbance differential equation (21.17). According to equation (21.17)

$$\varphi'' - \alpha^2\varphi = \frac{U''}{U - c}\varphi$$

or

$$\varphi'' \sim \frac{1}{y - y_K}; \quad \varphi' \sim \log\left(y - y_K\right), \text{ if } U''_K \neq 0$$

This singular behavior of the solution φ_2 in the critical layer stems of course from neglecting the friction. The frictionless differential equation here no longer gives a serviceable approximation. In the neighborhood of the critical layer the friction must be taken into consideration. Moreover, there is another inconvenience connected with the φ_2. For fulfillment of the boundary conditions one requires the solution for $y - y_K > 0$ as well as for $y - y_K < 0$. However, for φ_2 it is at first undetermined what branch of the logarithm should be chosen at transition from $y - y_K > 0$ to $y - y_K < 0$. This also can be clarified only if in the neighborhood of $y - y_K$, at least, the large friction terms of the complete differential equation (21.15) are taken into consideration. The details of the calculation will not be discussed here. The calculation leads, as Tollmien (reference 109) has shown, to the result that one obtains for the solution φ_2 a so-called transition-substitution in the critical layer which appears as follows:

$$\left.\begin{aligned} y - y_K > 0: \quad \varphi_2 &= P_2\left(y - y_K\right) + \frac{U''_K}{U'_K}\left(y - y_K\right) P_1\left(y - y_K\right) \log\left(y - y_K\right) \\ y - y_K < 0: \quad \varphi_2 &= P_2\left(y - y_K\right) + \frac{U''_K}{U'_K}\left(y - y_K\right) P_1\left(y - y_K\right) \log\left\{\left|y - y_K\right| - i\pi\right\} \end{aligned}\right\} \tag{21.27}$$

If one writes, according to this, the complete u'-component, then in the neighborhood of $y - y_K$:

$$\left.\begin{aligned} y - y_K > 0: \quad u' &= \ldots\ldots + \frac{U''_K}{U'_K} \log\left(y - y_K\right) \cos\left(\alpha x - \beta t\right) \\ < 0: \quad u' &= \ldots\ldots + \frac{U''_K}{U'_K} \log\left|y - y_K\right| \cos\left(\alpha x - \beta t\right) \\ &\quad + \pi \frac{U''_K}{U'_K} \sin\left(\alpha x - \beta t\right) \end{aligned}\right\} \qquad (21.28)$$

One obtains therefore in the critical layer a phase discontinuity for the u'-component. This is retained even in going to the limit, $R \to \infty$. It is lost, however, if one neglects the curvature of the basic flow U'' or if one operates only with the frictionless differential equation. This phase discontinuity is very significant for the development of the motion. The loss of the phase discontinuity is the reason that stability investigations neglecting the curvature U'' or operating only with the frictionless differential equation remain unsuccessful.

With this friction correction in the critical layer the pair of solutions φ_1, φ_2 is sufficiently determined. By taking the friction terms in equation (21.15) into consideration, one then obtains a second pair of solutions φ_3, φ_4 which can be represented by Hankel and Bessel functions. Of these two solutions φ_4 tends very strongly towards infinity and is therefore not used because of the boundary conditions, equation (21.16). φ_3 tends, for large y, towards zero.

The Boundary Value Problem

The general solution as a linear combination of the four particular solutions is:

$$\varphi = C_1\varphi_1 + C_2\varphi_2 + C_3\varphi_3 + C_4\varphi_4 \qquad (21.29)$$

Let us consider in particular the case where a boundary layer profile is investigated with respect to stability. For this case the boundary value problem can be somewhat simplified. The previous considerations showed that in the disturbance differential equation the friction essentially needs to be taken into consideration only in the neighborhood of the critical layer; also, of course, at the wall, because of non-slip. The critical layer is always rather close to the wall; hence for $y > \delta$,

where $U = U_m$ = constant, one may use the frictionless solution which is according to equation (21.19) $\varphi = e^{-\alpha y}$. Thus the condition that the solution for $y = \delta$ joins the solution for U = constant is

$$\varphi'_\delta + \alpha \varphi_\delta = \Phi_\delta = 0 \tag{21.30}$$

This mixed boundary condition is therefore to be set up on the outer edge. Furthermore, the particular solution φ_4 is a priori eliminated in the general solution (equation (21.29)), since it grows, for positive $y - y_K$, beyond all limits; thus $C_4 = 0$. Hence there remains for the boundary value according to equation (21.16)

$$\left.\begin{aligned} C_1 \varphi_{1o} + C_2 \varphi_{2o} + C_3 \varphi_{3o} &= 0 \\ C_1 \varphi'_{1o} + C_2 \varphi'_{2o} + C_3 \varphi'_{3o} &= 0 \\ C_1 \Phi_{1\delta} + C_2 \Phi_{2\delta} + C_3 \Phi_{3\delta} &= 0 \end{aligned}\right\} \tag{21.31}$$

A further simplification takes place because of the fact that because of the rapid fading away of the solution φ_3 on the outer edge $y = \delta$, the solution $\Phi_{1\delta}$ already practically equals zero. In the third equation of equation (21.31) $\Phi_{3\delta}$ may therefore be cancelled. The boundary value problem actually to be solved is, therefore,

$$\begin{vmatrix} \varphi_{1o} & \varphi_{2o} & \varphi_{3o} \\ \varphi'_{1o} & \varphi'_{2o} & \varphi'_{2o} \\ \Phi_{1\delta} & \Phi_{2\delta} & 0 \end{vmatrix} = 0 \tag{21.32}$$

This determinant gives the eigenvalue problem indicated above, which requires — as has been said before — the solution of the following problem: Given

1. basic flow $U(y)$

2. Reynolds number $Re = U_m\delta/\nu$

3. wave length of the disturbance $\alpha = 2\pi/\lambda$

One seeks from equation (21.32) the pertinent complex eigenvalue $c = c_r + i\,c_i$. Therein c_r gives the velocity of wave propagation and c_i the amplification or damping.

Equation (21.32) may formally be written in the form:

$$F(\alpha,\ c_r,\ c_i,\ R;\quad U'_o,\ U''_o,\ \ldots\ .) = 0 \tag{21.33}$$

where equation (21.33) signifies a complex equation, hence is equivalent to two real equations

$$\left.\begin{aligned} f_1\left(\alpha,\ c_r,\ c_i,\ R;\ U'_o,\ U''_o,\ \ldots\right) &= 0 \\ f_2\left(\alpha,\ c_r,\ c_i,\ R;\ U'_o,\ U''_o,\ \ldots\right) &= 0 \end{aligned}\right\} \tag{21.34}$$

If one imagines for instance c_r eliminated from these two equations, one obtains one equation between α, R, c_i:

$$g_1\left(\alpha,\ c_i,\ R;\ U'_o,\ U''_o,\ \ldots\right) = 0 \tag{21.35}$$

From this equation c_i can be calculated as a function of α and R. The constants U'_o, U''_o, . . . are parameters of the basic flow. Thus, if equation (21.35) is assumed solved with respect to c_i,

$$c_i = g_2\left(\alpha,\ R;\ U'_o,\ U''_o,\ \ldots\right) \tag{21.36}$$

Finally one obtains from it, for the neutral disturbances $c_i = 0$, a curve in the α, R–plane, given by the equation

$$g_2\left(\alpha,\ R;\ U'_o,\ U''_o,\ \ldots\right) \tag{21.37}$$

This is the sought for neutral stability curve (compare figure 103), which separates the unstable from the stable disturbances and also yields the theoretical stability limit, that is, the critical Reynolds number Re_{crit}.

The performance of the calculation, here only indicated, is analytically not possible since the quantities α, c_r, R enter into the determinant, equation (21.32), in a very complicated manner. One has therefore to resort to numerical and graphical methods. The critical Reynolds number is very largely dependent on the form of the velocity profile of the basic flow, in particular on whether the velocity profile of the basic flow has an inflection point, thus on $U''(y)$.

The critical Reynolds number found from such a calculation gives exactly the boundary between stability and instability, hence the first occurrence of a neutrally stable disturbance. In comparison with the transition point of test results it is therefore to be expected that the experimental transition point appears only for larger Reynolds numbers where an amplification of the unstable disturbance has already occurred.

c. Results

A few results of such stability calculations will be given. The completely calculated example concerns the boundary layer on the flat plate in longitudinal flow with the laminar velocity profile according to Blasius (compare chapter IXa). In figure 108 the streamline pattern of this plate boundary layer with the superimposed disturbance movement is given for a special neutral disturbance. Figure 109 shows, for the same neutral disturbance, the amplitude distribution and the energy balance. Since the disturbance in question is neutral, the energy transfer from the main to the secondary movement is of exactly the same magnitude as the dissipation of the energy of the secondary movement. Figure 110 shows the neutral-stability curve as result of the stability calculation according to which the critical Reynolds number is referred to the displacement thickness δ^* of the boundary layer $(U_m\delta^*/\nu)_{crit} = 575$. The connection between displacement thickness δ^* and length of run x is for the laminar boundary layer according to equation (9.21)

$$\frac{U_m\delta^*}{\nu} = 1.73\sqrt{\frac{U_m x}{\nu}}$$

Thus a critical Reynolds number formed with the length of run x $(U_m x/\nu)_{crit} = 1.1 \times 10^5$ corresponds to the critical Re-number $(U_m\delta^*/\nu)_{crit} = 575$. The critical number for this case observed in tests

was 3 to 5×10^5. It was explained above that it must be larger than the theoretical number. Furthermore, figure 110 shows that at the stability limit the unstable wave lengths are of the order of magnitude $\lambda = 58$. The unstable disturbances thus have rather long wave lengths.

This calculation, carried out by Tollmien (reference 109) for the flow without pressure gradient was later applied by Schlichting (reference 114, 115) to boundary layer flows with pressure drop and pressure rise. The boundary layer profiles with pressure rise and pressure drop can be represented in a manner appropriate for the stability calculation as a one-parameter family with the form parameter $\lambda_{P\,4}$ according to Pohlhausen's approximate calculation. One then obtains for each profile of this family a neutral-stability curve as indicated in figure 111. Hence the critical Reynolds number $(U_m\delta^*/\nu)_{crit}$ is a function of the form parameter $\lambda_{P\,4}$ according to figure 112. In retarded flow $(\lambda_{P\,4} < 0)$ the critical Re-number is smaller than for the plate flow $(\lambda_{P4} = 0)$, for accelerated flow $(\lambda_{P4} > 0)$ it is larger. With this result of a universal stability calculation the position of the theoretical transition point may be determined conveniently for an arbitrary body shape (plane problem) in the following manner: At first, one has to calculate for this body the potential flow along the contour, furthermore one has to carry out, with this potential flow, a boundary layer calculation according to the Pohlhausen method. This calculation yields the displacement thickness and the form parameter λ_{P4} as functions of the arc length along the contour, in the form

$$\frac{\delta^*}{t}\sqrt{\frac{U_o t}{\nu}} = f_1(s) \quad \text{and} \quad \lambda_{P4} = f_2(s)$$

Since in general there exists, accelerated flow at the front of the body and retarded flow at the rear λ_{P4} decreases from the front toward the rear. By means of the universal stability calculation according to figure 112 one may determine a critical Reynolds number $(U_m\delta^*/\nu)_{crit}$ for each point of the contour. The position of the transition point for a prescribed Re-number $U_o t/\nu$ is then given by the condition

$$s = s_{crit}: \quad \frac{U_m\delta^*}{\nu} = \left(\frac{U_m\delta^*}{\nu}\right)_{crit}$$

Figure 113 shows, for the example of an elliptic cylinder*, how to find the transition point. The curve $(U_m\delta^*/\nu)_{crit}$ decreases from the front

*The boundary layer calculation for this elliptic cylinder was given in figure 52.

toward the rear; the curve $U_m\delta^*/\nu$ for a fixed Re-number $U_o t/\nu$ increases from the front toward the rear. The intersection of the two curves gives the theoretical transition point for the respective Re-number $U_o t/\nu$. By determining this point of intersection for various $U_o t/\nu$ one obtains the transition point as a function of $U_o t/\nu$. The result is represented in figure 114. The transition point travels with increasing Re-number from the rear toward the front; however, the travel is considerably smaller than for the plate in longitudinal flow which is represented in figure 114 for comparison. Finally figure 115 shows the result of such a stability calculation for four different elliptic cylinders in flow parallel to the major axis. The shifting of the transition point with the Re-number increases with the slenderness of the cylinder. For the circular cylinder the shifting is very slight, which is caused by the strongly marked velocity maximum. As a last result, figure 116 shows the travel with Re-number of the transition point on a wing profile for various lift coefficients. The profile in question is a symmetrical Joukowsky profile with lift coefficients $c_a = 0$ to 1. With increasing angle of attack the transition point travels, for fixed Re-number toward the front on the suction side, toward the rear on the pressure side. (compare the velocity distirbutions for this profile, given in figure 54.) One recognizes that the shift of the transition point with the lift coefficient is essentially determined by the shift of the velocity maximum.

The last examples have shown that it is possible to calculate beforehand the position of the transition point as a function of the Re-number and the lift coefficient for the plane problem of an arbitrary body immersed in a flow (particularly a wing). Regarding the comparison with test results it was determined that the experimental transition point always lies somewhat further downstream than the theoretical transition point. The reason is that between the theoretical and the experimental transition points lies the region of amplification of the unstable disturbances. This amplification also can be calculated on principle according to methods similar to those previously described. (Compare Schlichting (reference 112) where this was done for the special case of the plate in longitudinal flow.) Presumably one can obtain a still closer connection between the theoretical instability point and the experimental transition point by applying such calculations to the accelerated and retarded flow.

CHAPTER XXII. CONCERNING THE CALCULATION OF THE TURBULENT FRICTION LAYER ACCORDING TO THE METHOD OF GRUSCHWITZ (REFERENCE 78)

a. Integration of the Differential Equation of the Turbulent Boundary Layer

In order to integrate the system of equations (18.16), one first introduces dimensionless variables. One refers the lengths to the

wing chord t and the velocity to the free stream velocity U_o, thus:

$$\frac{x}{t} = x^*; \quad \frac{\vartheta}{t} = \vartheta^*; \quad \frac{\zeta}{\frac{\rho}{2} U_o^2} = \zeta^* = \left(\frac{U}{U_o}\right)^2 \eta \tag{22.1}$$

Hence the system of equations (equation (18.16)) may be written:

$$\left.\begin{aligned} \frac{d\zeta^*}{dx^*} + 0.00894 \frac{\zeta^*}{\vartheta^*} &= 0.00461 \left(\frac{U}{U_o}\right)^2 \frac{1}{\vartheta^*} \\ \frac{d\vartheta^*}{dx^*} + 2\left(1 + \frac{H}{2}\right)\vartheta^* \frac{U_o}{U} \frac{d\left(\frac{U}{U_o}\right)}{dx^*} &= \frac{\tau_o}{\rho U^2} \end{aligned}\right\} \tag{22.2}$$

First, the second equation is solved with constant values for $\tau_o/\rho U^2$ and H, namely

$$\frac{\tau_o}{\rho U^2} = 0.002; \quad H = 1.5$$

The first approximation $\vartheta_1^*(x^*)$ obtained from that is then substituted in the first differential equation. From the latter one obtains a first approximation $\zeta_1^*(x^*)$ and from that, according to equation (22.1), $\eta_1(x^*)$. With $\eta_1(x^*)$ one determines according to figure 92 the course of $H(\eta)$ and corrects τ_o according to equation (18.15). Then one obtains from the second differential equation a second approximation $\vartheta_2^*(\eta)$, etc.

For the solution of the differential equations one uses the isocline method which can be applied for the present case, according to Czuber, in the following manner: Both differential equations have the form:

$$\frac{dy}{dx} + f(x)y = g(x) \tag{22.3}$$

As can be easily shown, this differential equation has the property that all line elements on a straight line x = constant radiate from one point. The coordinates of this point (= pole) are:

$$\xi = x + \frac{1}{f(x)}; \quad X = \frac{g(x)}{f(x)} \tag{22.4}$$

Thus one has only to calculate a sufficient number of these poles and can then easily draw the integral curve.

Figure 93 indicates the result of such a calculation for the profile J 015; $c_a = 0$. The calculation of the laminar boundary layer for the same profile was performed in chapter XII, figure 49, table 6.

Initial values: The transition point was placed somewhat arbitrarily at the velocity maximum of the potential flow $(x/t = 0.141)$. It was assumed that:

$$Re = \frac{U_o t}{\nu} = 10^6$$

For the laminar boundary layer was found:

$$\frac{x}{t} = 0.141: \quad \frac{\delta^*}{t}\sqrt{\frac{U_o t}{\nu}} = 1.56 \text{ (table 6)}$$

Hence there results, with $\delta^*/\vartheta = 2.55$;

$$\frac{x}{t} = 0.141: \quad \left(\frac{\vartheta}{t}\right)_o = 0.611 \times 10^{-3} \quad \text{(table 8)}$$

The corresponding η – value was assumed to be

$$\eta = 0.1 \qquad \text{(table 8)}$$

Calculation to the second approximation suffices. The result is compiled in table 8 and figure 93. A turbulent separation point does not exist since η remains below 0.8. From the variation of the shearing stress τ_o along the wing chord the drag coefficient of the surface friction may be determined:

$$W = 2b\int_o^t \tau_o \, dx \quad (x = \text{measured along chord})$$

or $c_w = W/2\ b\ t\ \frac{\rho}{2} U_o^2$

$$c_w = \int_o^l \frac{\tau_o}{\frac{\rho}{2} U_o^2}\, d\,\frac{x}{t} \tag{22.5}$$

The evaluation of the integral gives

$$c_w = 0.0090$$

b. Connection Between the Form Parameters η and $H = \vartheta/\delta^*$ of the Turbulent Boundary Layer

According to Pretsch (reference 80) one may also represent analytically the relation between the form parameters $\eta = 1 - (u\,\vartheta/U)^2$ and $H = \delta^*/\vartheta$ which was found empirically by Gruschwitz, compare figure 92. A power law is set up for the velocity distribution, of the form:

$$\frac{u}{U} = \left(\frac{y}{\delta}\right)^n = z^n \tag{22.6}$$

with $n = 1/6, 1/7, 1/8 \ldots$, according to the experiments so far. Hence results:

$$\frac{\delta^*}{\delta} = \int_{y/\delta=0}^{l} \left(1 - \frac{u}{U}\right) d\,\frac{y}{\delta} = \int_0^l \left(1 - z^n\right) dz = \frac{n}{n+1} \tag{22.7}$$

Furthermore:

$$\frac{\vartheta}{\delta} = \int_{y/\delta=0}^{l} \frac{u}{U}\left(1 - \frac{u}{U}\right) d\,\frac{y}{\delta} = \int_0^l z^n \left(1 - z^n\right) dz \tag{22.8}$$

$$= \int_{z=0}^{l} \left(z^n - z^{2n}\right) dz = \frac{1}{n+1} - \frac{1}{2n+1} = \frac{n}{(n+1)(2n+1)}$$

From equations (22.7) and (22.8) follows:

$$H = \frac{\delta^*}{\vartheta} = 2n + 1$$

or

$$n = \frac{H - 1}{2} \tag{22.9}$$

From equation (22.8) follows further

$$\frac{\vartheta}{\delta} = \frac{H - 1}{H(H + 1)} \tag{22.10}$$

The Gruschwitz form parameter η is defined according to equation (18.2) by:

$$\eta = 1 - \left(\frac{u_\vartheta}{U}\right)^2$$

With equation (22.6) η becomes:

$$\eta = 1 - \left(\frac{\vartheta}{\delta}\right)^{2n} \tag{22.11}$$

Substitution of equation (22.10) into (22.11) gives:

$$\boxed{\eta = 1 - \left[\frac{H - 1}{H(H + 1)}\right]^{H-1}} \tag{22.12}$$

The connection between H and η calculated according to this equation is given in the following table and is also plotted in figure 92. The curve calculated according to equation (22.12) almost coincides with the curve found empirically by Gruschwitz.

H	η
1	0
1.1	0.270
1.2	0.404
1.4	0.573
1.6	0.688
1.8	0.772
2.0	0.833
2.2	0.881
2.4	0.916
2.6	0.941
2.8	0.959
3.0	0.972

Translated by Mary L. Mahler
National Advisory Committee
for Aeronautics

BIBLIOGRAPHY

Part B. — Turbulent Flow

Chapters XIII to XX

*60. Darcy: Memoires des Savants etrangers. Vol. VII, 1858.

61. Reynolds, Osborn: Phil. Trans. Roy. Soc., 1883 or Collected papers, vol. II, p. 51.

62. Prandtl, L.: Ueber den Luftwiderstand von Kugeln, Göttingen Nachrichten, p. 177, 1914.

63. Lorenz, H. A.: Abhandlungen üb. theoretische Physik. Bd. 1, pp. 43 — 47, 1907.

64. Boussinesq, T. V.: Mem. Pres. par div. Sav., vol XXIII, Paris, 1877. Theorie des l'écoulement tourbillant, Paris 1987.

65. Reichardt, H.: Messungen turbulenter Schwankungen. Naturw. 1938, p. 404.

66. Prandtl, L.: Ueber die ausgebildete Turbulenz. ZAMM 1925, p. 136 and Verhdl. II. internat. Kongress f. angew. Mech. Zürich, 1926.

67. Schmidt, W.: Massenaustausch in freier Atmophäre und verwandte Erscheinungen. Hamburg, 1925.

68. V. Kármán, Th.: Mechanische Aehnlichkeit und Turbulenz. Nachr. Ges. Wiss. Göttingen, Math. Phys. Klasse, p. 58, 1930.

69. Blasius, H.: Forschungsheft 131 des Vereins deutscher Ingen.. 1911.

70. Nikuradse, J.: Strömung in glatten Rohren. VDI-Forschungsheft 356, 1932.

71. Nikuradse, J.: Strömungsgesetze in rauhen Rohren VDI-Forschungsheft 361, Berlin 1933.

72. Schlichting, H.: Experimentelle Untersuchungen zum Rauhigkeitsproblem. Ing.-Arch. Bd. 7, 1936, p. 1.

73. Prandtl, L.: Ueber den Reibungswiderstand strömender Luft. Results of the Aerodynamic Test Institute, Göttingen, III. Lieferung, 1927.

74. Prandtl, L.: Zur turbulenten Strömung in Rohren und Längs Platten. Results of the Aerodynamic Test Institute, Gottingen, IV. Lieferung, 1932.

---

*The reference numbers used herein have been taken directly from the original German Version.

75. V. Kármán, Th.: Verhdlg. III. Internat. Mech. Kongress, Stockholm, 1930.

76. Prandtl, L., and Schlichting, H.: Das Widerstandsgesetz rauher Platten. Werft, Reederei, Hafen. 1934, p. 1.

77. Tani, Hama, Mituisi: On the Permissible Roughness in the Laminar Boundary Layer. Aeron Res. Inst. Tokyo Rep. 15, 419, 1940.

78. Gruschwitz, E.: Die turbulente Reibungsschicht in ebener Strömung bei Druckabfall und Druckanstieg. Ing.-Arch. Bd.II, p. 321, 1931.

79. Millikan, C. B.: The Boundary Layer and Skin Friction for figure of Revolution. Trans. Americ. Soc. Mech. Eng., vol. 54, No. 2, 1932.

80. Pretsch, J.: Zur theoretischen Berechnung des Profilwiderstandes. Jb. 1938 d. deutschen Luftfahrtforshung, p. I 61.

81. Tollmien, W.: Berechnung der turbulenten Ausbreitungsvorgänge. ZAMM Bd. IV, p. 468, 1926.

82. Schlichting, H.: Ueber das ebene Windschattenproblem. Ing.-Arch. Bd. I., p. 533, 1930.

83. Swain, L. M.: Proc. Roy. Soc. London. A. 125, 129, p. 647.

84. Betz, A.: Ein Verfahren zur direkten Ermittlung des Profilwiderstandes. Z. f. M. Bd. 16., p. 42, 1925.

85. Jones, B. M.: The Measurement of Profile Drag by the Pitot Transverse Method. ARC Rep. 16888, 1936.

86. Elias, F.: Die Wärmeübertragung einer geheizten Platte an strömende Luft. ZAMM, 1929, p. 434.

87. Reichardt, H.: Die Wärmeübertragung in turbulenten Reibungsschichten. ZAMM 20, 1940, p. 297.

88. Olsson, Gran.: Geschw.- und Temperatur-Verteilung hinter einem Gitter bei turbulenter Strömung. ZAMM, 1936, p. 257.

89. Schultz-Grunow, F.: Neues Reibungswiderstandsgesetz für glatte Platten. Luftf. Forschung 1940, p. 239.

90. . . . . : Widerstandsmessungen an rauhen Kreiszylindern. ARC Rep. 1283, 1929.

91. Förthmann, E.: Ueber turbulente Strahlausbreitung. Ing.-Arch. Bd. V, p. 42, 1934.

92. Taylor, G. I.: The Transport of Vorticity and Heat Trough Fluids in Turbulent Motion. Proc. Roy. Soc. A, Vol. 135, p. 685, 1932.

93. Fage and Falkner: Note on Experiments on the Temperature and Velocity in the Wake of a Heated Cylindrical Obstacle. Proc. Roy. Soc. A. Vol. 135, p. 702, 1932.

94. Lorenz, H.: Zeitschr. F. techn. Physik 15, p. 376, 1934.

95. Hagen: Pogg. Ann. Bd. 46, p. 423, 1839.

96. Froude: Experiments on the Surface Friction. Brit. Ass. Rep., 1872.

97. Dryden, H. L. and Kuethe, A. M.: Effect of Turbulence in Windtunnel Measurements. NACA Rep. No. 342, 1929.

BIBLIOGRAPHY

Origin of Turbulence (chapter XXI)

101. Reynolds, O.: Sci. papers 2, 1883.

102. Rayleigh, Lord: Papers 3, 1887.

103. Lorenz, H. A.: Abhandlungen über theoretische Physik. I 43, Leipzig, 1907.

104. Sommerfeld, A.: Ein Beitrag zur Hydrodynamischen Erklärung der turbulenten Flüssigkeitsbewegung. Atti. d. IV congr. int. dei Mathem. Rom 1909.

105. V. Mises, R.: Beitrag zum Oszillationstheorem. Heinrich Weber Festschr. 1912. Derselbe: Zur Turbulenz-Theorie. Jahresbericht d. deutsch. Mathem. Ver. 1912.

106. Hopf, L.: Der Verlauf kleiner Schwingungen in einer Strömung reibender Flüssigkeit. Ann. Phys. 44, p. 1, 1914; and: Zur Theorie der Turbulenz. Ann. Phys., 59 p. 538, 1919.

107. Prandtl, L.: Bemerkungen über die Entstehung der Turbulenz. Zeitschr. angew. Math. u. Mech. 1, 431, 1921.

108. Tietjens, O.: Beitrage zum Turbulenzproblem. Diss. Gottingen, 1922, and Zeitschr. angew. Math. u. Mech 5, 200, 1925.

109. Tollmien, W.: Ueber die Entstehung der Turbulenz. Nachr. Ges. Wiss. Göttingen. Math. Phys. Klasse 1929, p. 21.

110. Tollmien, W.: Ein allgemeines Kriterium der Instabilität laminarer Geschwindigkeitsverteilungen. Nachr. Ges. Wiss. Göttingen. Math. Phys, Klasse Bd. I, Nr. 5, 1935.

111. Prandtl, L.: Ueber die Entstehung der Turbulenz. Zeitschr. angew. Math. u. Mech. 11, 407, 1931.

112. Schlichting, H.: Zur Entstehung der Turbulenz bei der Plattenströmung. Nachr. Ges. Wiss. Göttingen. Math. Phys. Klasse, 1933, p. 181.

113. Schlichting, H.: Amplitudenverteilung und Energiebilanz kleiner Störungen bei der Plattenströmung. Nachr. Ges. Wiss. Göttingen. Math. Phys. Klasse 1935, P. 48.

114. Schlichting, H.: Berechnung der kritischen Reynoldsschen Zahl einer Reibungsschicht in beschleunigter und verzögerter Strömung. Jahrbuch 1940 der deutschen Luftfahrt-Forschung, p. I 97.

115. Schlichting, H. and Ulrich, A.: Zur Berechnung des Umschlages laminar/turbulent. (Preisausschreiben 1940 der Lilienthal Gesellschaft). Lilienthal-Gesellschaft Bericht S. 10, 1941.

TABLE VII. — THE DRAG LAW OF THE SMOOTH PLATE

$$\text{I} \quad c_f = \frac{0.074}{Re^{1/5}} \qquad Re = \frac{U_o l}{\nu}$$

$$\text{Ia} \quad c_f = \frac{0.074}{Re^{1/5}} - \frac{1700}{Re}$$

$$\text{II} \quad c_f = \frac{0.455}{(\log Re)^{2.58}}$$

$$\text{IIa} \quad c_f = \frac{0.455}{(\log Re)^{2.58}} - \frac{1700}{Re}$$

$$\text{III} \quad c_f = \frac{0.427}{(-0.407 + \log Re)^{2.64}}$$

	I	Ia	II	IIa	III
$Re = \frac{U_o l}{\nu}$	$c_f \times 10^3$	$c_f \times 10^3$	$c_f \times 10^3$	$c_f \times 10^3$	$c_f \times 10^3$
10^5	7.40		7.13		7.63
2×10^5	6.43		6.11		6.50
3×10^5	5.93		5.62		5.85
4×10^5	5.60		5.33		5.50
5×10^5	5.37		5.06		5.23
6×10^5	5.18	2.35	4.92	2.17	5.06
8×10^5	4.88	2.76	4.62	2.50	4.74
10^6	4.67	2.97	4.46	2.76	4.51
2×10^6	4.07	3.22	3.96	3.11	3.95
3×10^6	3.74	3.17	3.67	3.10	3.68
4×10^6	3.54	3.11	3.50	3.07	3.50
5×10^6	3.38	3.04	3.40	3.06	3.33
6×10^6	3.26	2.98	3.28	3.00	3.21
8×10^6	3.08	2.87	3.09	2.88	3.07
10^7	2.94	2.77	2.99	2.82	2.94
2×10^7	2.56	2.47	2.67	2.58	2.62
5×10^7	2.13	2.16	2.38	2.35	2.26
10^8	1.85	1.83	2.14	2.12	2.03
2×10^8			1.93	1.92	1.87
5×10^8			1.70	1.70	1.61
10^9			1.56	1.56	1.47
2×10^9			1.43	1.43	1.33
5×10^9			1.30	1.30	1.19
10^{10}			1.20	1.20	1.10

TABLE VIII. — CALCULATION EXAMPLE FOR THE TURBULENT BOUNDARY LAYER ACCORDING TO GRUSCHWITZ (REFERENCE 78)

PROFILE J 015; $c_a = 0$; COMPARE FIGURE 93. (LAMINAR BOUNDARY LAYER FOR THE SAME PROFILE; COMPARE FIGURE 49 AND TABLE 6.)

			I. Approximation					II. Approximation						
$\frac{x}{t}$	$\frac{U}{U_o}$	$\frac{t}{U_o}\frac{dU}{dx}$	$H = \frac{\delta^*}{\vartheta}$	$\frac{\tau_o}{\rho U^2}$	$\left(\frac{\vartheta}{t}\right)_1 10^3$	ζ^*_1	η_1	H	$\frac{\tau_o}{\rho U^2}$	$\left(\frac{\vartheta}{t}\right)_2 10^3$	ζ^*_1	η_2	$\frac{\delta^*}{t} 10^3$	$\frac{2\tau_o}{\rho U_o^2} 10^3$
0.141	1.271	0	1.5	0.002	0.611	0.162	0.1	1.01	0.00237	0.611	0.162	0.1	0.617	7.66
0.173	1.267	−0.215	↓	↓	0.67	0.407	0.254	1.15	0.00232	0.70	0.407	0.254	0.805	7.42
0.235	1.245	−0.398			0.84	0.636	0.410	1.25	0.00214	0.87	0.630	0.406	1.09	6.64
0.305	1.212	−0.482			1.05	0.712	0.485	1.37	0.00211	1.11	0.704	0.478	1.52	6.21
0.380	1.178	−0.498			1.31	0.726	0.525	1.41	0.00200	1.40	0.720	0.521	1.97	5.53
0.461	1.136	−0.500			1.63	0.713	0.555	1.45	0.00191	1.74	0.710	0.553	2.52	4.91
0.546	1.095	−0.500			2.01	0.689	0.575	1.48	0.00183	2.17	0.686	0.574	3.22	4.38
0.631	1.053	−0.488			2.45	0.662	0.596	1.49	0.00176	2.65	0.662	0.596	3.95	3.91
0.713	1.014	−0.471			2.96	0.635	0.619	1.50	0.00169	3.18	0.635	0.619	4.77	3.47
0.791	0.977	−0.455			3.50	0.611	0.642	1.55	0.00165	3.75	0.611	0.642	5.81	3.14
0.861	0.945	−0.431			4.07	0.591	0.664	1.58	0.00160	4.33	0.593	0.665	6.84	2.85
0.919	0.917	−0.427			4.59	0.574	0.683	1.61	0.00156	4.86	0.577	0.687	7.83	2.62
0.964	0.899	−0.430			5.03	0.562	0.695	1.64	0.00153	5.28	0.565	0.699	8.66	2.47
0.990	0.889	−0.421			5.30	0.555	0.704	1.65	0.00152	5.60	0.558	0.708	9.25	2.40
1.000	0.884	−0.421	↓	↓	5.41	0.552	0.707	1.65	0.00151	5.72	0.557	0.715	9.44	2.36

$c_w = 0.0090$

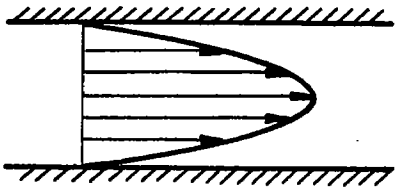

Laminar

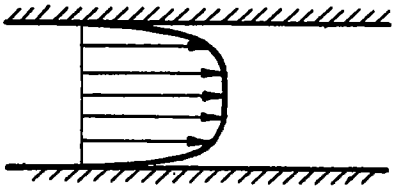

Turbulent

Figure 71.- Laminar and turbulent velocity distribution in pipe.

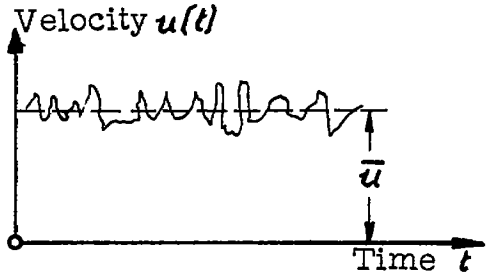

Figure 72.- Fluctuation with time of the velocity of turbulent flow at a fixed position.

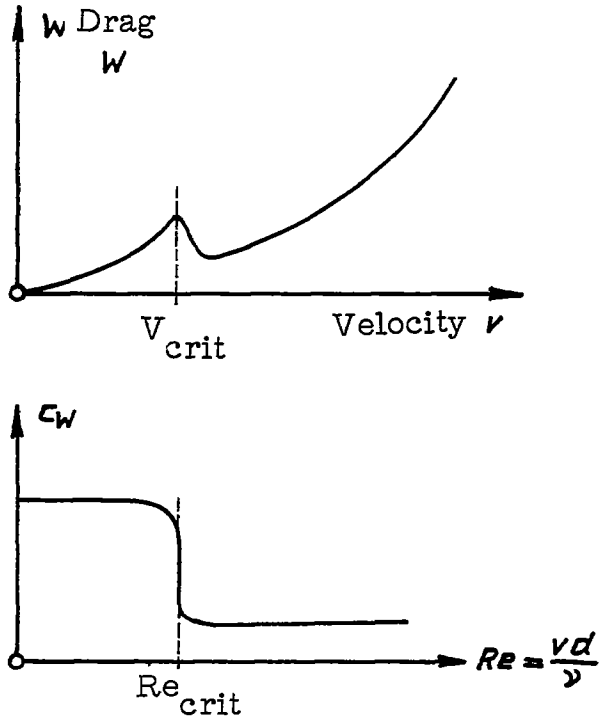

Figure 73.- Drag and drag coefficient of a sphere.

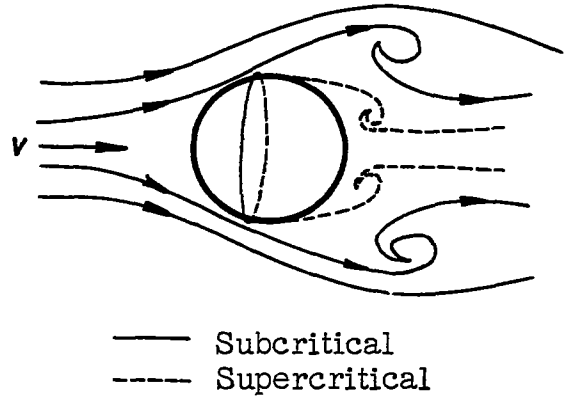

Figure 74.- Flow around a sphere; subcritical and supercritical (schematic).

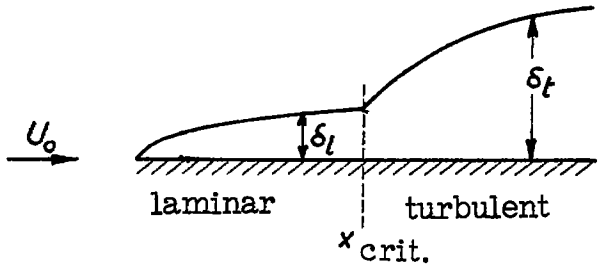

Figure 75.- Laminar and turbulent boundary layer on a flat plate in longitudinal flow.

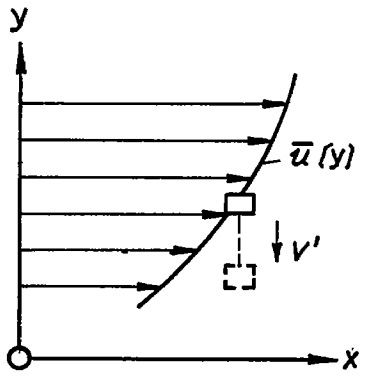

Figure 76.- Transfer of momentum by the turbulent fluctuation velocity.

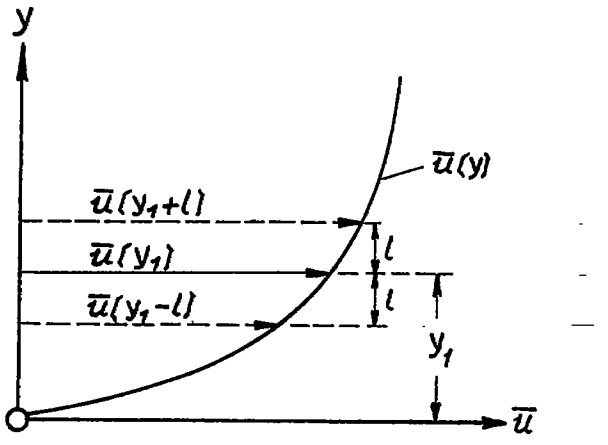

Figure 77.- Explanation of the mixing length.

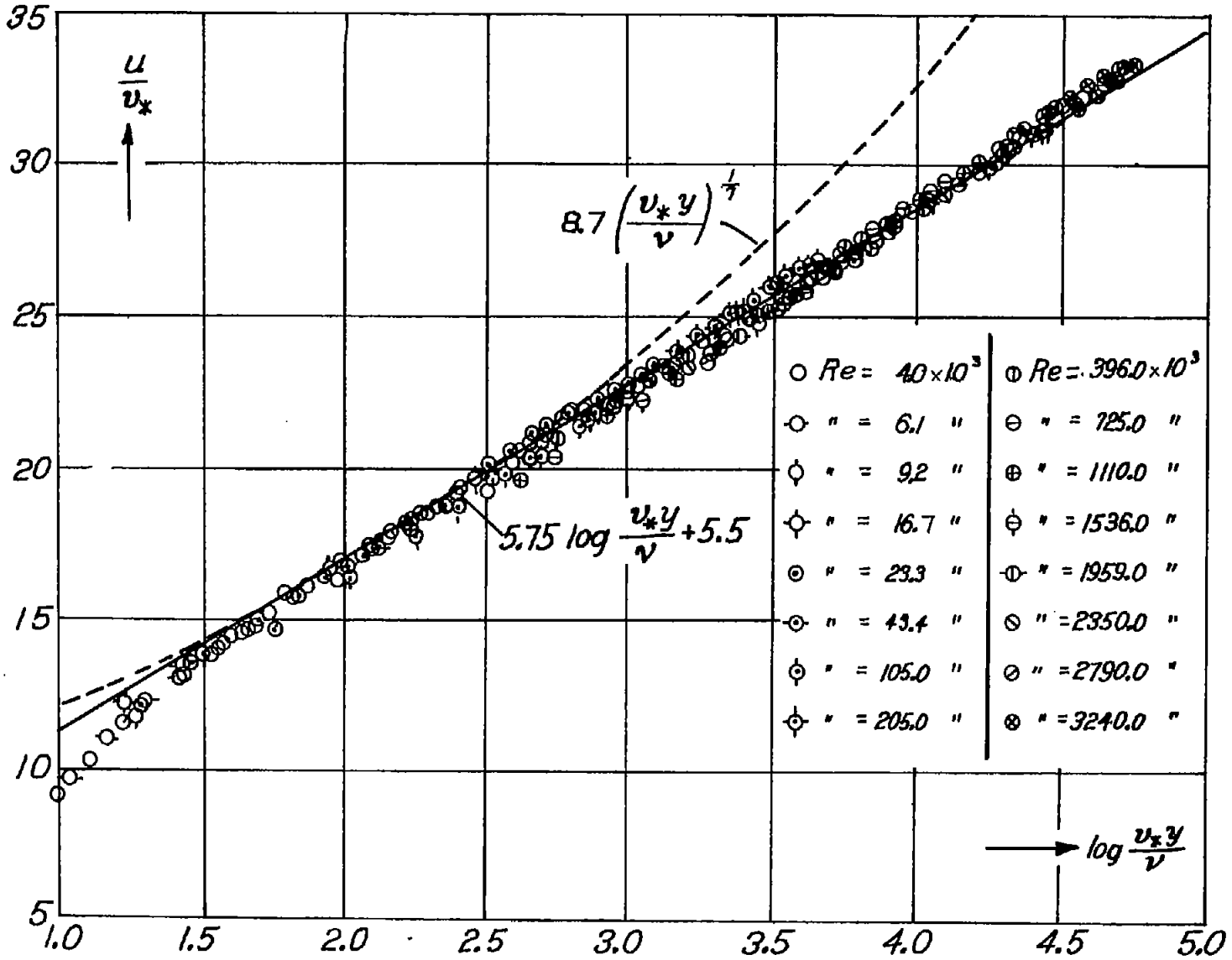

Figure 78.- Universal velocity distribution law in the smooth pipe.

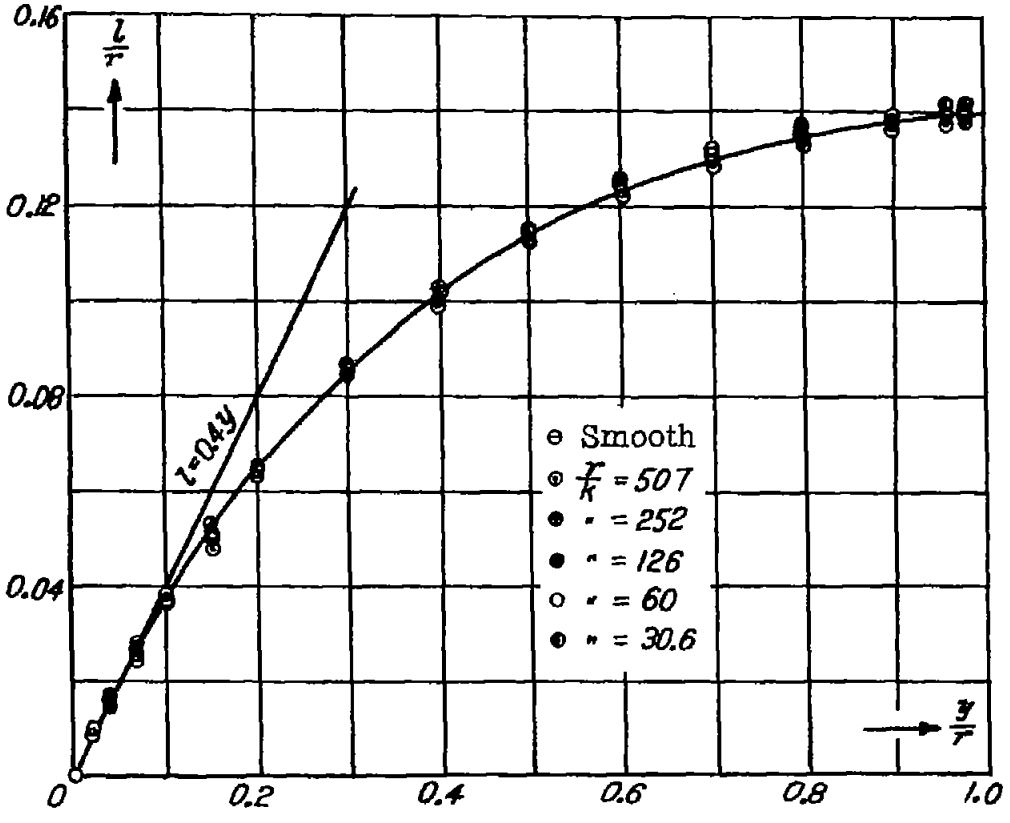

Figure 79.- Mixing length distribution in the smooth pipe.

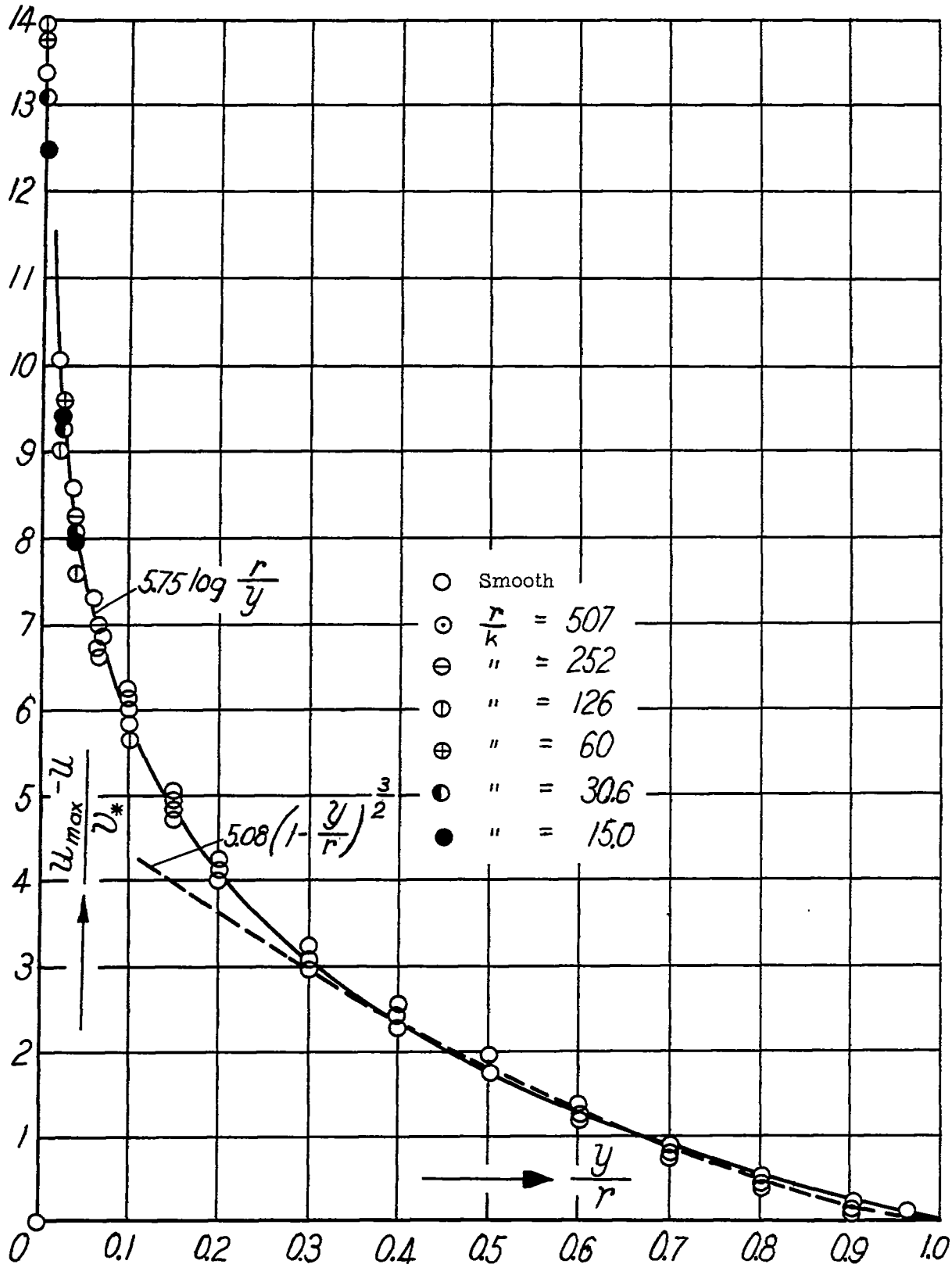

Figure 80.- Universal velocity distribution law for smooth and rough pipes.

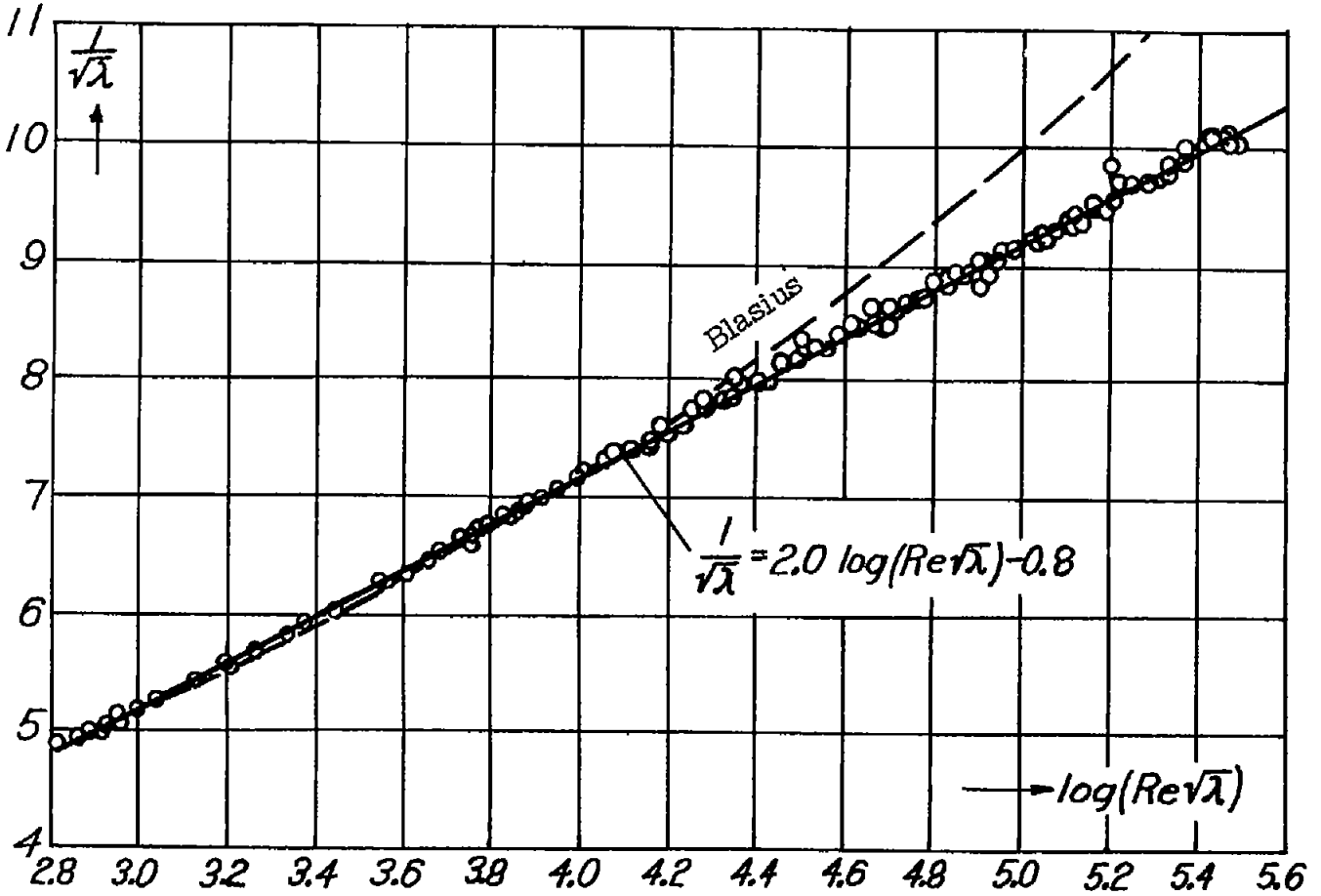

Figure 81.- Universal resistance law of the smooth pipe.

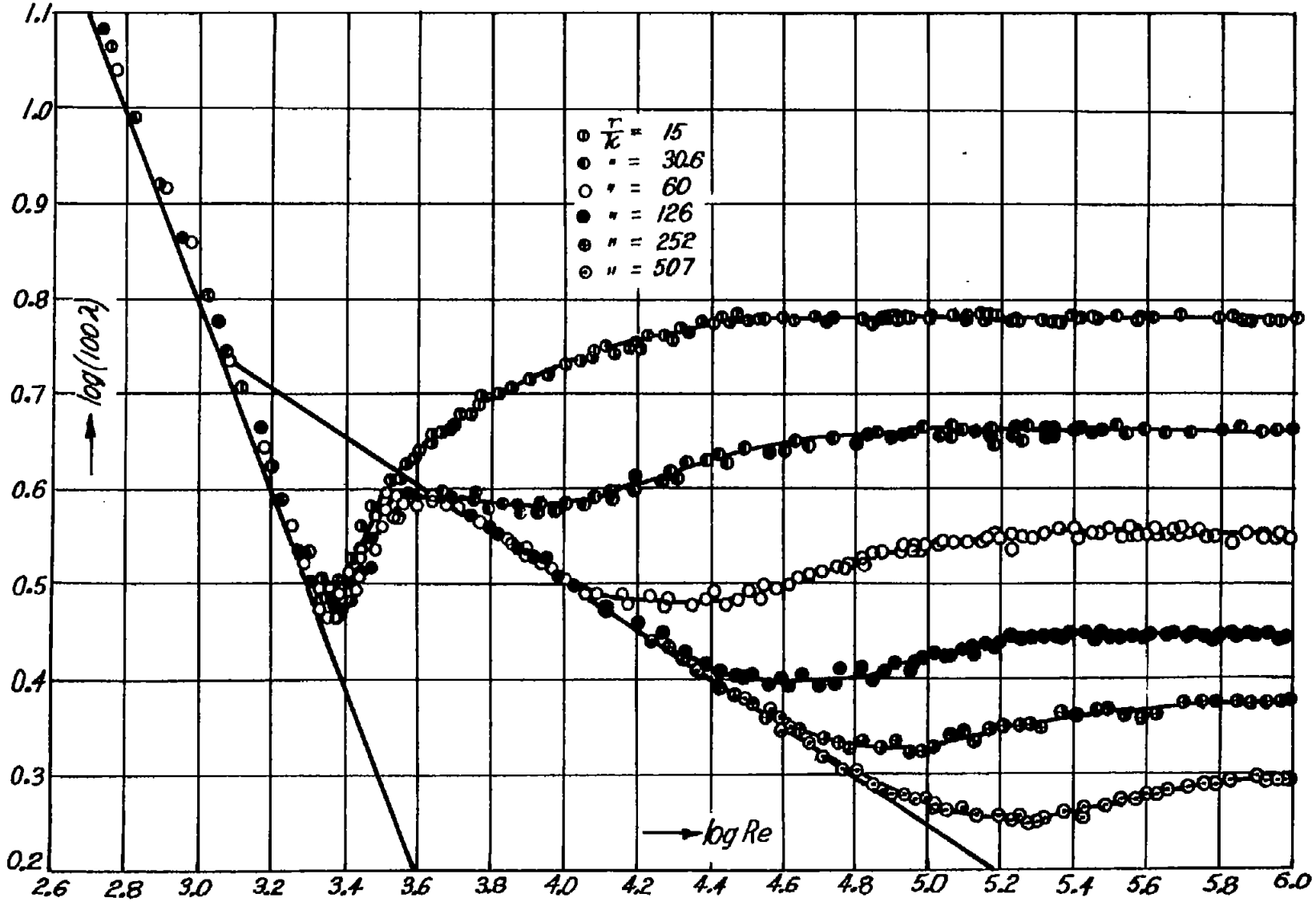

Figure 82.- Resistance law of the rough pipe.

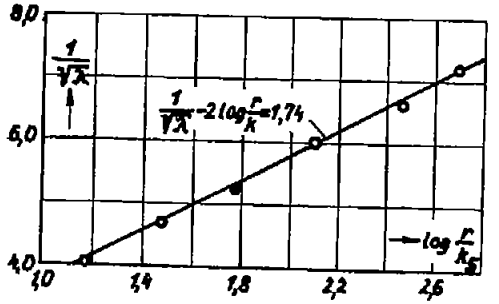

Figure 83.- Resistance law of the rough pipe for fully developed roughness flow.

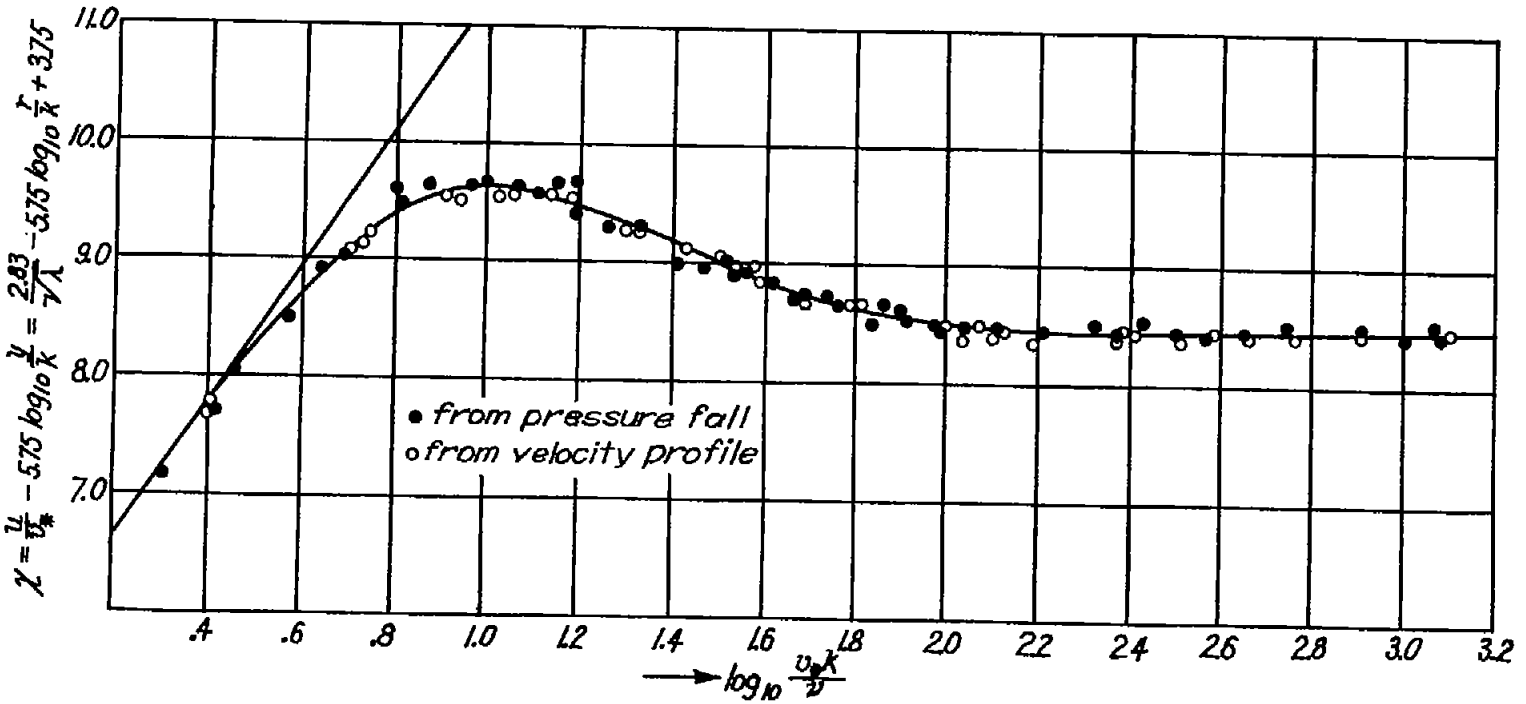

Figure 84.- The roughness function B as a function of $v\, k_s / \nu$.

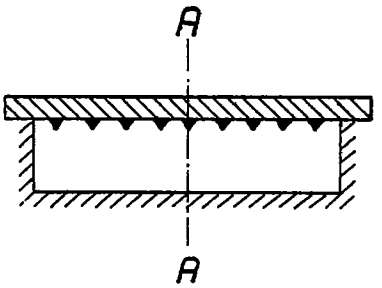

(a) Roughness tunnel.

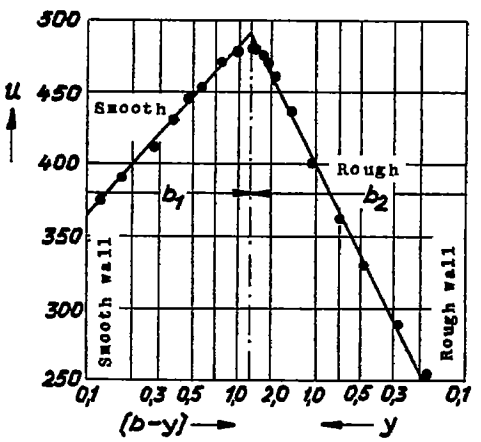

(b) Velocity distribution in the section A A.

Figure 85.- Measurement of the drag of an arbitrary roughness.

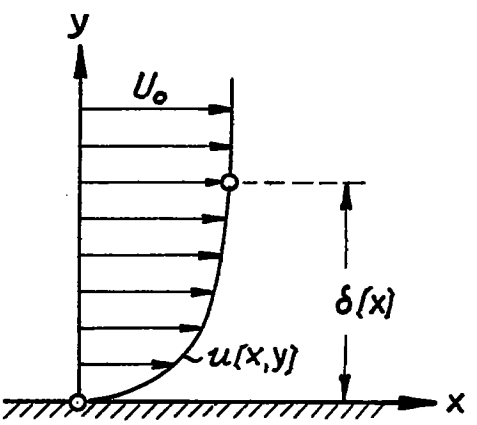

Figure 86.- Calculation of the turbulent plate drag.

$$\text{I}: c_f = \frac{0{,}074}{Re^{1/5}} \qquad \text{II}: c_f = \frac{0{,}455}{(\log Re)^{2{,}58}} \qquad \text{III}: c_f = \frac{0{,}427}{(-0{,}407 + \log Re)^{2{,}64}}$$

$$\text{Ia}: c_f = \frac{0{,}074}{Re^{1/5}} - \frac{1700}{Re} \qquad \text{IIa}: c_f = \frac{0{,}455}{(\log Re)^{2{,}58}} - \frac{1700}{Re}. \qquad \text{laminar } c_f = \frac{1{,}328}{\sqrt{Re}}$$

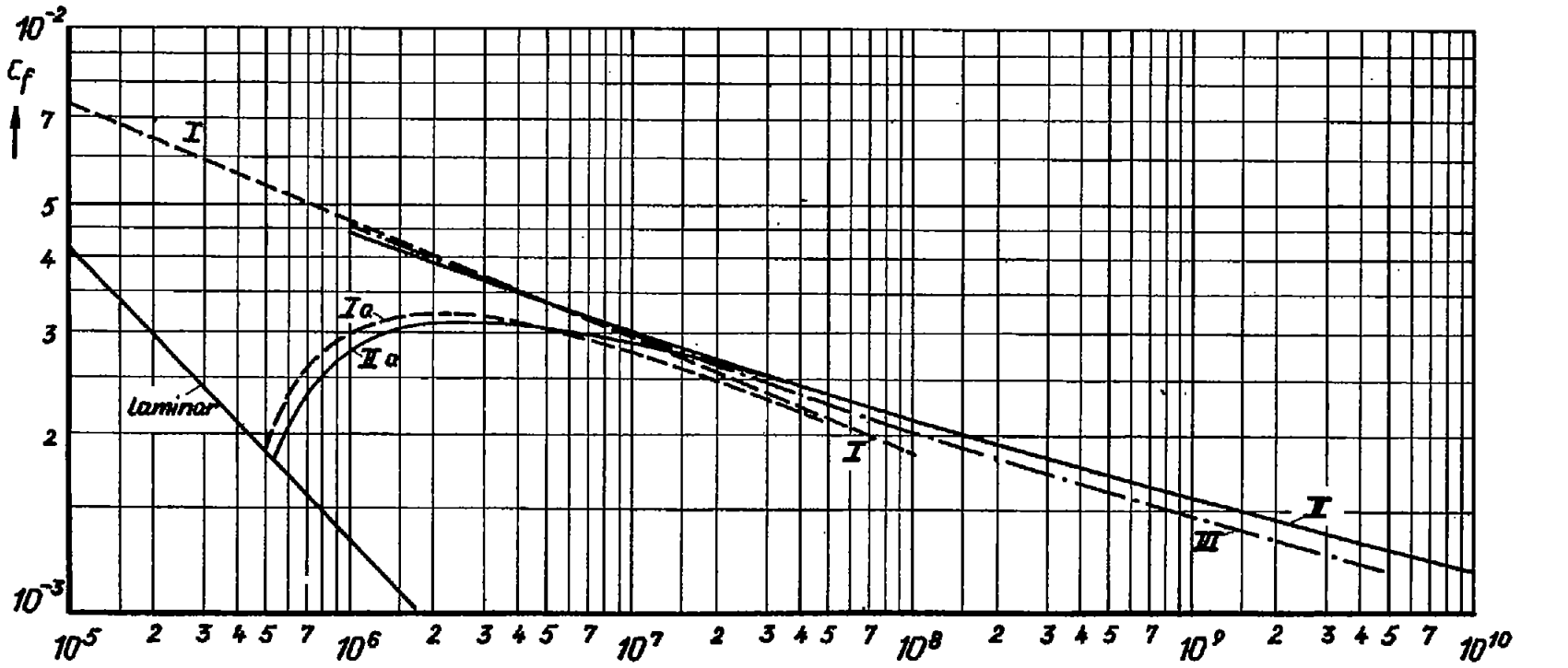

Figure 87.- The drag law of the smooth flat plate in longitudinal flow (theoretical curves).

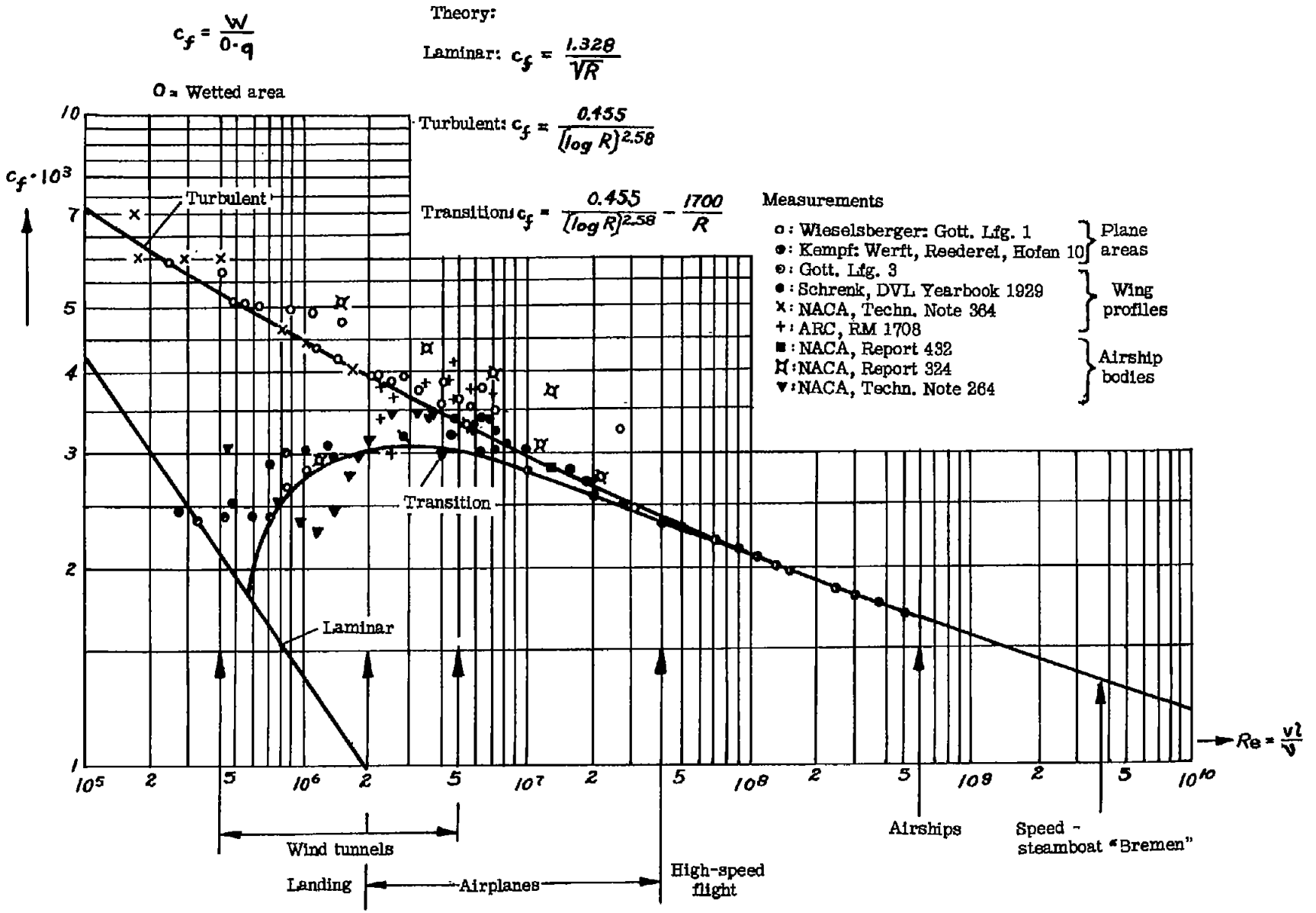

Figure 88.- The drag law of the smooth plate; comparison with measurements.

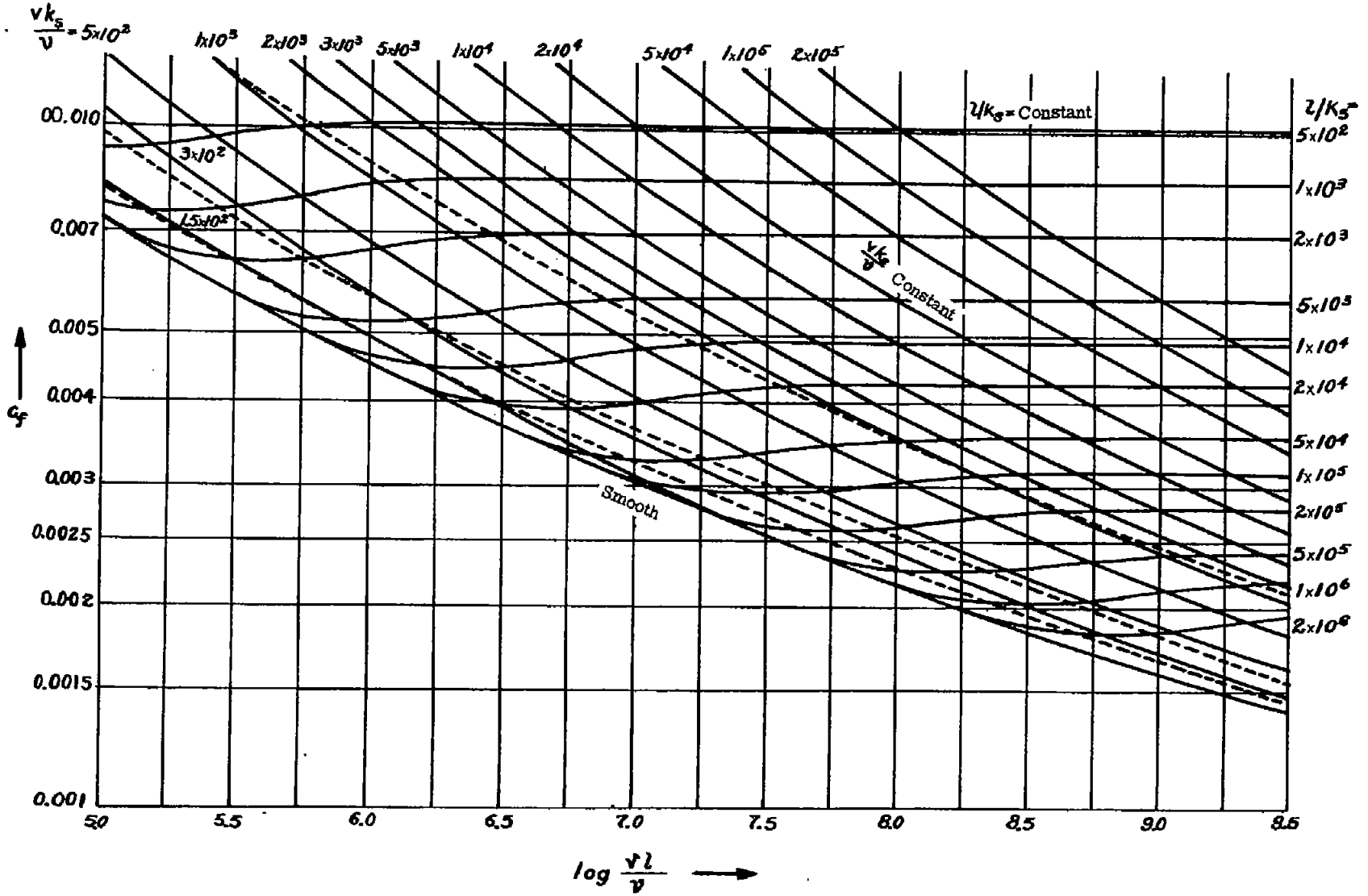

Figure 89.- The drag law of the rough plate.

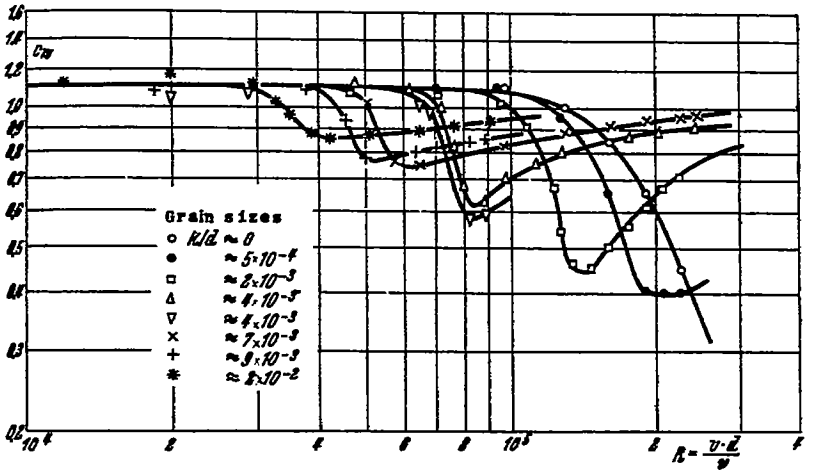

Figure 90.- Drag of the circular cylinder for various relative roughnesses.

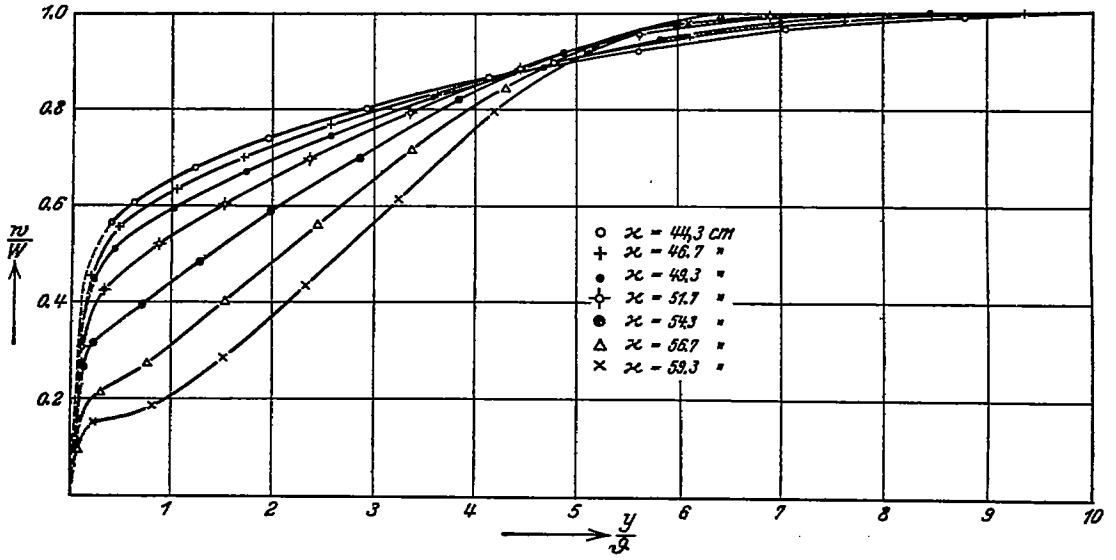

Figure 91.- Velocity profiles in the turbulent friction layer with pressure decrease and pressure increase (according to Gruschwitz [78]).

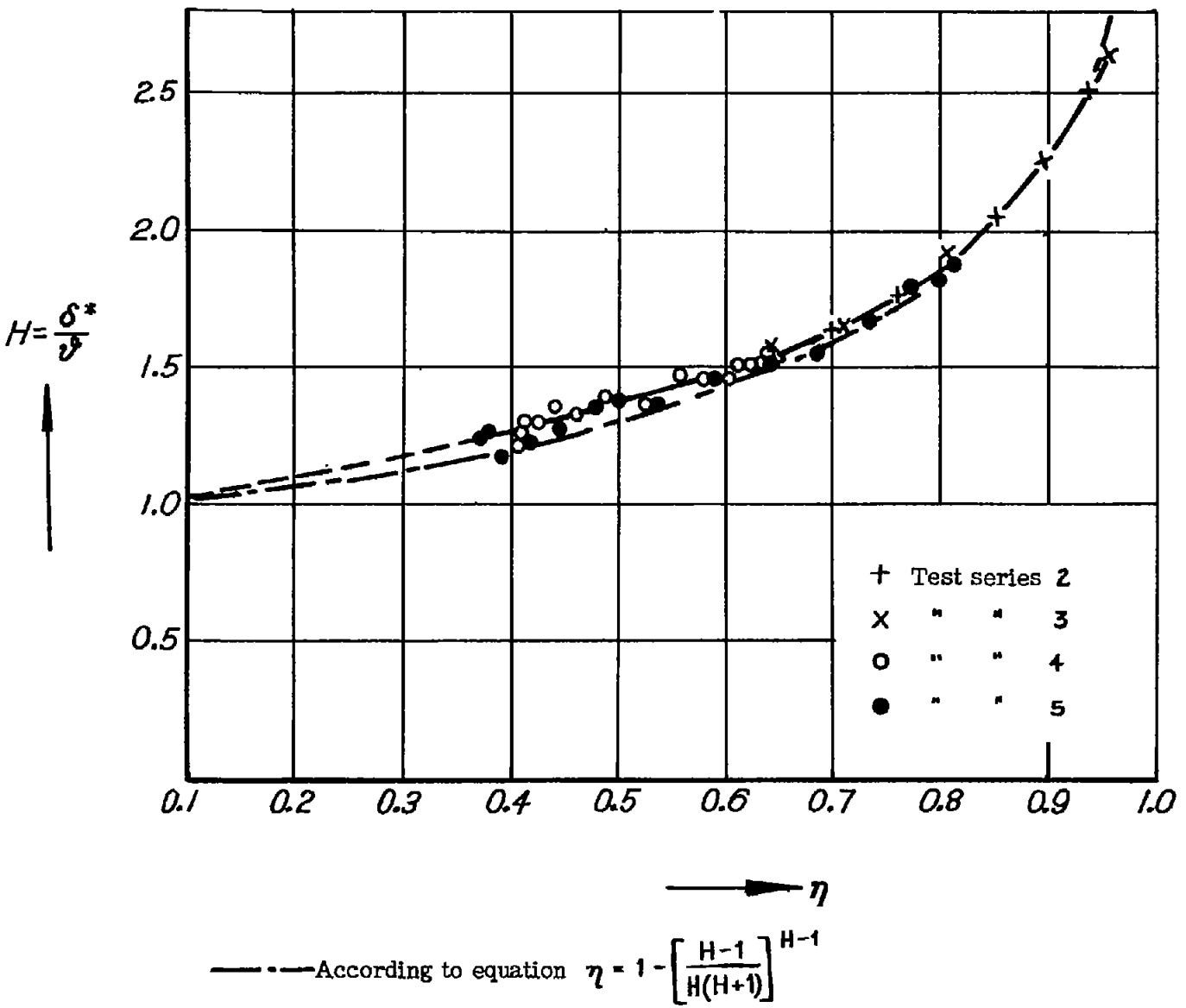

Figure 92.- The ratio $H = \delta^*/\vartheta$ as a function of the form parameter η (according to Gruschwitz [78]).

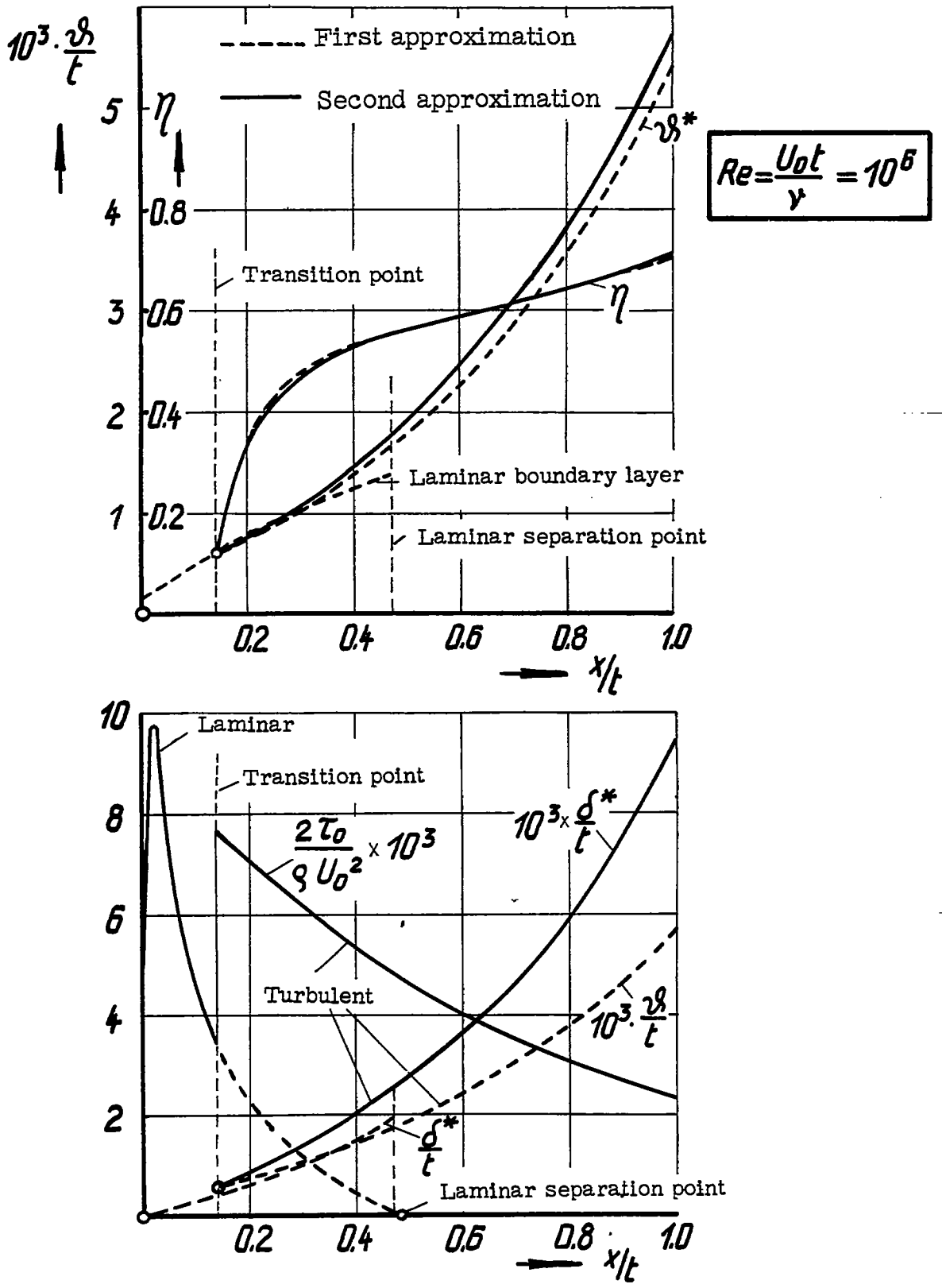

Figure 93.- Result of the calculation of the turbulent friction layer according to Gruschwitz. Example profile J 015; $c_a = 0$.

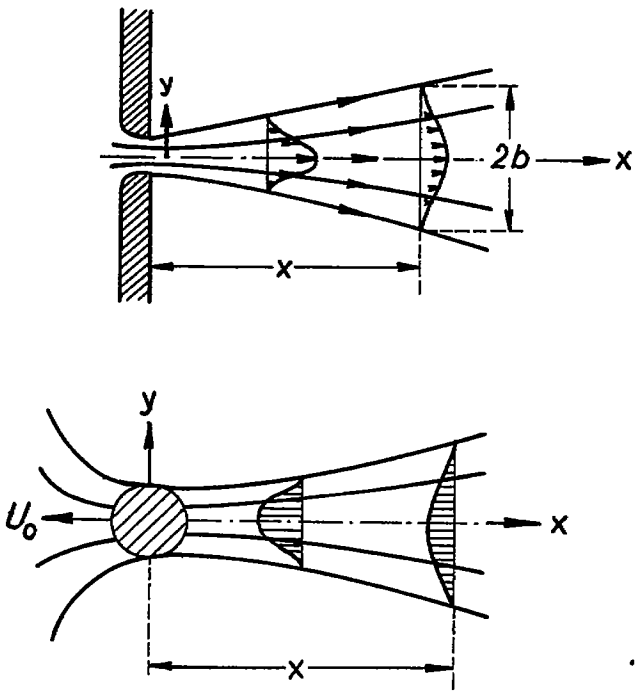

Figure 94.- Free turbulence: free jet and wake.

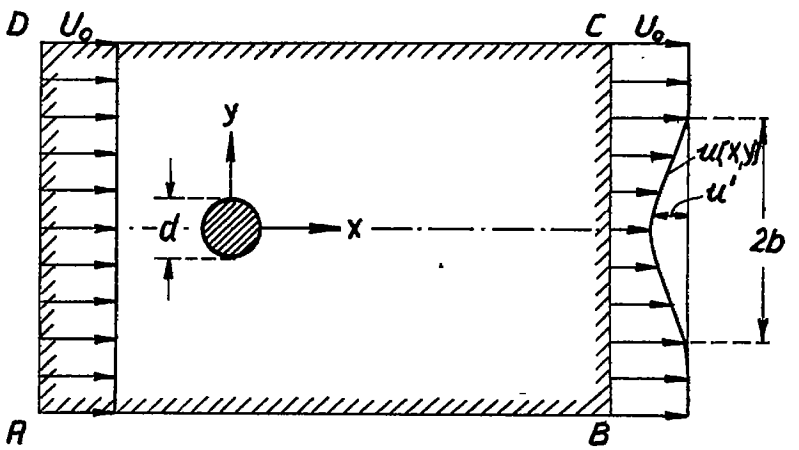

Figure 95.- Plane wake flow; explanatory sketch.

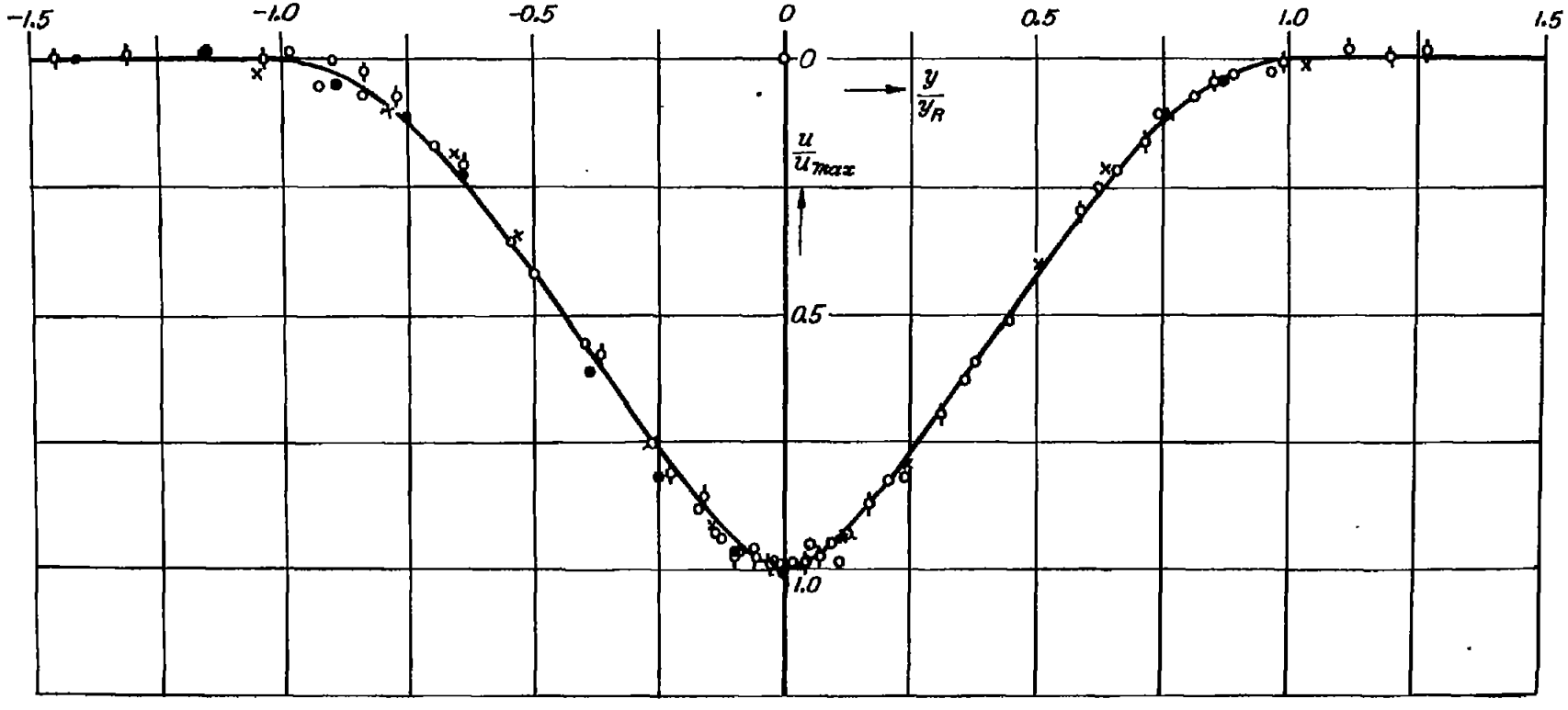

Figure 96.- Plane wake flow; comparison of measurement and calculation.

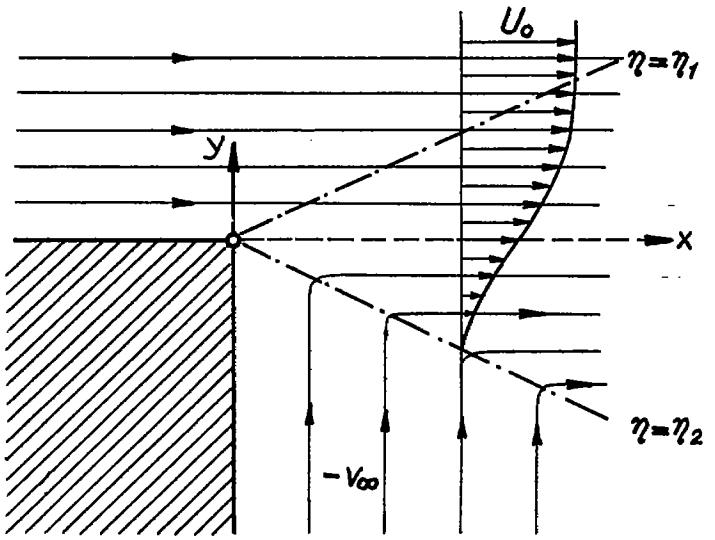

Figure 97.- The free jet boundary; explanatory sketch.

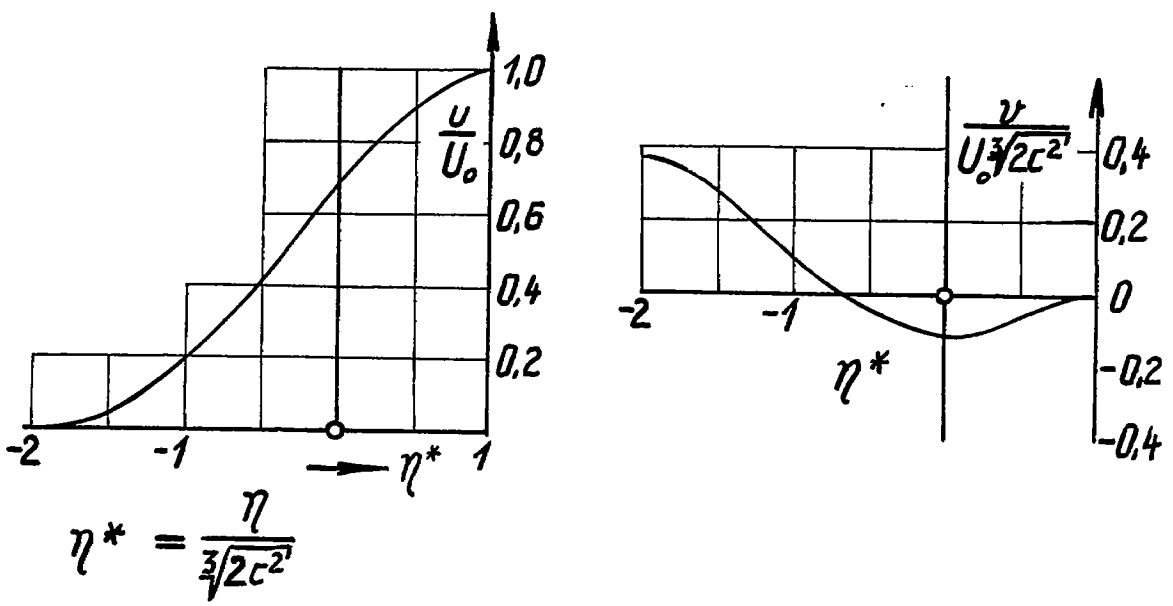

Figure 98.- Free jet boundary; distribution of the longitudinal and transverse velocity.

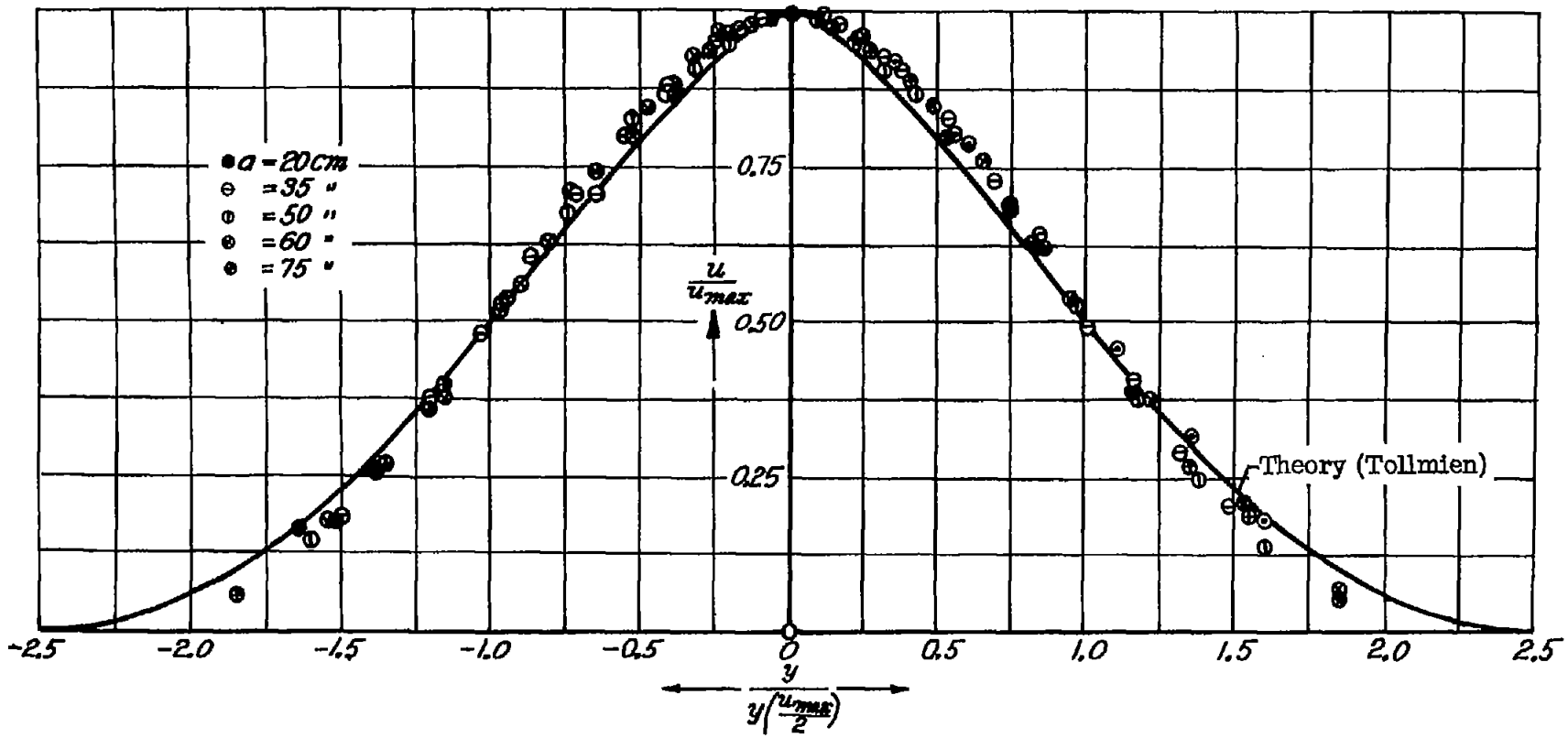

Figure 99.- The plane free jet; comparison of measurement and calculation.

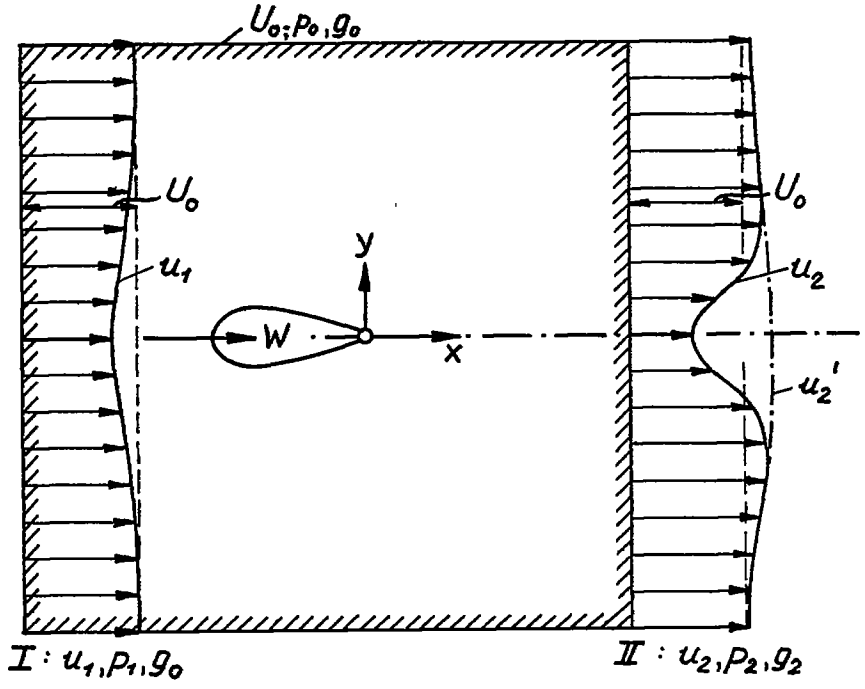

Figure 100.- Determination of the profile drag according to Betz.

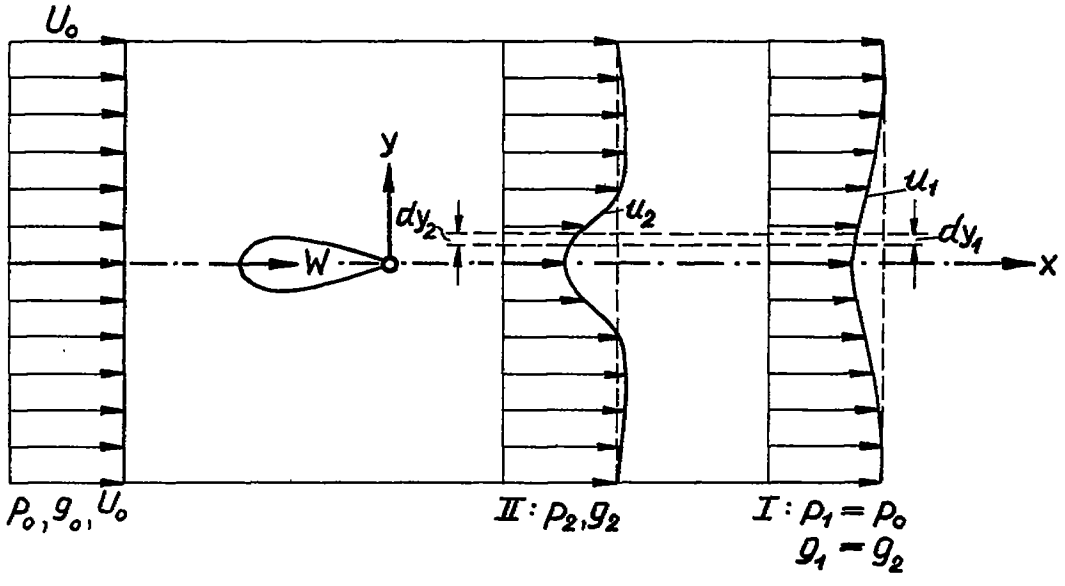

Figure 101.- Determination of the profile drag according to Jones.

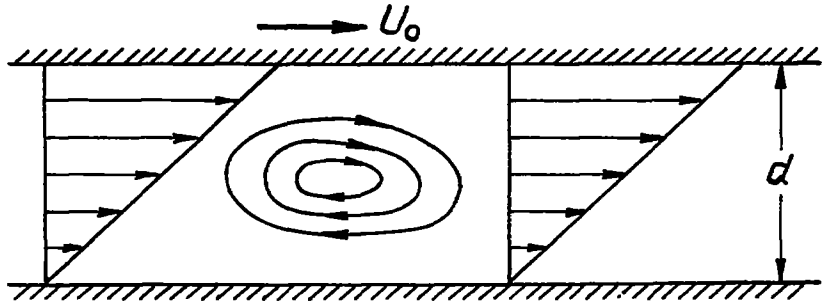

Figure 102.- The stability investigation of the Couette flow.

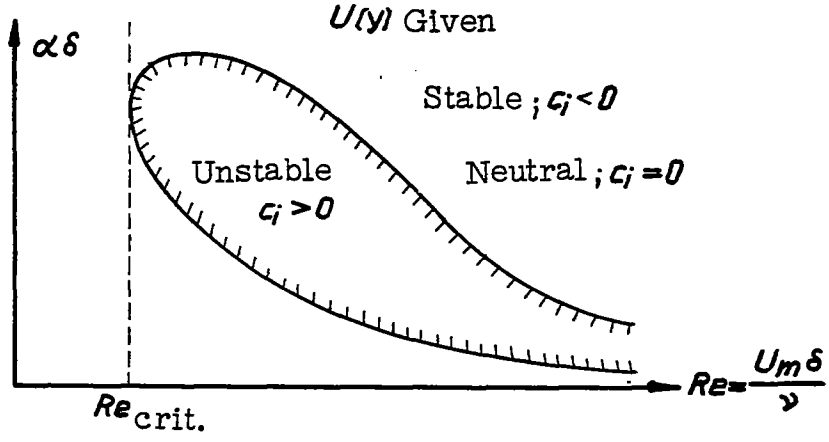

Figure 103.- The neutral stability curve as result of a stability investigation (schematic).

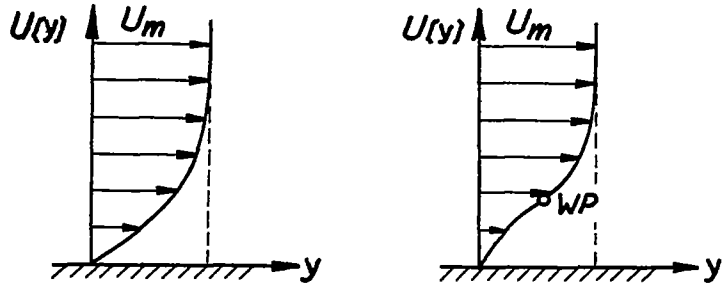

Figure 104.- Basic flow without and with inflection point.

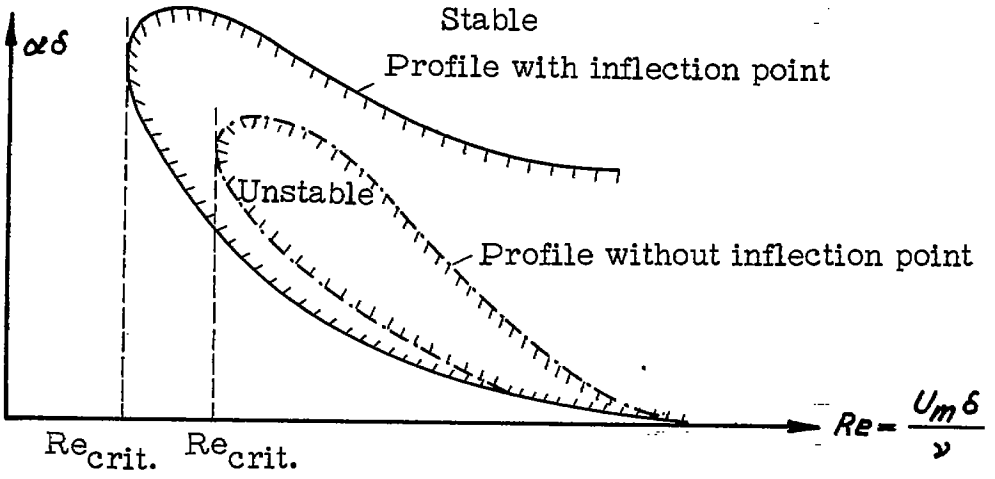

Figure 105.- Neutral stability curves for velocity profiles without and with inflection point (schematic).

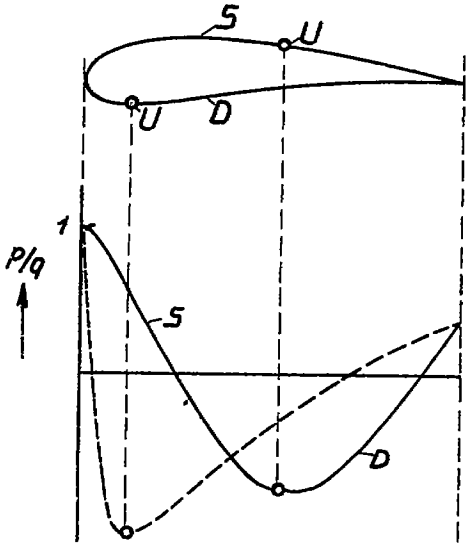

D = Pressure side

S = Suction side

U = Transition point

Figure 106.- Wing profile with pressure distribution.

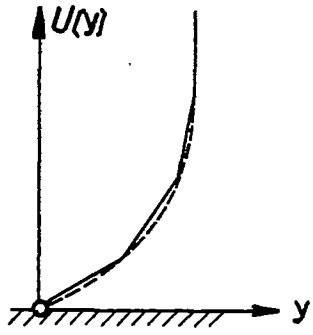

Figure 107.- Approximation of a velocity profile by a polygon.

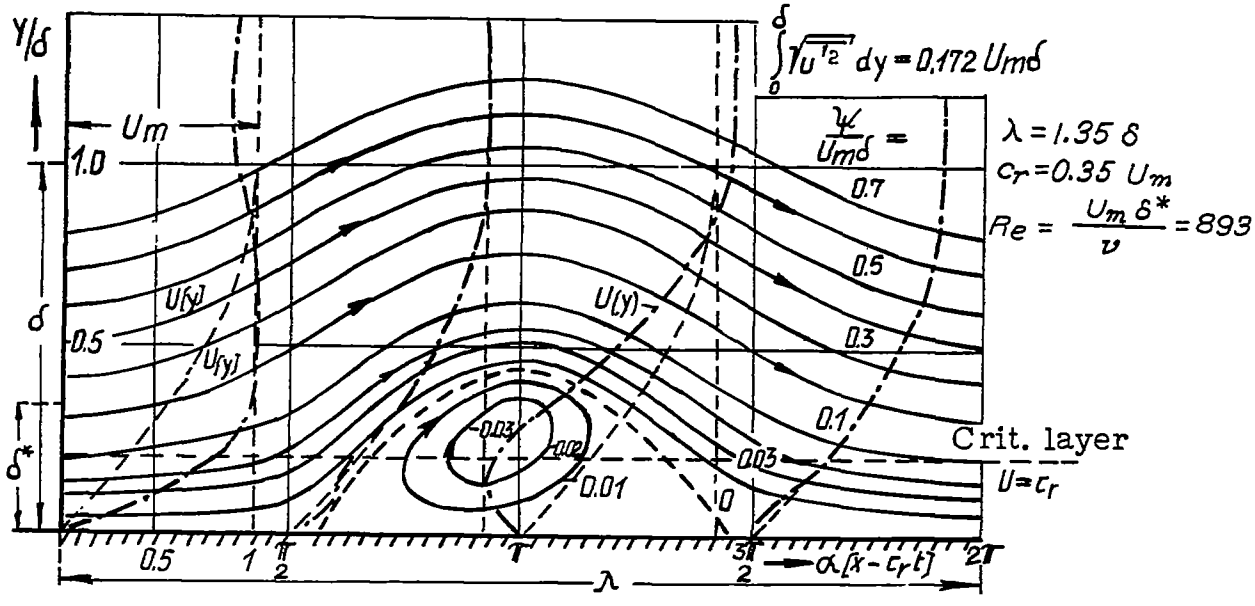

Figure 108.- Streamline pattern and velocity distribution of the plate boundary layer for neutrally stable disturbance U(y) = basic flow; u(y) = U(y) + u'(x,y,t) = disturbed velocity distribution; $\lambda = 2\pi/\alpha$ = wave length of the disturbance.

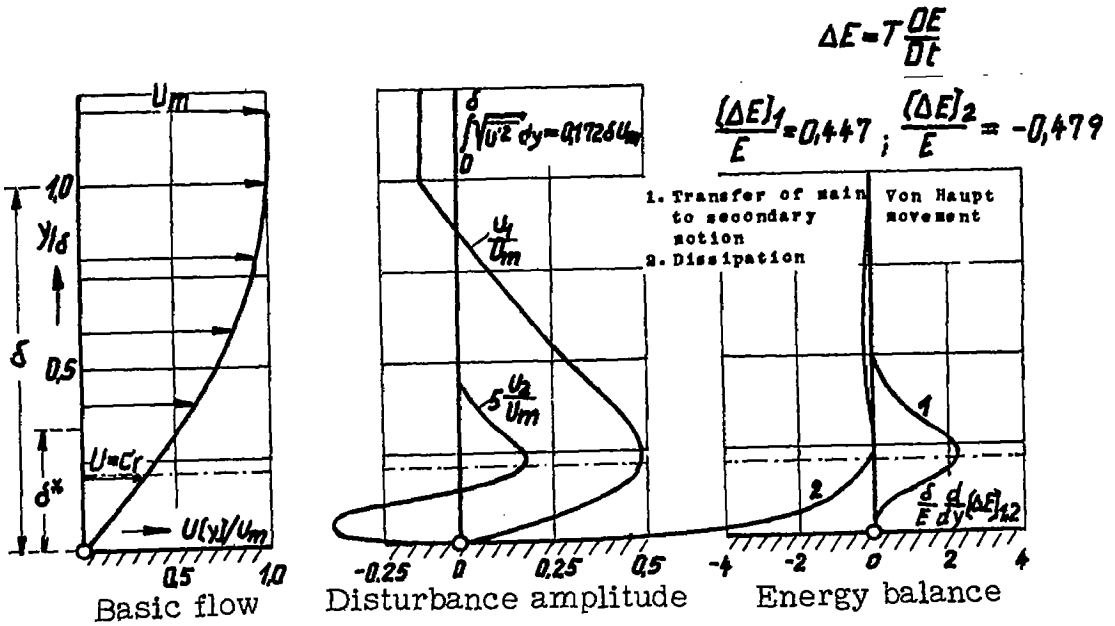

Basic flow Disturbance amplitude Energy balance

Parameters of the disturbance:

Wave length $\lambda = 13.5\,\delta$; $\alpha\delta = 0.466$

Velocity of wave propagation $c_r = 0.35\,U_m$

Angular frequency $\beta_r = \frac{2\pi}{T} = 0.163\,\frac{m}{\delta}$ $\qquad \frac{U_m\delta^*}{\nu} = 893$.

Figure 109.- Neutral disturbance for the friction layer on the flat plate. Amplitude of the disturbance velocity:
$u'(x,y,t) = u_1(y)\cos(x - \beta_r t) - u_2(y)\sin(x - \beta_r t)$.

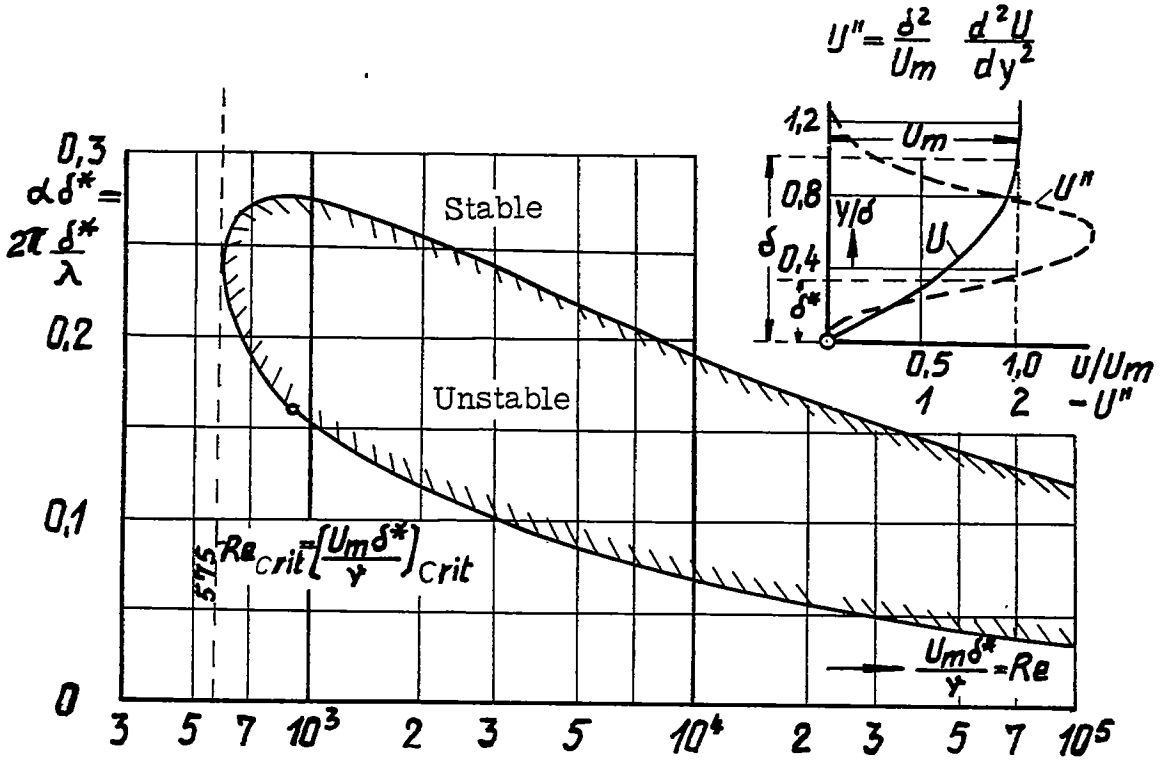

Figure 110.- Neutral stability curve for the friction layer on the flat plate in longitudinal flow.

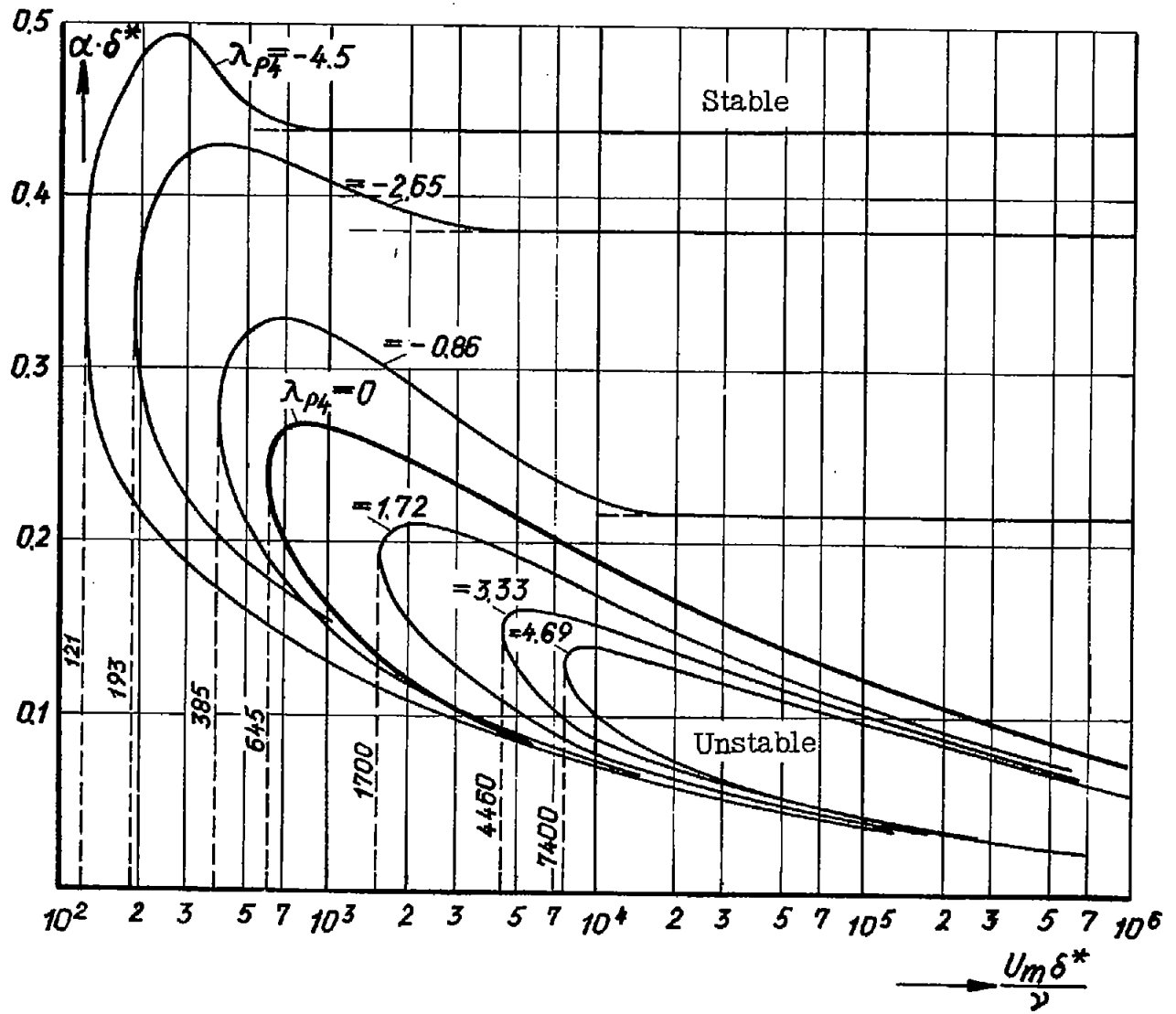

Figure 111.- Neutral stability curves for the boundary-layer profiles in accelerated and retarded flow.

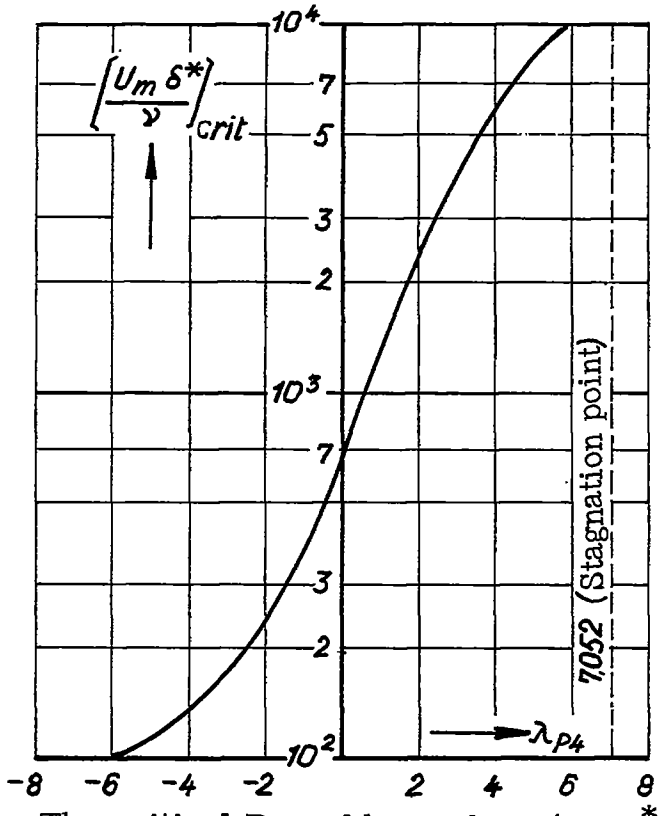

Figure 112.- The critical Reynolds number $(U_m \delta^* / \nu)_{crit}$ as a function of λ_{p4}.

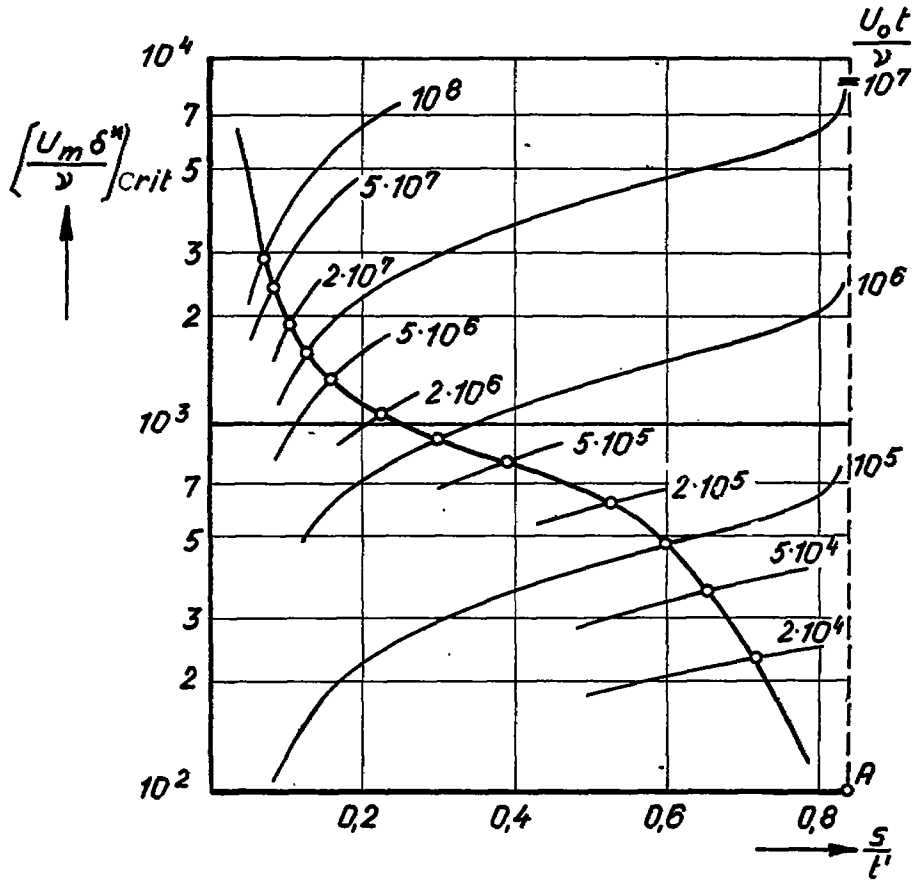

Figure 113.- Stability calculation for the elliptic cylinder of axis ratio $a_1/b_1 = 4$.

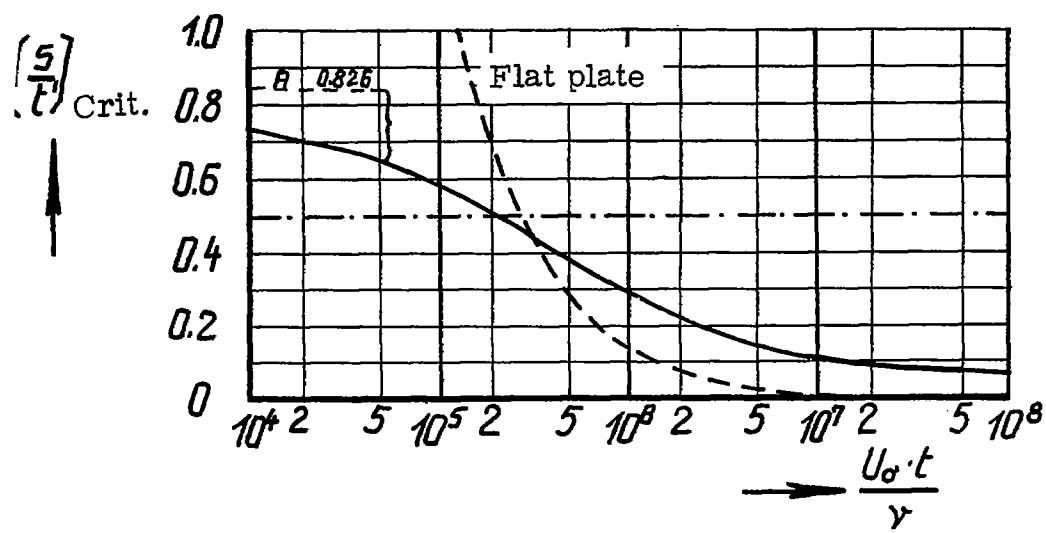

Figure 114.- Result of the stability calculation for the elliptic cylinder of axis ratio $a_1/b_1 = 4$.

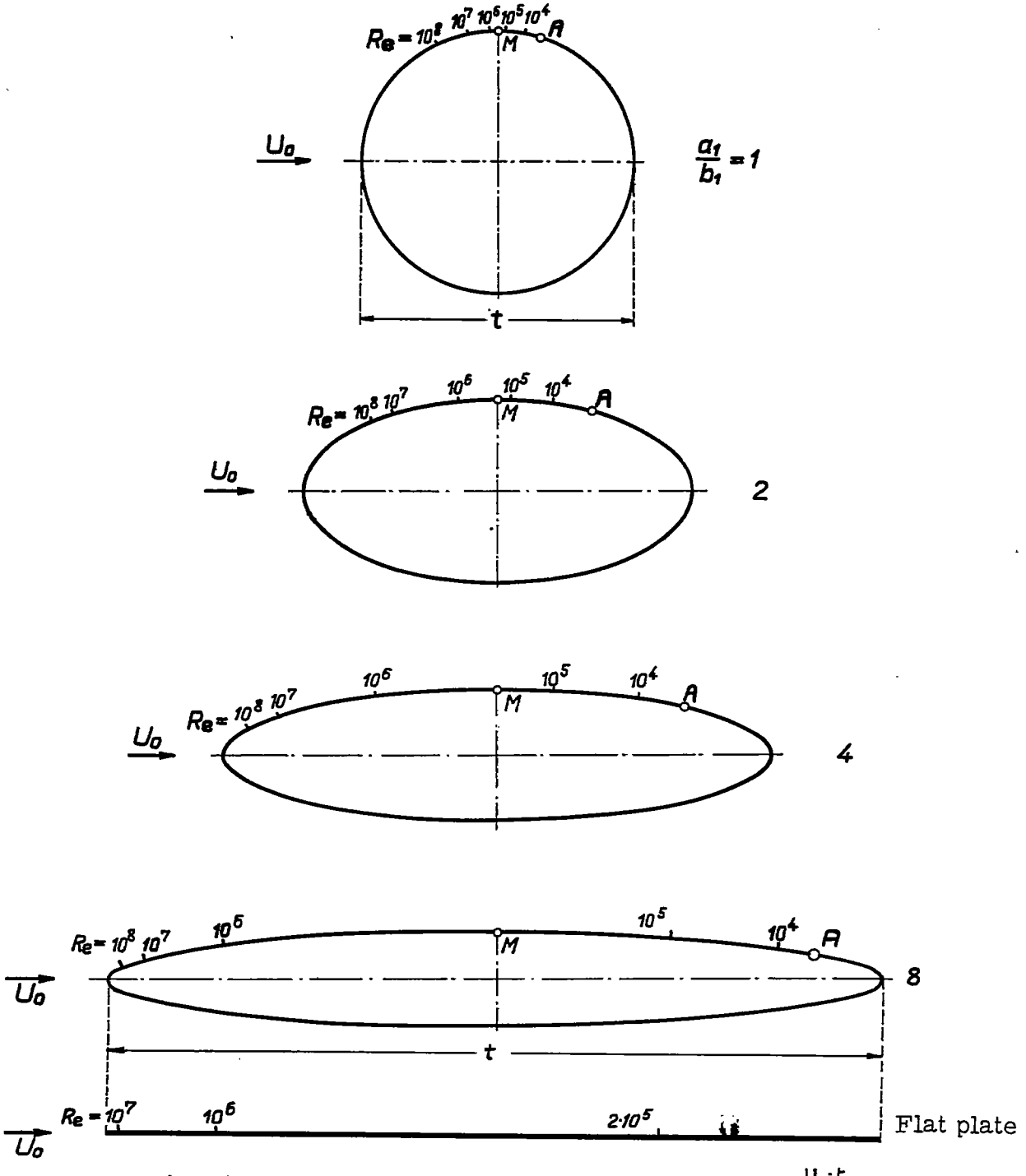

A = laminar separation point (independent of $R_e = \frac{U_o \cdot t}{\nu}$)

M = maximum velocity of the potential flow.

Figure 115.- The position of the instability point as a function of the Reynolds number for the elliptic cylinders of axis ratios $a_1/b_1 = 1, 2, 4, 8$.

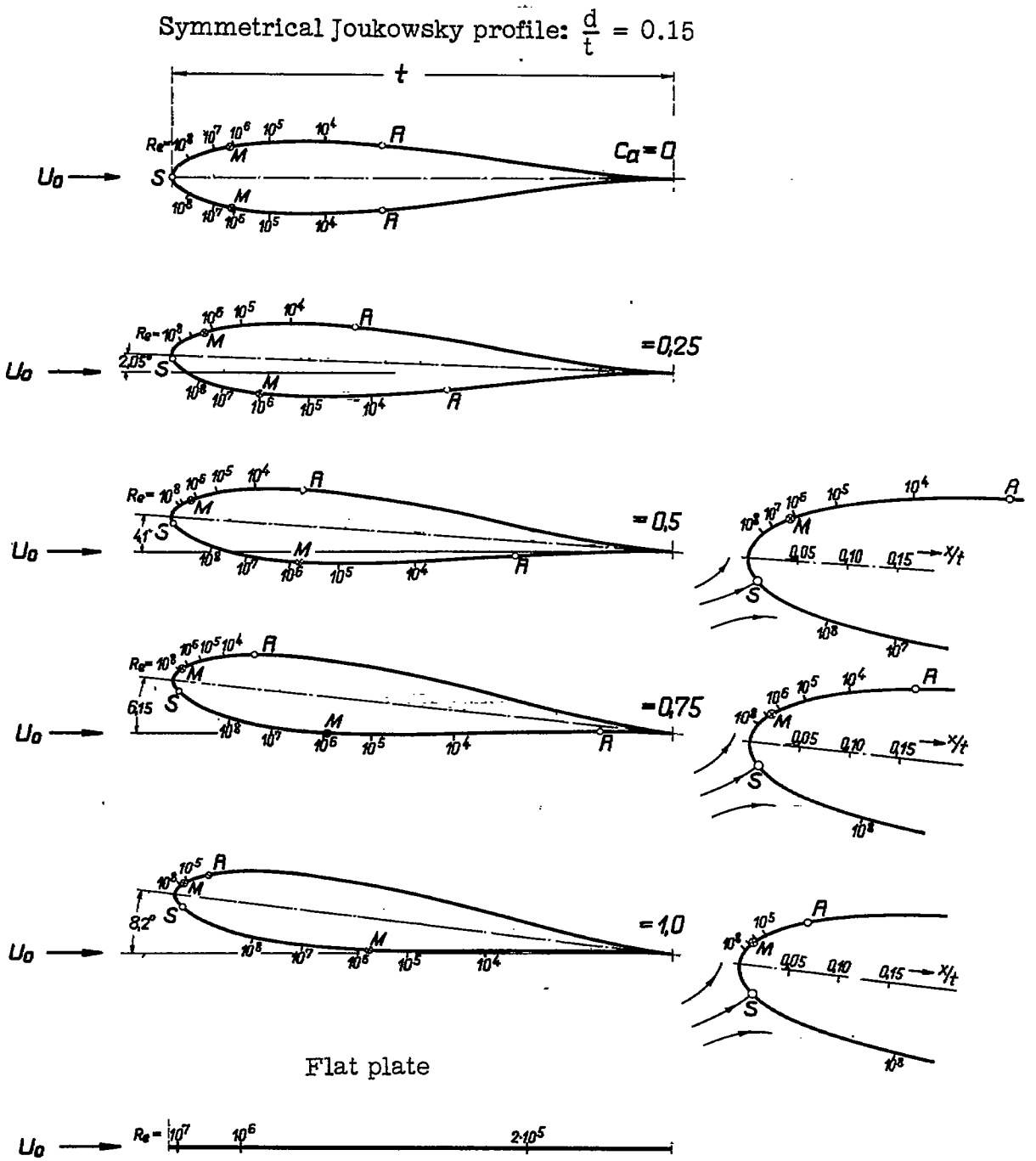

A = laminar separation point (independent of $R_e = \frac{U_o \cdot t}{\nu}$)
M = maximum velocity of the potential flow
S = stagnation point

Figure 116.- The position of the instability point as a function of the Reynolds number for a Joukowsky profile for lift coefficients of $c_a = 0$ to $c_a = 1$.